Electrochemical Energy Reviews (2022) 5:18
https://doi.org/10.1007/s41918-022-00170-6

REVIEW ARTICLE

Versatile Electrospinning for Structural Designs and Ionic Conductor Orientation in All-Solid-State Lithium Batteries

Qiang Li[1] · Xiao Sun[1] · Daxian Cao[1] · Ying Wang[1] · Pengcheng Luan[1] · Hongli Zhu[1]

Received: 18 January 2021 / Revised: 1 July 2021 / Accepted: 15 December 2021

Abstract
Recent advances in next-generation energy storage devices have focused on flexible and wearable all-solid-state lithium batteries (ASSLBs), mainly because of their advantages in terms of safety and extensive applications. Among various technologies for the preparation of flexible electrodes, electrospinning is a straightforward operation and cost-effective mean for the facile fabrication of flexible nanofibers and the versatile design of nanofiber structure. Herein, current technologies for engineering electrospun nanofiber structures and their state-of-the-art implementation in flexible ASSLBs are reviewed. First, current strategies for nanofiber structural design, including advances in high-specific surface area, superior mechanical flexibility, and various nanostructures, are systematically discussed. Subsequently, the utilization of electrospun nanofibers in ASSLBs is reviewed. Electrospinning of flexible and highly ion-conductive solid-state electrolytes (SSEs) is emphasized, and current nanofiber structural designs for SSEs and electrodes for ASSLBs are introduced. Despite these advances, there have not been enough studies of the integration of versatile electrospinning techniques in nanofiber structural design for both SSEs and electrodes. In the final section, promising pathways to implement versatile electrospinning in flexible ASSLBs with superior electrochemical performance and stable cycling properties are discussed. Thus, this review provides a holistic overview of the state of the art of electrospinning for high-performance flexible ASSLBs, which could safely power next-generation flexible devices.

Keywords Electrospinning · Nanofibers · All-solid-state lithium battery · Solid-state electrolytes · Flexible device

1 Introduction

Recently, numerous efforts have been made to make flexible and wearable all-solid-state lithium (Li) batteries (ASSLBs) that are considered a promising power source for next-generation emerging electronics due to their safety, high energy density, excellent mechanical performance that integrates bendability, foldability and stretchability, and, in general, light weight [1, 2]. These combined characteristics are highly desired in the modern electronics industry due to their great potential for the fabrication of various flexible and wearable electronics, such as roll-up displays, touchable screens, smart textiles and clothing, portable electronic devices, electronic skin, wearable health monitors, and military garment devices [3, 4]. Flexibility represents one of the most significant and challenging issues for flexible and wearable ASSLBs because flexibility is required to maintain electrochemical performance under repeated external mechanical bending, folding, and stretching [5]. One technology to fabricate flexible and wearable electronics is that of clothing. Textiles are ubiquitous in our daily life and an excellent substrate in which to embed nanomaterials for the fabrication of devices [6]. Functional textiles have been developed that are flexible, lightweight, and comfortable to wear, and they have great potential for use in smart clothing, with novel functions such as communicating, sensing, monitoring, computing, and actuating [7]. Despite these attractive potential opportunities, clothing technology has limitations; for example, it is challenging to permanently maintain the functions of smart clothing after frequent washing. In this regard, versatile fiber technology to integrate functional materials into fabrics is one of the most important technologies that can be applied to fabricate flexible and wearable electronics [7]. The as-spun fibers

✉ Hongli Zhu
h.zhu@neu.edu

[1] Department of Mechanical and Industrial Engineering, Northeastern University, Boston, MA 02115, USA

Published online: 03 October 2022

are generally flexible, bendable, lightweight, and long lasting. Spinning technologies have been widely used for next-generation energy storage devices with high energy density, high power density, flexibility, portability, and manufacturing scalability [4].

Numerous fiber spinning technologies have been developed to fabricate fibers with diameters ranging from microns to nanometers. Nanofibers have many attractive characteristics, such as high surface area, large surface-to-volume ratio, superior mechanical strength, and excellent flexibility [8, 9], which have attracted extensive interest for fabricating energy storage devices. The techniques to make polymers into nanofiber materials are diverse, including self-assembly, phase separation, templating synthesis, mechanical drawing, melt blowing, centrifugal spinning, and electrospinning (Table 1) [8, 10–13]. These nanofiber fabrication technologies have different working principles and advantages; however, each technology has disadvantages. As summarized in Table 1, self-assembly, mechanical drawing and melt blowing are only applicable for certain polymers that satisfy specific requirements. Phase separation and templating synthesis involve systems with elaborate and complex controls, and centrifugal spinning lacks the capability to be used in the design of nanofiber structures. Different from these nanofiber spinning technologies, electrospinning represents one of the most facile and versatile technologies that can easily manipulate the diameters of the produced fine fibers from tens of nanometers to microns [14]. More importantly, electrospinning is suitable for fiber structural design. Aligned patterns with oriented fiber deposition can be implemented by using different fiber collectors [9, 15]. The compositional structures of nanofibers can be designed as various types of structures that are comprised of binary, ternary, and even higher-order blends of polymer precursors [16]. Electrospinning possesses several additional advantages, such as low-cost facilities, and is feasible for most synthetic and natural polymers or polymer blends [17]; it also has excellent operability, reproducibility, and scalability [9, 18]. The resultant electrospun nanofibers generally have high aspect ratios and are randomly deposited to form a bendable, flexible, and freestanding mesh with nano-scale vacancies among the fibers. Notably, electrospun nanofibers are generally deposited to form mats that have been referred to as nanowires, nanomeshes, nanomembranes, nanofilms, or nanocomposites (of polymer blends) in different fields. Owing to these numerous advantages, electrospinning has demonstrated its great potential as the next-generation nanotechnology for practical applications to address current challenges in energy-related devices, such as fuel cells, dye-sensitized solar cells, supercapacitors, Li-ion batteries, sodium ion batteries, Li-sulfur batteries, sodium-sulfur batteries, and Li-oxygen batteries [19–28]. In this review, we specifically introduce the applications of electrospun nanofibers in

Table 1 Comparison of different technologies used to prepare nanofibers [8, 10–13]

Nanofiber technology	Principle	Advantages	Disadvantages
Electrospinning	Electrostatic repulsion under high electric fields	Facile and versatile; can spin a wide range of organic and inorganic materials into continuous nanofibers; easy to design nanofiber nanostructures and control nanofiber geometries	High voltage setups; low production rates
Self-assembly	Spontaneous organization	Fine nanofibers with diameters to several nanometers	Only for natural and synthetic polymers; complex operations and low throughput; requires elaborate setups
Phase separation	Thermal-induced polymer gelation by liquid/liquid or liquid/solid phase separation and fixed by low temperature quenching	No requirement for expensive specialized equipment	Involves multiple steps; small-scale technique; only amenable for certain polymers; difficult for nanostructure design
Templating synthesis	Fill a nanoporous template to form solid or hollow nanofibers	Amenable for metals, semiconductors, and polymers; uniform nanofibers; relatively simple and easy	Cannot make a continuous fiber one at a time; fiber formation heavily depends on template
Mechanical drawing	Extensive deformation under mechanical pulling	Forms a long single fiber one at a time	Only for viscoelastic materials
Melt blowing	Melts polymers to extrude them followed by high-speed air blowing to form nanofibers	High production rates; low cost; easy to scale up; solvent free	Only for certain polymers; needs careful operational control to produce nanoscale fibers
Centrifugal spinning	Radial centrifugal force stretches polymer jets	High production rates; spinnable for a wide range of organic and inorganic materials	Amenable for spinning randomly deposited nanofibers

flexible and wearable ASSLBs and, unlike existing reviews, we focus on this emergent next-generation energy storage technology.

Electrospinning technology has attracted increasing attention for preparing flexible and wearable ASSLBs, especially high-performance solid-state electrolytes (SSEs). Current SSEs can be generally divided into solid-state inorganic electrolytes (SIEs) made from glasses and ceramics, solid-state polymer electrolytes (SPEs) made of polymeric solid hosts and Li salts without liquid solvents, and composite electrolytes of these organic polymers and inorganic substances [2]. One of the most significantly challenging issues of these SSEs is their low ionic conductivity (IC) compared to liquid electrolytes, especially for SPEs in which most polymers have weak IC [29–31]. Multiple strategies have been developed to enhance IC, primarily including the integration of ion conductive inorganic nanofillers and the nanoengineering of ion conduction routes [32–34]. Among these improvements, electrospinning is a versatile means to functionalize each part of the ASSLBs. For example, electrospinning has enabled the fabrication of aligned nanowires that remarkably increased the IC of SSEs and used to prepare nanostructured anodes of ASSLBs [35] and cathode carbon nanofiber hosts in all-solid-state Li-sulfur batteries [36]. More importantly, the excellent flexibility and bendability of as-electrospun nanofibers are critical for fabricating portable and safe ASSLBs. The integration of electrospinning technology in ASSLB manufacturing, therefore, has opened a promising avenue to transform the IC of SSEs, the performance of assembled ASSLBs, and the practical implementation of ASSLBs.

In this review, we synthesize current knowledge of electrospinning technology for nanofiber structure design and key challenges of flexible and wearable ASSLBs. As shown in Fig. 1, we systematically review the versatility of electrospinning in designing nanofiber structures and their current applications in SSEs, anodes, and cathodes of ASSLBs. This review begins with a comprehensive overview of electrospun nanofibers and strategies to control their patterns, porous structures, and compositional nanostructures. In the following section, we emphasize the mechanism of how these structural designs can enhance the IC of SSEs and the performance of ASSLBs. The application of electrospun nanofibers as hosts for fabrication of both anodes and cathodes of ASSLBs is investigated thereafter. In the last parts of the review, future directions and perspectives for utilizing electrospinning nanofibers to make flexible and wearable ASSLBs are discussed.

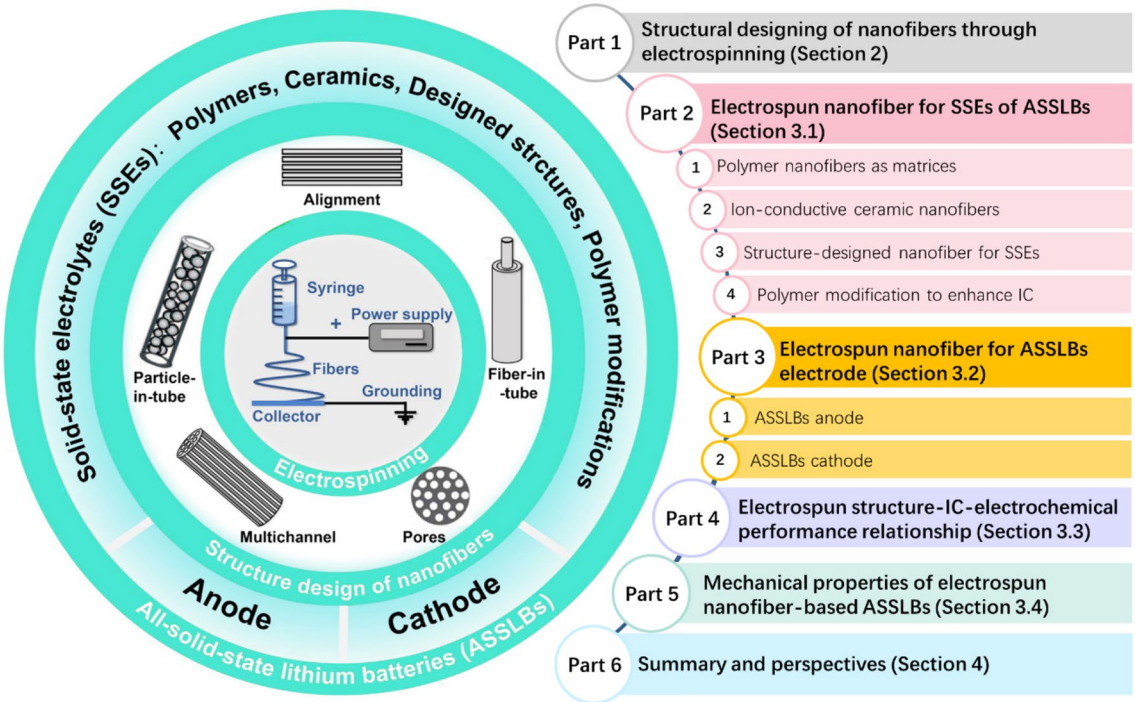

Fig. 1 The scope of this review consists of a timely overview of the versatility of electrospinning technology in the structural design of nanofibers and their applications in SSEs, anodes, and cathodes of ASSLBs

2 Structural Design of Nanofibers Through Electrospinning

The inherent merits of a high specific surface area and good mechanical flexibility have built the foundation of electrospun nanofibers for extensive applications in both conventional and next-generation energy storage devices. These properties of electrospun nanofibers can be further enhanced through facile control of nanofiber geometrical and architectural structures [27, 37]. In this section, we introduce the mechanism of how electrospinning produces nanofibers and summarize the widely used strategies to generate aligned patterns, porous structures, and complex nanostructures. These structural designs of electrospun nanofibers have broadly impacted the synthesis of nanofibers for tissue engineering, drug delivery, nanocomposites, membranes, and biomedical and many other functional applications [37–41]. In particular, some structural designs have enabled the enhancement of the electrochemical performance of energy storage devices, such as supercapacitors, Li-ion batteries, and ASSLBs [26, 27, 35, 42, 43]. Reviewing these mechanisms and nanostructural engineering technologies will provide holistic guidance for the future development of flexible and wearable ASSLBs as promising flexible energy storage devices.

2.1 Mechanism of Electrospinning For Nanofiber Fabrication

Overall, an electrospinning system is simply comprised of three main components: a micropumping unit, a high-voltage power supply system, and a winding system (Fig. 2A). The micropumping system controls the injection of the precursors at a certain low rate, the electric voltage is variable from 5 to 35 kV, depending on the spinnability of the precursors, and the winding system uses a rotating metal collector to gather the as-spun nanofibers. Most commercial electrospinning units are built in sealed boxes that contain a ventilation system to remove evaporated solvents (Fig. 2A) [44] and means to easily control the temperature, humidity, and atmosphere in the box when sensitive precursors are applied.

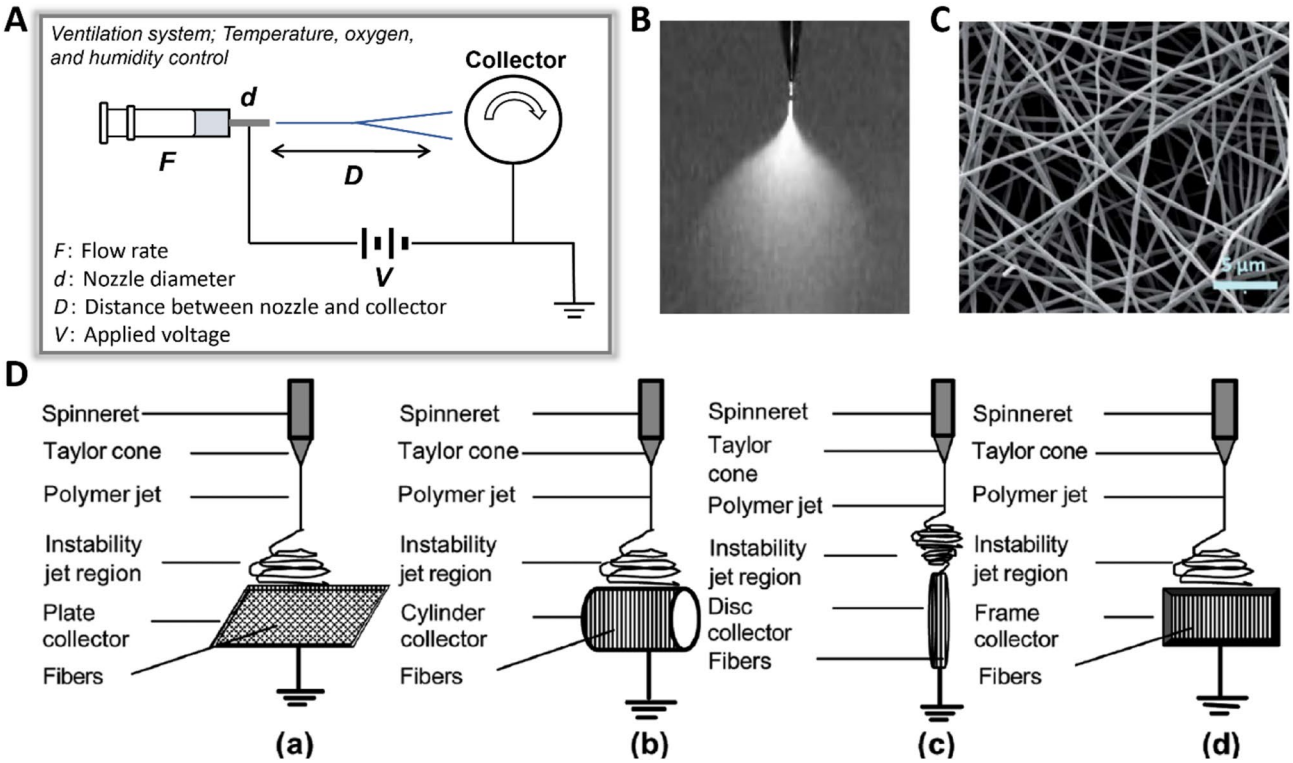

Fig. 2 **A** Fundamentals of electrospinning and manipulation of the patterns of the as-spun nanofibers. Schematic illustration of the electrospinning setup. Reprinted with permission from Ref. [44]. Copyright 2017, The Royal Society of Chemistry. **B** A typical electrospinning jet showing the bending instability of the Taylor cone. Reprinted with permission from Ref. [45]. Copyright 2012, Elsevier Ltd. **C** A representative scanning electron microscopy (SEM) image of nanofibers fabricated from electrospinning, which were randomly deposited to form a nanomesh. Reprinted with permission from Ref. [48]. Copyright 2018, Elsevier Ltd. **D** Strategies to electrospin nanofibers with aligned patterns. Reprinted with permission from Ref. [50]. Copyright 2007, Mary Ann Liebert, Inc.

The formation of nanofibers and their electrostability are complex since all the electrospinning parameters can have large effects on the morphologies, diameters, and uniformities of the resultant nanofibers. When a pendant droplet of precursor is injected from the spinneret, an electric potential is applied to the spinneret to electrify the droplet, and electric charge subsequently accumulates on the droplet surface and deforms the droplet into a Taylor cone (Fig. 2B) [12, 45, 46]. The shape of this Taylor cone is controlled by two electrostatic forces, i.e., electrostatic repulsion between the surface charge of the droplet and the Coulombic force exerted by the applied strong external electric field [14]. Nevertheless, to form a well-shaped Taylor cone, both characteristics of electrospinning dopes and operation parameters should be well-controlled. The characteristics include the electrical conductivity and molecular weight of the polymer precursor, the viscosity and concentration of the spinning dope, the surface tension of the droplet, and the dielectric constant of the solvent, while the operation conditions are mainly comprised of the injection rate, applied voltage, distance between the tip of the spinneret and the collector, needle size and shape, collector geometry and winding speed, and ambient parameters [14, 15, 47]. It is still impractical to quantitatively determine the effects of each factor on the quality of the as-spun nanofibers; however, the manipulation of some key parameters can generally produce a stable Taylor cone and corresponding uniform, defect-free, fine nanofibers (as shown in Fig. 2C) [48].

2.2 Manipulation of the Aligned Patterns of Nanofibers

As-spun nanofibers are commonly deposited on the collector at random (Fig. 2C and 2D-a). However, the design of aligned nanopatterns and the structured orientation of the formed nanofibers has enabled the implementation of electrospinning in numerous fields where structured materials are essential. Applying electrospun biopolymers as scaffolds in tissue engineering has motivated the manipulation of nanofiber patterns because cells cultured on aligned nanofiber scaffolds can proliferate along the fiber orientation [49]. The alignment of the electrospun nanofibers can be regulated by controlling the winding system, including the rotation speed and the collector shape [50]. A rotatable cylindrical collector (Fig. 2D-b) has been widely used to dynamically collect as-spun nanofibers. When the rotating speed matches the deposition rate of the polymer jet, the spun nanofibers can be wound tightly on the surface of the collector in a circumferential manner, resulting in oriented patterns to some extent [50, 51]. Nevertheless, increasing the winding speed has limitations. The Taylor cone can be destabilized when the rotating speed exceeds the deposition rate of the polymer jet, which could lead to the formation of discontinuous fibers. Another strategy to form aligned nanofibers is to replace a smooth collector with one that has sharp edges, such as a disc-type fiber collector (Fig. 2D-c), which can effectively concentrate the electrical field onto the collector edge and attract and continuously wind jet fibers [14, 52]. In general, a rotating disc collector that combines the merits of faster winding and sharp edges can successfully form highly aligned nanofibers.

Furthermore, additional strategies have been developed to form aligned nanofibers. For example, a frame collector (Fig. 2D-d) has been widely used for forming thin nanofiber mesh, and single nanofibers can be easily peeled off the mesh [50, 53]. This method has enabled the study of single nanofiber properties. For instance, single polyacrylonitrile (PAN) nanofibers have been obtained by using a frame collector, and the relationship between nanofiber mechanical performance and molecular orientation of PAN in the nanofibers has been demonstrated [53, 54]. Furthermore, other fiber collectors with very complicated structural designs, such as drum collectors, tube collectors with knife-edge electrodes, and twin blade collectors, have been used for aligning nanofiber jets [15]. Xie et al. [55] prepared radially aligned nanofibers by using a collector with a ring electrode and a sharp needle located in the center. In addition, Kessick et al. [56] reported that changing the power supply system can benefit alignment. They replaced the typically used direct current (DC) power supply with an alternating current (AC) high-voltage power supply to charge the electrospinning dopes of polyethylene oxide (PEO). The alignments of the PEO nanofibers were much improved.

2.3 Generation of Porous Structures in Electrospun Nanofibers

Porous structures can enable high specific surface areas of carbon nanofibers, which are highly preferable for energy storage devices such as supercapacitor electrodes and Li-ion battery anodes [57, 58]. In addition to high specific surface areas, porous nanofibers fabricated from electrospinning have high aspect ratios and improved pore interconnectivity, all of which have been extensively investigated to improve the mechanical strength and performance of electrodes in conventional batteries [57]. Recently, porous electrospun nanofibers have been prepared as hosts for solid electrolytes for ASSLBs (details are provided in Sect. 3.1). Some porous structures can provide sufficient amounts of interconnected voids to contain solid electrolytes. The resultant solid electrolyte can have improved mechanical strength and flexibility and greater Li-ion conductivity for some polymer electrolytes. When a battery undergoes external bending and twisting, the porous structures can dissipate the generated strain because of their relatively low bending stiffness [5]. The underlying relationship between the porosity of the porous structures and their relative flexibility

(α), as shown in the following equation, reveals that the flexibility of a solid material increases exponentially with its structural porosity [5, 59]. Therefore, applying porous structures in battery components can certainly enhance the flexibility of entire ASSLBs [5].

$$\alpha = \frac{B_b}{B_p(\rho)} = \left(\frac{2\left(1+\sqrt{2}\right)^2}{15} \frac{5\pi + 3(1-\rho)\left(1+\sqrt{2}\right)^3}{25\pi + 7(1-\rho)\left(1+\sqrt{2}\right)^3}(1-\rho) \right)^{-1} \quad (1)$$

where α is the relative flexibility of the solid material, B_b is the bending stiffness ratio of the solid structure, and B_p is the bending stiffness ratio of the porous structure with porosity ρ.

As mentioned above, vacancies can naturally form between fibers in as-spun nanofibers and contribute to mesoporous structures. These pores can be regulated by controlling electrospinning conditions, such as the applied voltage, tip-to-disc distance, and injection rate. More porous structures in nanofibers have been produced with the development of several technologies.

2.3.1 Pore Formation by Solvent Evaporation

Porous structures can be produced by designing the solvent composition of electrospinning dopes. Selecting a binary solution system of two solvents that have significantly different boiling points can induce different evaporation rates and thus generate pores in the electrospun nanofibers. In another approach, two precursors can form an emulsion (so-called emulsion electrospinning, Fig. 3A) [57]. For instance, a blend of a high molecular weight polyacrylonitrile (PAN) in *N,N*-dimethylformamide (DMF) (solvent with a low molecular weight pitch in tetrahydrofuran (THF)) was used to prepare electrospun nanofibers [60]. Fast evaporation of THF produced ultramicroporous structures in the as-spun nanofibers, which were then carbonized; the ultramicroporous structures improved the specific capacitance and energy density when the carbonized PAN/pitch nanofibers were used as the electrode of a supercapacitor [60].

2.3.2 Pore Formation by Sacrificial Polymers

Porous structures can be generated by using sacrificial polymers. With this strategy, electrospinning dopes are generally comprised of two polymer components, one of which serves as the sacrificial polymer that can be easily removed by dissolution or thermal treatment. Poly(methyl methacrylate) (PMMA) is a widely used sacrificial polymer that can be thermally degraded and thus creates abundant porous structures when the as-electrospun nanofibers are thermostabilized (normally at 250 °C). PMMA has been used to prepare PMMA/

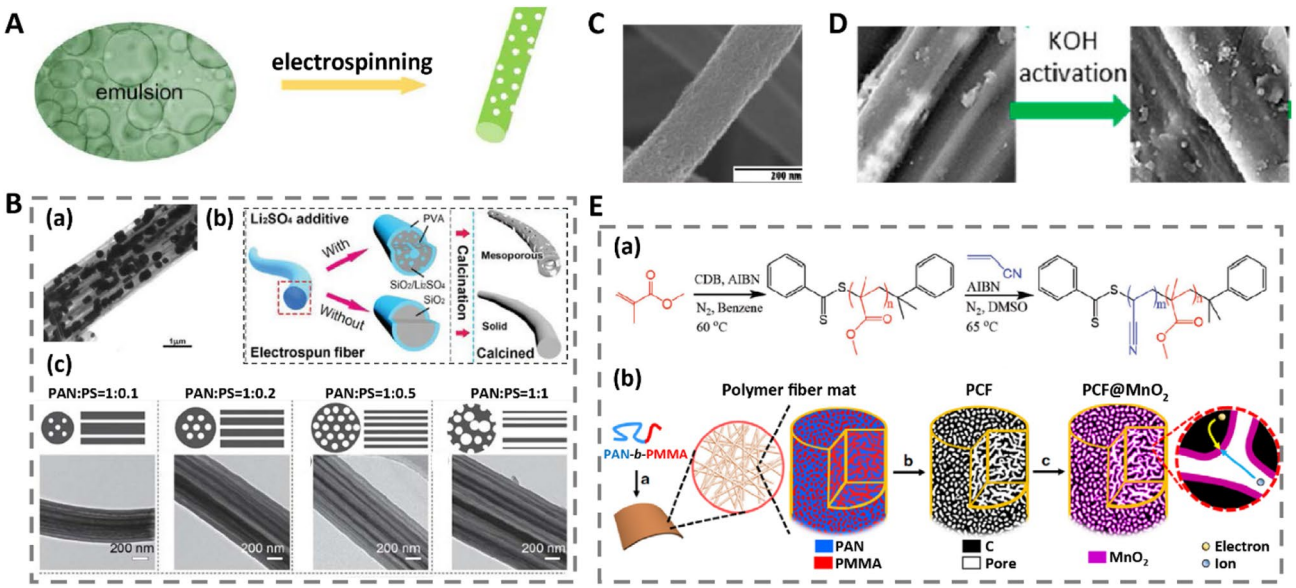

Fig. 3 Different strategies to produce porous structures in electrospun nanofibers for energy storage applications: **A** emulsion electrospinning. Reprinted with permission from Ref. [57]. Copyright © 2017, Elsevier Ltd.; **B** sacrificial polymer. Reprinted with permission from Ref. [61]. Reprinted with permission from Ref. [62]. Reprinted with permission from Ref. [65]. Copyrights © 2009, 2019 and 2015, American Chemical Society, John Wiley & Sons, Inc. and Springer Nature Ltd., respectively; **C** catalytic carbonization. Reprinted with permission from Ref. [69]. Copyright © 2011, Elsevier Ltd.; **D** chemical activation. Reprinted with permission from Ref. [75]. Copyright © 2018, American Chemical Society; and **E** self-assembly of a block copolymer. Reprinted with permission from Ref. [78]. Copyright © 2017, John Wiley & Sons, Inc. Reprinted with permission from Ref. [79]. Copyright © 2019, American Association for the Advancement of Science

metallic tin/PAN electrospun nanofibers [61]. The porous structures created by PMMA thermal degradation were carbonized to encapsulate tin (Fig. 3B-a), which significantly improved the cycling stability of tin in Li-ion batteries [61]. Other widely used sacrificial polymers and organics include poly(vinyl alcohol) (PVA), polyvinyl pyrrolidone (PVP), polystyrene (PS), and paraffin oil. For example, a porous SiO_2/Li_2SO_4/PVA nanofiber was prepared by electrospinning and used as the host of the polymer electrolyte in an ASSLB [62]. The PVA polymer was degraded to generate mesopores in the SiO_2 nanofiber when it was calcined at 500 °C (Fig. 3B-b) [8]. The porous structure can facilitate the infiltration of the polymer electrolyte of PEO/LiTFSI (lithium bis(trifluoromethanesulfonyl)imide) and improve the contact of the polymer electrolyte with the fibers, which can thus enhance the IC and electrochemical stability of the assembled ASSLBs [62]. A similar strategy was used to synthesize a TiO_2 nanofiber in which PVP, paraffin oil and $Ti(OBu)_4$ were blended and electrospun. After heating to 500 °C to convert $Ti(OBu)_4$ into TiO_2, PVP and paraffin oil degraded and generated porous structures in the TiO_2 nanofiber [63]. PS has also served as the sacrificial phase to prepare porous PAN nanofibers. PS can be decomposed during the carbonization processing of PAN [64, 65]. Controlling the PS dosage in the electrospinning dopes has enabled the regulation of the porous structures in the resultant carbon nanofibers (Fig. 3B-c) [65].

2.3.3 Catalytic Formation of Pores

Catalysts have been used to generate mesopores during nanofiber carbonization processing. Catalysts are generally added to polymer solutions during the preparation of electrospinning dopes (also called template electrospinning) and used to simultaneously catalyze the graphitization of the precursor polymer and create porous structures. Such a strategy has been widely used to prepare PAN-based mesoporous carbon nanofibers for supercapacitor electrodes. Various catalysts have been used, such as zinc chloride [66], nickel acetate [67], and vanadium pentoxide [68]. Moreover, a carbon nanofiber made from a tetraethyl orthosilicate (TEOS)/PAN blend was prepared with ultramicropores on the outer surface (Fig. 3C), which TEOS served as the bifunctional component that produced gases to generate pores and formed SiO_x to catalyze the formation of the porous structures by etching the carbon atoms that were formed in the thermostabilization process [69]. Controlling the catalyst content in the spinning dopes can normally result in different pore sizes and volumes and thus enhanced specific surface areas.

2.3.4 Activation of Carbon Nanofibers

Activation is efficient for creating micropores in carbon nanofibers, which can significantly increase the specific surface areas. Thus, nanofibers with activated carbon have broad applications, such as separation, purification, storage for natural gas and catalysts, and energy storage [70–73]. The activation reaction can be carried out using both steam [74] and powdery potassium hydroxide (Fig. 3D) [75]. The reactions are normally conducted under an inert atmosphere and at a high temperature (900 °C) for 1 h [75, 76]. Moreover, activation has been integrated with the abovementioned catalytic carbonization to develop micropores after the generation of mesopores and thus create hierarchical porous structures in the carbon nanofibers [66, 77].

2.3.5 Pore Formation in Block Copolymer-Based Nanofibers

In a recent breakthrough, self-assembly of block copolymers was used to generate and control the alignment of electropun nanofibers. A PAN-*b*-PMMA block copolymer was synthesized by addition-fragmentation chain transfer polymerization and electrospun to fabricate carbon nanofibers for electrodes (Fig. 2E-a) [78]. Under thermal annealing, microphase-separated structures formed with well-aligned PAN and PMMA microdomains. Under high-temperature carbonization, the PAN was converted into carbon and generated mesopores, while the PMMA degraded and created micropores (Fig. 2E-b) [79]. These designed hierarchical pores served as ion-buffering reservoirs and reduce ion transport distances, which largely improved the capacitive performance of the assembled pseudocapacitor (Fig. 2E-b) [80, 81]. Additionally, many block copolymers have been synthesized and used as SSEs of ASSLBs for their enhanced Li-ion conductivities, which are reviewed in Sect. 3.1.4.1.

Notably, hollow nanofibers from electrospinning have also been thought to be porous structures. We review their structure in the following section of nanostructure design, since most hollow nanofibers were enabled by core–shell nanofiber architecture design.

2.4 Nanostructure Design of Electrospun Nanofibers

Designing the nanostructure of electrospun nanofibers has greatly expanded their functionalization and application. Building complex nanostructures, on the other hand, poses challenges to researchers, as they cannot be easily and robustly fabricated through conventional "bottom-up" or "top-down" methods [82]. Electrospinning represents a novel and versatile simple technique to achieve the nanoscale design of the structure and architecture of nanofibers. Currently, most nanostructure designs using electrospinning are based on a core–shell structure that is produced by coaxial electrospinning (Fig. 4A) [82, 83]. The structure of the spinneret with the associated pumping system can enable the electrospinning of binary liquids, ternary liquids, and even

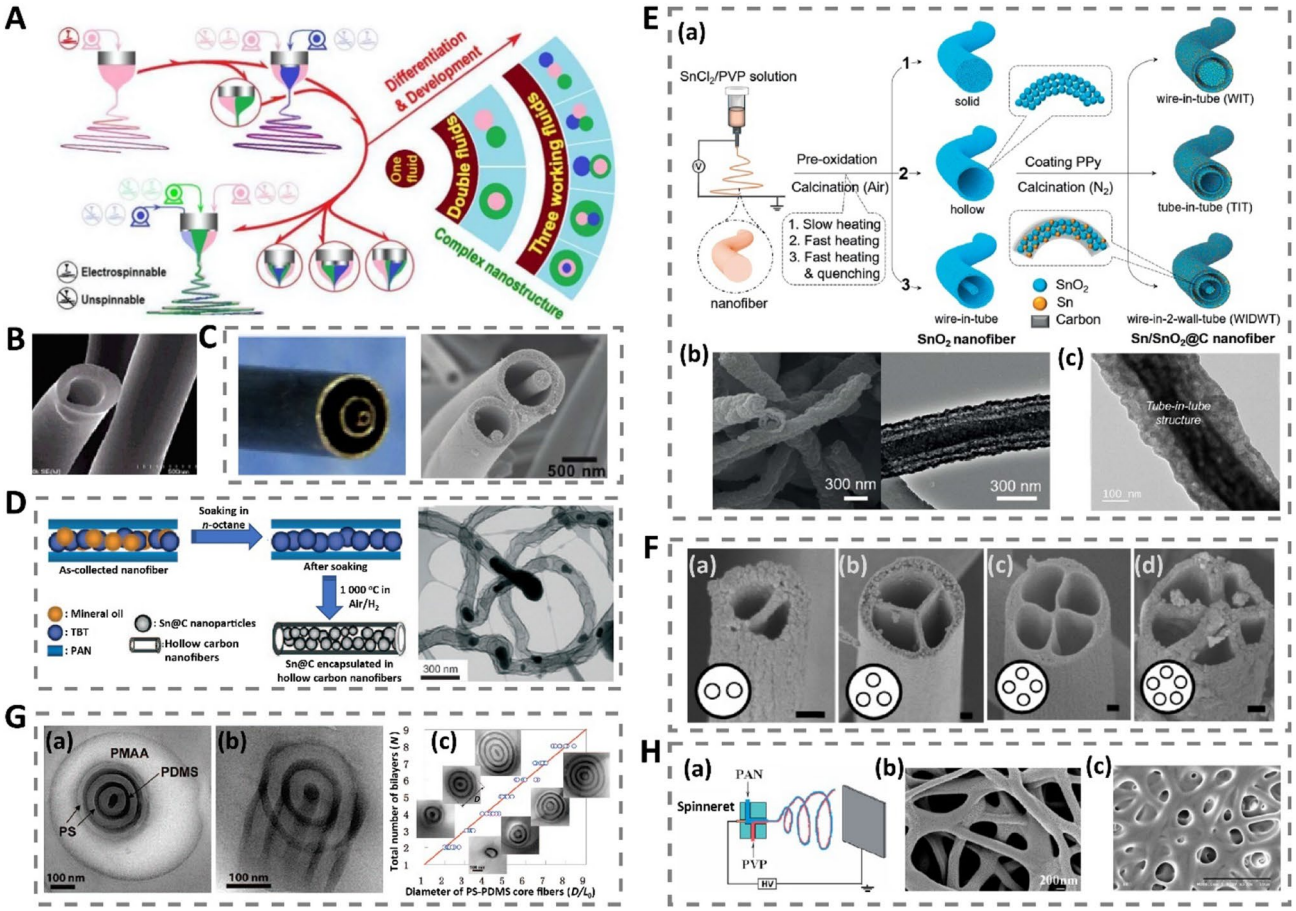

Fig. 4 Design of nanostructures of electrospun nanofibers: **A** coaxial electrospinning enables the design of core–shell and complex nanostructures. Reprinted with permission from Ref. [82]. Copyright © 2020, John Wiley & Sons, Inc.; **B** a typical hollow nanofiber. Reprinted with permission from Ref. [90]. Copyright © 2004, American Chemical Society; **C** an electrospun nanofiber with a fiber-in-tube structure enabled by tricoaxial electrospinning using a specially designed tricoaxial spinneret. Reprinted with permission from Ref. [91]. Copyright © 2019, Elsevier Ltd. Reprinted with permission from Ref. [93]. Copyright © 2010, American Chemical Society; **D** an example of the fabrication of a nanoparticle-in-tube nanofiber. Reprinted with permission from Ref. [97]. Copyright © 2009, John Wiley & Sons, Inc.; **E** a typical strategy to prepare a tube-in-tube nanostructured electrospun nanofiber (a) and its morphologies (b and c). Reprinted with permission from Ref. [98]. Copyright © 2020, Royal Society of Chemistry. Reprinted with permission from Ref. [99]. Copyright © 2020, Royal Society of Chemistry and John Wiley & Sons, Inc.; **F** multichannel microtube structures of electrospun nanofibers. Reprinted with permission from Ref. [101]. Copyright © 2007, American Chemical Society; **G** a concentric lamellar structure of nanofibers enabled by self-assembly of a coaxially electrospun block copolymer. Reprinted with permission from Ref. [104]. Copyright © 2006, American Chemical Society. Reprinted with permission from Ref. [105]. Copyright © 2009, American Chemical Society; **H** nanofibers with interconnection structures among fibers prepared by coaxially electrospinning two different polymers (a and b) or electrospinning a polymer with two fractions that have distinct thermostability. Reprinted with permission from Ref. [108]. Copyright © 2011, Elsevier Ltd.

higher-order mixtures of liquids to define the nanostructure of the resultant nanofibers. As shown in Fig. 4A, core–shell, side-by-side, and Janus structures can be formed by the coaxial electrospinning of two fluids, while the tricoaxial electrospinning of three liquids can fabricate much more complex nanostructures. Using these coaxial electrospinning technologies, multiple types of hollow nanofibers have been developed to encapsulate functional nanomaterials into electrodes for energy storage applications. These nanostructures mainly include single microtube (hollow nanofiber); fiber-in-tube, tube-in-tube, and multichannel microtubes; and inter-fiber connections. The mechanisms for preparing these nanostructures and their typical applications in energy storage are discussed in this section.

2.4.1 Hollow Nanofibers

Hollow nanofibers have received extensive attention for their wide applications in energy storage, microfluidics, catalysis, drug release, nerve guidance, oxygenators, and many other

devices [84–88]. Generally, hollow nanofibers are prepared from core–shell nanofibers fabricated by using coaxial electrospinning, where the sacrificial phase is used as the core to generate the hollow nanotube [89]. The first hollow electrospun nanofiber was reported by Loscertales et al. [90] who used olive oil or glycerin as the core fluid to produce hollow silica nanofibers (Fig. 4B). The method was later modified by Lallave et al. [16] by adding ethanol into the outer shell phase to prepare hollow carbon lignin nanofibers. Many other polymers have also been reported as sacrificial fluids for coaxial electrospinning. For example, a PAN-derived hollow carbon nanofiber was prepared by coaxially electrospinning a PAN/PMMA core/shell nanofiber in which PMMA was subsequently degraded during a thermostabilizing process to form the hollow structures [77]. The resultant hollow PAN-based carbon nanofiber displayed excellent capacity and load-bearing capability when it was used as the electrode material for a supercapacitor [77].

2.4.2 Fiber-in-Tube Structure

The fiber-in-tube structure is generally fabricated by using tricoaxial electrospinning, although the technology was first introduced to prepare hollow carbon nanofibers [16]. For tricoaxial electrospinning, the middle fluid serves as the sacrificial phase that separates the core and shell fluids during spinning and results in as-spun nanofibers with sandwich-like structure; the outer shell and inner core can be prepared from the same dope or different dopes to fabricate homogenous fiber-in-tube and a heterogeneous fiber-in-tube nanostructures, respectively [91, 92]. For example, a TiO_2 fiber-in-TiO_2 tube nanofiber was prepared by using the TiO_2 precursor tetrabutyl titanate [$Ti(OBu)_4$] for both outer and inner fluids, while paraffin oil was used as the middle fluid [93]. The collected as-spun nanofibers were calcinated at 450 °C to degrade the middle layer and synthesize TiO_2 in situ, forming a TiO_2 nanofiber in the TiO_2 nanotube structure (Fig. 4C) [93]. Moreover, two incompatible polymers can be incorporated into a heterogeneous fiber-in-tube nanofiber using this tricoaxial electrospinning technology. In a typical example, PS, PAN, and paraffin oil served as the shell, core, and sacrificial fluid, respectively, to fabricate a PAN fiber-in-PS core nanofiber [93]. These fiber-in-tube nanostructures might be used in microelectronics, luminescent devices, nanocables, drug delivery devices and other applications [94–96].

2.4.3 Nanoparticle-in-Tube Structure

Hollow carbon nanofibers can be encapsulated in situ or infiltrated with guest functional nanomaterials. An interesting example was reported by Yu et al. [97] who used mineral oil/tributyltin (TBT) as the core fluid and PAN in the shell fluid to coaxially electrospin tin nanoparticle-encapsulated hollow carbon nanofibers for the anodes of Li-ion batteries. Mineral oil was easily removed by dissolving the as-spun nanofibers in a solvent (*o*-octane), while tin nanoparticles were synthesized in-situ from TBT and encapsulated in the hollow PAN carbon nanofibers during the carbonization process (Fig. 4D) [97].

2.4.4 Tube-in-Tube Structure

Nanofibers with tube-in-tube nanostructure have been the subject of strong interest for energy storage applications due to their relatively large specific surface area and abundant inner surface, which can provide an effective area for contact between the electrode and electrolyte and many active sites for redox reactions [98]. In addition to energy storage, tube-in-tube nanofibers have also been applied in drug delivery systems owing to their inherent structural merits. Theoretically, a tube-in-tube nanofiber can be fabricated by tetracoaxial electrospinning with the second and fourth inner fluids as the sacrificial phases. However, the limited ability to spin most nanofibers with very fine inner layers might hinder this application. In practice, most tube-in-tube nanofibers were prepared from a solid electrospun nanofibers derived from polymer blends (mostly commonly PAN and PVP) combined with thermally active materials, such as SnO_2 [99] and cobalt(II) acetylacetonate-iron(III) acetylacetonate ($Co(acac)_3$-$Fe(acac)_3$) [100]. In these studies, the first-stage thermal treatment converted them into hollow nanofibers of Sn/SnO_2 and $CoFe_2O_4$. After that, polypyrrole (PPy) was infiltrated into the hollow fibers, which could generate tubes by partial pyrolysis during the next stage of thermal treatment for polymer carbonization (Fig. 4E-a). In this process, the thermal reaction of the active materials assisted the tube generation. The resultant Sn@C (Fig. 4E-b) and $CoFe_2O_4$@C nanofibers (Fig. 4E-c) with tube-in-tube structures were used as the anode of a Li-ion battery, which had high specific capacity with excellent long cycle performance.

2.4.5 Multichannel Microtubular Structures

Nanofibers with interesting multichannel microtubular structures were first reported by Zhao et al. [101] who used multifluid electrospinning. This complex nanostructure was inspired by the multichannel microtubular structures of many birds' feather that were thought to function as heat shields and thermal insulators. TiO_2 nanofibers with two to five microchannels (Fig. 4F-a to 4F-d, respectively) were fabricated by using a spinneret with the corresponding number of channels. The TiO_2 precursor Ti(O*i*Pr)$_4$, and PVP were dissolved in ethanol

and used as the shell dope, while paraffin oil served as the core dope. The microtubes were generated by sacrificing the organic compounds during calcination at 500 °C. Compared with the single hollow nanofibers introduced above, multichannel structures may possess considerable advantages, such as independent addressable channels, better mechanical stability, and larger surface-to-volume area [102]. However, such multichannel microtubular structures have not been extensively applied in functional material synthesis, perhaps due to their complex structures for practical control. Nevertheless, such nanofibers showed great potential for biomimetic super lightweight thermo-insulated textiles, multicomponent drug delivery devices, vessels for macro- and nanofluidic devices, highly efficient catalysts, and electrodes [102].

2.4.6 Concentric Lamellar Structure

Block copolymers generally present self-assembly properties such as microphase separation driven by the degree of incompatibility between the A and B blocks [103]. This self-assembly can result in the formation of interesting ordered aggregates that have been used to produce porous (Sect. 2.3.5) and ordered lamellar structures. The ordered lamellar property of a PS-*b*-PDMS block copolymer has been integrated with the advantages of electrospinning to fabricate a concentric lamellar structure with long-range order [104, 105] which is highly interesting for applications such as wearable power sensors, drug release systems, photonic bandgap fibers, and optical waveguides [106, 107]. In their study, PMMA and PS-*b*-PDMS copolymers were used as the outer and inner liquids for coaxial electrospinning, respectively. After thermal annealing at 160 °C for ten days, the PS and PDMS moieties in the block copolymer separated to form a lamellar structure in which the dark layers were identified to be PDMS, due to their higher electron density, and the light layers were PS (Fig. 4G-a). More interestingly, PMMA as the outer shell layer confined the self-assembly into a concentric cylindrical structure (Fig. 4G-a) and the number of layers (N in Fig. 4G-b). The PMMA outer shell determined the diameter of the as-spun nanofiber (D in Fig. 4G-b), and the layer thickness (L_0 in Fig. 4G-b, defined for an AB-BA layer) produced by the self-assembly was 56 nm. As shown in Fig. 4G, N equals D/L_0, which provides a simple strategy to control the self-assembly of the layers. By this technology, nanofibers as many as nine concentric lamellar layers have been fabricated (Fig. 4G). The continuity of the concentric lamellar structure was confirmed by transmission electron microscopy (TEM) (Fig. 4G-c), which reached 1–10 cm in length.

2.4.7 Interfiber Connection

In general, the as-spun fibers from electrospinning are randomly deposited to form a nanomesh with a lack of interfiber connections, which could result in unstable pore structures and charge transfer efficiency when they are used as electrodes for energy storage [108]. Building sufficient fiber–fiber connections can shorten the charge transfer pathway and facilitate charge transfer among fibers [109]. Side-by-side coaxial electrospinning has been used to prepare interconnected PAN-based carbon nanofibers (Fig. 4H-a) [108]. PAN was electrospun on one side of the fiber, and PVP was electrospun on the other side. PVP is a thermoplastic polymer that serves as the sacrificial polymer, which can be melted first to form connections among fibers and then partly degraded during carbonization processing to maintain the interconnection structure (as displayed in Fig. 4H-b). The capacitance was increased approximately 1.5-fold when this interconnected PAN-based carbon nanofiber was used as the electrode of a supercapacitor compared to that of a PAN/PVP carbon nanofiber without interconnection structures. Moreover, the fused structure of the interfiber connection can be tuned by changing the composition of the electrospinning dopes. Dallameyer [110, 111] studied industrial lignin/PEO electrospun nanofibers. Two lignin fractions with distinct glass transition temperatures (T_g, 152 and 230 °C) were blended. By increasing the ratio of the low-T_g lignin fractions, the as-spun nanofibers can form largely fused interfiber structures under thermostabilization while keeping the fiber scaffold (Fig. 4H-c). Since lignin is an abundant industrial waste derived from natural plants, lignin and lignin-based electrospun nanofibers have been widely used to fabricate sustainable energy storage devices [112–117]. Similar to the abovementioned fused PAN/PVP nanofibers, this interfiber-connected structure could benefit electrochemical performance, if lignin-based nanofibers are used, for energy storage devices.

Overall, these studies have provided novel strategies to generate various nanostructures in nanofibers or fused interconnection structures among nanofibers. These interesting nanostructures have enabled multiple functionalizations of electrospun nanofibers in electrodes and many other applications, which can inspire innovative designs of transfer pathways to enhance ion or charge transference when electrospun nanofibers are used for SSEs or electrodes of ASSLBs, respectively.

3 Advances of Electrospinning in ASSLBs: The-State-of-the-Art

Current applications of electrospinning technology have been focused on the fabrication of flexible and highly ion-conductive SSEs, including electrospinning polymer nanomeshes as hosts, electrospinning ion-conductive ceramic nanofibers for solid composite electrolyte fabrication, and designing special electrospun nanofibers

for enhancing Li-ion transportation. All these applications represent state-of-the-art use of electrospinning technology for ASSLBs. However, these applications have not yet integrated the versatility of electrospinning in nanofiber structure design, except for the preparation of aligned ceramic nanofibers. Despite the SSEs, applications of electrospinning in the electrodes of ASSLBs have been the subject of relatively few studies, and only a few publications have focused on the anodes of ASSLBs, the cathodes of all-solid-state Li-sulfur batteries and an all-solid-state sodium-ion battery. In this section, we systematically summarized these existing applications of electrospinning technology in the fabrication of both SSEs and electrodes of ASSLBs, which represents a timely review of how electrospun nanofibers can perform in advancing the development of next-generation flexible and wearable battery technologies.

3.1 Electrospun Nanofiber for SSEs

SSEs, key components of ASSLBs, are critical for battery safety, high temperature resistance, and nonvolatilization [118]. Nevertheless, current SSEs still encounter great challenges with regard to low ionic conductivity, poor interfacial contact with electrodes, and narrow electrochemical stability windows [29, 31]. Electrospinning technologies can address these challenging issues of SSEs through structural designs. Current strategies for making SSEs from electrospun nanofibers include electrospinning ion-conductive polymer nanofibers, ion-conductive ceramic nanofibers, and nanofibers with aligned or porous structures for enhanced ion conductivity. It is possible that regulating polymer chemistry can concurrently enhance ion conductivity and electrospinnability. All these studies have demonstrated the great potential and promising future of electrospinning technology in fabricating high-profile SSEs.

3.1.1 Electrospun Polymer Nanofibers as Matrices

Electrospinning is a facile approach to fabricate membranes composed of polymer nanofibers that have controllable thickness, high porosity, and good flexibility. Such electrospun membranes are good matrices for the preparation of SSE layers. In comparison with conventional preparation protocols, infiltrating SSEs, including solid polymer electrolytes (SPEs) and solid ceramic electrolytes (SCEs), into the electrospun polymer matrix endows the solid electrolyte layers with unique properties, such as decreased thickness, considerable flexibility, enhanced film formability, and accelerated ion conduction. In this section, the application of an electrospun polymer nanofiber matrix in the preparation of SPEs and SCEs is discussed.

Conventional SSEs layers are prepared through cold pressing methods and generally are limited by their large thickness and high rigidity. Such thick SSEs can decrease the energy density of the assembled cell, and the pellet is not

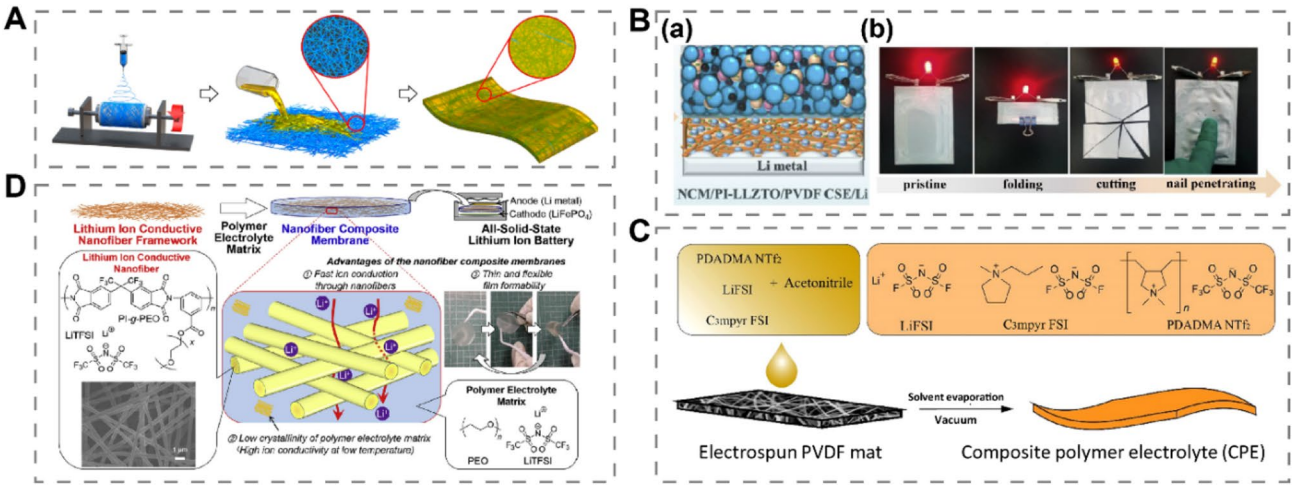

Fig. 5 Electrospinning of polymer nanofibers as a matrix for infiltrating SSEs: **A** electrospinning of randomly deposited PI as the host for the infiltration of a sulfide ($Li_6PS_5Cl_{0.5}Br_{0.5}$) for solid ceramic electrolytes. Reprinted with permission from Ref. [119]. Copyright © 2010, Elsevier Ltd.; **B** electrospinning of PI nanofibers as the host for casting a solid ceramic electrolyte ($Li_{6.75}La_3Zr_{1.75}Ta_{0.25}O_{12}$, LLZTO) and the punched ASSLBs working in harsh environments. Reprinted with permission from Ref. [120]. Copyright © 2019, American Chemical Society; **C** electrospinning of the randomly deposited PVDF nanomat as the host for a composite polymer electrolyte. Reprinted with permission from Ref. [118]. Copyright © 2020, American Chemical Society; and **D** electrospinning of ion-conductive nanofibers from PI-*g*-PEO polymer as the framework for a composite polymer electrolyte. Reprinted with permission from Ref. [123]. Copyright © 2005, IOP Publishing

suitable for flexible batteries to be used in wearable electronics. To overcome these limitations, combining rigid SSEs with soft polymers is a promising strategy. Recently, Kim et al. [119] developed a thin and flexible SSE through the infiltration of a sulfide ($Li_6PS_5Cl_{0.5}Br_{0.5}$) into an electrospun polyimide (PI) membrane, as shown in Fig. 5A, which delivered excellent thermal stability (> 400 °C) along with reasonable ion conductivity (5×10^{-5} S cm^{-1}). The PI polymer has high thermal stability, making it a suitable host for the hybrid solid electrolyte layer. In addition, the PI-derived nanomats obtained through electrospinning were flexible, robust, and porous. The assembled $LiNi_{0.6}Co_{0.2}Mn_{0.2}O_2$ (NCM)/graphite ASSLBs using $Li_6PS_5Cl_{0.5}Br_{0.5}$-infiltrated PI had a high capacity (146 mAh g_{NCM}^{-1}, 30 °C), high energy density (110 $Wh_{kg\ cell}^{-1}$, 30 °C), promising cycling performance (88.1% capacity retention after 25 cycles at 0.2 C, 30 °C) and excellent thermal stability (only marginal degradation at 180 °C).

Electrospun PI nanofibers have also been used as hosts for electrolyte fillers composed of $Li_{6.75}La_3Zr_{1.75}Ta_{0.25}O_{12}$ (LLZTO), polyvinylidene fluoride (PVDF) and LiTFSI to fabricate hybrid polymer electrolytes (Fig. 5B-a) [120]. This hybrid polymer electrolyte had an ion conductivity of 1.23×10^{-4} S cm^{-1}, where PI nanofibers provided a network to host LLZTO in PVDF and prevented Li dendrite growth (Fig. 5B-a). The assembled solid-state $LiNi_{0.5}Co_{0.2}Mn_{0.3}O_2$/Li pouch cells exhibited excellent cycling stability (152.6 mAh g^{-1} with capacity retention of 94.9% at 0.1 C after 80 cycles at 25 °C), even in harsh external environments, such as folding, cutting, and nail penetration (Fig. 5B-b), suggesting the high safety of this ASSLB [120].

A similar strategy that introduced SPEs into an electrospun polymeric matrix was also developed to address the challenges in the formation of films from some polymer electrolytes, such as PEO and polymerized ionic liquids. These polymer electrolytes have considerable ionic conductivities but poor film formability and weak mechanical strength, which have significantly impeded their applications in ASSLBs. Employing an electrospun polymer matrix has successfully addressed this challenging issue. Wang et al. [121] reported using a PVDF nanomat prepared by electrospinning to cast polymerized ionic liquids for a composite polymer electrolyte (Fig. 5C) that had a high ionic conductivity (4.5×10^{-4} S cm^{-1}). The robust PVDF membrane successfully enhanced the mechanical strength of ionic liquid-based electrolytes. Similarly, Zhou et al. [122] cast organic ionic plastic crystals (OIPCs) on an electrospun PVDF template to prepare a composite polymer electrolyte. The resultant freestanding and robust electrolyte layer had an ionic conductivity of 1.0×10^{-5} S cm^{-1} at room temperature. Notably, the ionic conductivity of the PVDF/OIPC electrolyte decreased slightly compared with that of OIPCs alone because the PVDF polymer matrix has no ion conduction property. Moreover, it is still debated whether electrolytes derived from ionic liquids and polymerized ionic liquids can be considered as solid electrolytes, although such electrolytes generally do not undergo leakage and solvent evaporation.

To circumvent the low ionic conductivity of the polymer matrix itself, grafted copolymers with higher ionic conductivity have been synthesized and electrospun into nanofibers for composite polymer electrolytes. Watanabe et al. [123] grafted PEO onto PI to synthesize a PI-*g*-PEO copolymer, which was then electrospun into nanofibers to infiltrate the PEO/LiTFSI electrolyte (Fig. 5D). The as-prepared composite polymer electrolyte was as thin as 19 μm and had an ionic conductivity (1×10^{-4} S cm^{-1} at 40 °C) much higher than that of each individual component (2.8×10^{-5} S cm^{-1} for the PI nanofiber membrane and 3×10^{-6} S cm^{-1} for the PEO electrolyte matrix at 40 °C). The enhanced ionic conductivity was attributed to the decreased crystallinity of the PEO moieties and the intrinsically high ionic conductivity of the nanofibers.

General guidance for electrospinning polymers for SSEs can be summarized from the above studies. The following characteristics are preferable for the polymeric matrix: (1) porous structures formed between fibers to enable the infiltration of ceramic electrolyte and percolation for efficient ion conduction; (2) high thermal stability to avoid degradation in the subsequent annealing process for solution-processed sulfide electrolyte; (3) good mechanical strength to maintain the intact structure; and (4) good chemical and electrochemical stability with respect to the solvent and ceramic electrolyte.

3.1.2 Electrospun Ion-Conductive Ceramic Nanofibers

In addition to polymer nanofibers, electrospinning has been used to fabricate ion-conductive ceramic nanofibers. Compositing polymer electrolytes with ceramic nanofibers is another promising strategy to fabricate composite polymer electrolytes with enhanced ionic conductivity and mechanical strength. As mentioned above, employing ionic conductors in composite polymer electrolytes can accelerate ionic conduction due to the decreased degree of crystallization of the ion-conductive polymers and the generated ion-conductive paths in the solid polymer electrolytes. In other words, 3D solid-state electrolytes fabricated on 1D nanofibers can facilitate Li^+ transport. This compositing polymer electrolyte generally can not only enable higher ionic conductivity but also reinforce the composite electrolyte.

As early as 2005, Wang et al. [124] reported the integration of ceramic conductive fibers made of $La_{0.55}Li_{0.35}TiO_3$ into a polymer electrolyte (PEO-$LiN(SO_2CF_2CF_3)_2$), which demonstrated an enhanced room temperature ionic conductivity of 5.0×10^{-4} S cm^{-1} and an increased transference

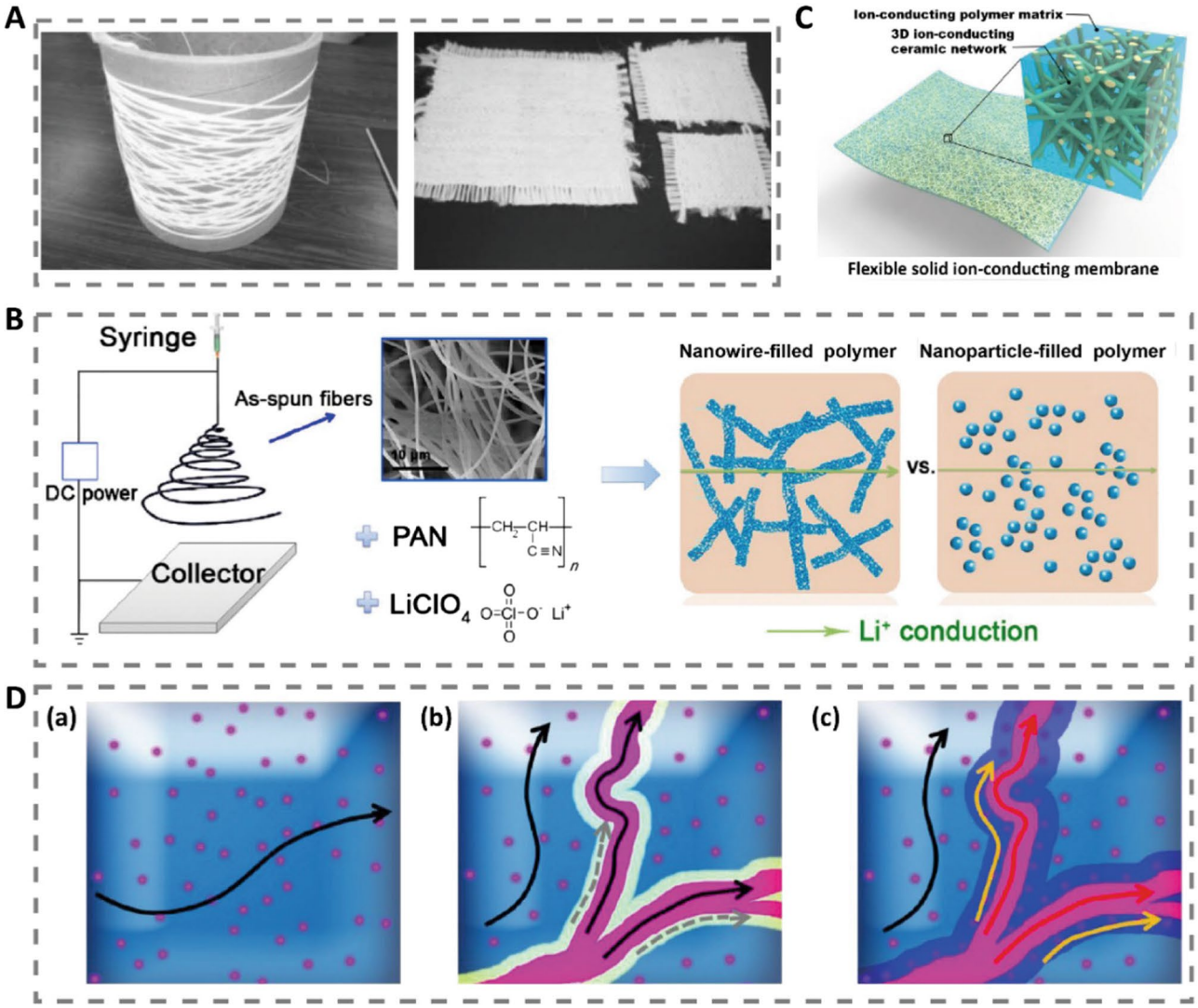

Fig. 6 Electrospinning of ceramic/polymer composites into nanofibers as templates for polymer electrolyte infiltration: **A** photos of $La_{0.55}Li_{0.35}TiO_3$ fibers with diameters of 15 μm. Reprinted with permission from Ref. [124]. Copyright © 2015, American Chemical Society; **B** schematics of the preparation of $La_{0.55}Li_{0.35}TiO_3$ nanofibers via electrospinning and the ion conduction paths in the PAN/$La_{0.55}Li_{0.35}TiO_3$ composite electrolyte. Reprinted with permission from Ref. [125]. Copyright © 2019, American Chemical Society; **C** electrospinning of ceramics/polymer (LLZO/PVP) nanofibers for polymer composite electrolytes (PEO/LiTFSI). Reprinted with permission from Ref. [128]. Copyright © 2018, Royal Society of Chemisty; and **D** schematic illustration of ion conduction pathways in composite polymer electrolytes by using (a) no fillers, (b) ion-conductive fillers, and (c) ion-conductive fillers with enhanced surface ionic conductivity. Reprinted with permission from Ref. [134]. Copyright © 2019, Elsevier Ltd.

number of 0.7. However, the $La_{0.55}Li_{0.35}TiO_3$ fibers, as shown in Fig. 6A, had diameters as large as 15 μm, since these fibers were made from a wet spinning method that can only produce micron-scale fibers. As a comparison, Liu et al. [125] fabricated $Li_{0.33}La_{0.557}TiO_3$ (LLTO) nanowires through electrospinning. The electrospun LLTO nanofibers had much smaller diameters of 140 nm (Fig. 6B). An unprecedented room temperature ionic conductivity of 2.4×10^{-4} S cm^{-1} was achieved when 15 wt% (wt% means the weight percentage) nanowires were incorporated with the PAN-$LiClO_4$ electrolyte, which represented an improvement of more than three orders of magnitude compared with the ionic conductivity of the PAN-$LiClO_4$ electrolyte without LLTO nanowires. When a certain number of ceramic nanowires was added, the conduction of Li ions in this composite electrolyte mainly took place in the polymers and on the surfaces of the ceramic wires, as illustrated in Fig. 6B. The A-site vacancy-enriched surfaces provided fast pathways for Li ion hopping. Likewise, PVDF-based electrolytes were also reinforced by other ceramics, such as $Li_{0.33}La_{0.55}TiO_3$ [126] and $Li_7La_3Zr_2O_{12}$ [127].

In the preparation of ceramic nanowire-based SSEs, the dispersion of ceramic nanowires in the polymer is critical because ceramic nanowires easily aggregate, which can reduce the ionic conductivity. To address this challenge that occurs in the mixing process, Fu et al. [128] developed a freestanding ion-conductive ceramic ($Li_{6.4}La_3Zr_2Al_{0.2}O_{12}$) membrane through electrospinning and then infiltrated it with polymer electrolyte (PEO-LiTFSI), as shown in Fig. 6C. The ceramic nanofibers had diameters of 138 nm and formed a 3D network for ionic conduction that enabled a high room temperature ionic conductivity of 2.5×10^{-4} S cm^{-1}. Meanwhile, this solid-state composite electrolyte had enhanced mechanical strength. When it was coupled with Li metal, good cycling stability was achieved, suggesting effective dendrite suppression. Similar designs were also reported in other works, where the fabricated solid composite electrolyte delivered enhanced ionic conductivities ($>10^{-4}$ S cm^{-1}), good stability with respect to Li, and a widened electrochemical stability window [129–133]. Notably, employing solid-state nuclear magnetic resonance, Yang et al. [134] confirmed that the transport of Li ions in these solid-state composite electrolytes is based on intrapolymer, intraceramic fiber, and interfacial transport, as illustrated in Fig. 6D. The ionic conductivity was greatly increased when the interfacial transport was enhanced.

3.1.3 Structure-Designed Electrospun Nanofibers For SSEs

Although electrospinning is versatile for designing numerous nanostructures of nanofibers that have attracted extensive attention for applications in supercapacitors and multiple types of batteries using liquid electrolytes, their current applications in ASSLBs are just at the initial stage. The utilization of randomly fabricated nanofibers as scaffolds for polymer electrolyte infiltration was the main focus. Reported nanostructure designs of electrospun nanofibers for the enhancement of ionic conductivity of solid polymer electrolytes have started to use the well-aligned patterns and porous structures of electrospun nanofibers. It was reported for the first time, by Liu et al. [35], that well-aligned LLTO nanowires have been fabricated by electrospinning and used as fillers to be added to PAN/$LiClO_4$/DMF solutions. The SSEs were prepared by casting the well-aligned LLTO nanowires and PAN/$LiClO_4$ solution into a film by using a doctor blade. In comparison with random LLTO nanofibers, the aligned nanowires can provide a straight pathway, without crossing junctions to interrupt ionic transport, resulting in fast ion conduction along the nanowire (Fig. 7A). The ion conductivity measured at 30 °C was 6.05×10^{-5} S cm^{-1}, representing a tenfold increase compared with that of the random ceramic nanowires (5.40×10^{-6} S cm^{-1}).

Likewise, a well-aligned ceramic $Li_{6.4}La_3Zr_2Al_{0.2}O_{12}$ (LLZO) nanofiber film was prepared by electrospinning its precursors with PVP polymers [135]. After calcination at 800 °C in air for 4 h, densified LLZO ceramic nanofibers were obtained (Fig. 7B). Their SSEs were prepared by casting the PVDF/$LiClO_4$/*N*-methyl pyrrolidone solution into aligned LLZO nanofiber films, which had an ion conductivity of 1.16×10^{-4} S cm^{-1} at 30 °C. The ASSLBs made of this aligned LLZO-based SSE, a high-voltage cathode of $LiNi_{0.8}Co_{0.15}Al_{0.05}O_2$ (NCA), and a lithium metal anode, have exhibited a high termination charging voltage (4.6 V under 0.2 C at 25 °C), high initial discharge capacity (146 mAh g^{-1} at 0.2 C), and high coulombic efficiency (> 95%).

In addition to the aligned patterns, porous structures of nanofibers have been advanced for SSE fabrication. Yu et al. [62] prepared a freestanding Li_2SO_4-doped mesoporous SiO_2 nanofiber film through electrospinning and used it as a host for polymer electrolytes. As shown in Fig. 7C-a, the electrospinnability of tetraethyl orthosilicate (TEOS, as the SiO_2 precursor) and Li_2SO_4 was enabled by PVA polymers. The porous structure was generated by the degradation of the PVA polymer during calcination at 500 °C in air, as introduced in Sect. 2.3.2. PEO and LiTFSI were dissolved in acetonitrile and dropped onto SiO_2 porous nanofibers to make SSEs. Li_2SO_4, which is inherently Li-ion conductive, improved the interaction between PEO and SiO_2 nanofibers at their interfaces (Fig. 7C-b). All these SiO_2 nanofiber structural designs enabled the preparation of SSEs with a Li-ion conductivity of 3.9×10^{-5} S cm^{-1} at 25 °C. The ASSLB full cell assembled from this SiO_2 nanofiber-based SSE, $LiFePO_4$ cathode, and Li metal anode had stable cycling performance with high specific capacities (over 80 mAh g^{-1}, 50 cycles at 0.5 C, 60 °C).

In summary, with the incorporation of these structurally designed electrospun nanofibers to enhance Li-ion conductivity, it is certain that a more complex functional nanostructure design has great potential to enhance the ionic conductivity of SSEs and the electrochemical performance of assembled ASSLBs.

Notably, solvents have been used in the preparation of all the above SSEs. Although the solvents were removed, the utilization of solvents for ASSLB fabrication is still under debate for the possible deterioration in the ionic conductivity of SSEs and the cycling performances of ASSLBs. First, the electrospinning of the precursors of ceramic nanofibers must be enabled by a polymer, which needs to be dissolved for electrospinning. As summarized in Table 2, PVP is the most commonly used polymer, and a DMF/acetic acid cosolvent with a certain ratio is a generally used solvent to dissolve PVP and disperse the precursors. Most solvents used for the preparation of ceramic nanofibers can be removed during the electrospinning process. The possibly remaining trace solvents can be completely removed in subsequent high-temperature heating treatments, such as calcination/sintering. Second, all aforementioned SSEs were prepared

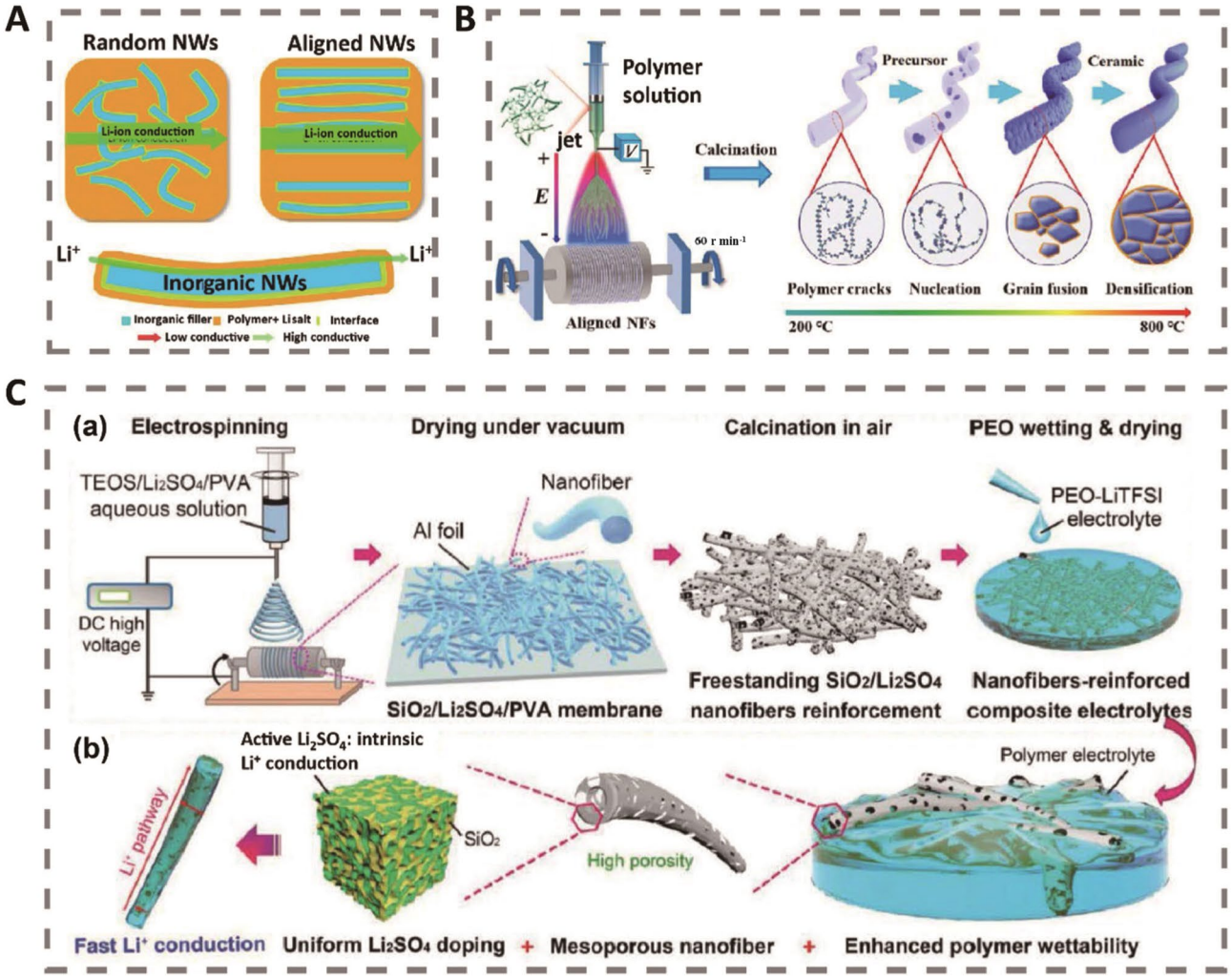

Fig. 7 Nanostructural design of nanofibers through electrospinning to enhance the ionic conductivity of the SSEs: **A** illustration of the possible mechanism by which aligned electrospun ceramic nanofibers enhance Li-ion conductivity. Reprinted with permission from Ref. [35]. Copyright © 2017, Springer Nature; **B** an example of the preparation of well-aligned LLZO ceramic nanofibers through electrospinning as a scaffold for polymer electrolyte preparation. Reprinted with permission from Ref. [135]. Copyright © 2012, American Chemical Society; and **C** preparation of a SiO_2 nanofiber with mesoporous structures through electrospinning for a composite polymer electrolyte. Reprinted with permission from Ref. [62]. Copyright © 2019, John Wiley & Sons, Inc. In panel (C), (a) is the schematic for the preparation of the SiO_2/Li_2SO_4/PEO composite polymer electrolyte, and (b) displays the fast Li^+ conduction of the composite polymer electrolyte that is enabled by the embedded SiO_2/Li_2SO_4 nanofibers. Reprinted with permission from Ref. [62]. Copyright © 2019, John Wiley & Sons, Inc.

by dissolving the ion conductive polymer and Li salt in organic solvents and then compositing them with ceramic nanofibers. The most common solvents used in this process are DMF, acetonitrile, and NMP (Table 2). Acetonitrile has a relatively low boiling point (82 °C), while DMF and NMP have much higher boiling points at 153 and 202 °C, respectively (Table 2). Even though vacuum drying has been widely used to remove solvents, as summarized in Table 2, trace solvents may remain in the SSEs, especially when high-boiling point solvents such as DMF and NMP are used [35]. Additionally, the strength of the interactions between the solvent and polymer in SSEs can impact the removal of the solvents; for example, PAN with abundant nitrile groups is very polar and can form strong dipole–dipole interactions with DMF, which can remain in the SSEs even after drying at 120 °C for 1 week [136]. Boiling points, interactions with the polymer used for SSEs, and proper drying methods should thus be considered during the selection of solvents.

Foran et al. [137] systematically reviewed the impacts of retained solvents on the performances of both solid polymer electrolytes and ASSLBs, although most understanding presented in the work is based on conventional lithium-ion batteries using liquid electrolytes. On the one hand, the remaining solvents in the SSEs, even at ppm-level content,

can enhance the lithium ion conductivity [137]. The underlying mechanism for such enhancement is (1) solvents may decrease the crystallinity of the polymer and lower its T_g, which can improve the mobility of the polymer and enhance lithium ion hopping in and/or between polymer chains; (2) polar solvent has a high affinity to lithium ions, which can enhance ion dissociation and increase ion mobility; and (3) solvent can serve as a plasticizer to better separate polymer chains, which can increase the free volume between polymer chains and thus improve polymer segmental mobility [137]. On the other hand, although solvent can enhance the ionic conductivity of SSEs, it may reduce the electrochemical performance of the assembled ASSLBs when the solvent content exceeds a certain amount, for example, several hundred ppm [137, 138]. The impacts of solvents on the assembled lithium battery performance mainly include: (1) solvent interaction with the anode to trap lithium ions and induce irreversible loss in rate capacity; for example, moisture can form C–OH sites with a graphite anode to disturb the formation of the solid-electrolyte interface (SEI) layer [137, 139] and acetonitrile has been reported to degrade the SEI layer formed between a lithium metal anode and a $LiPF_6$-acetonitrile electrolyte [140]; (2) a hygroscopic cathode may absorb moisture, and water decomposition during charging can increase the rate of aging and corrosion, thus decreasing battery cycling stability [141, 142]; (3) the polymer electrolyte might be more hygroscopic than the cathode and absorb moisture that can result in decreased cycling performance, rate capacity, and mechanical performance [137, 139].

Overall, complete removal of solvents is certainly an essential requirement for ASSLBs. Studies on conventional lithium batteries can deliver fundamental understanding about how remaining trace solvents impact battery performance, but how the trapped solvents can impact the electrochemical and other performance attributes (such as mechanical properties) of ASSLBs is still under study. The most commonly used drying technologies, as presented in Table 2, are probably not capable of reducing the solvent content to an acceptable level, such as several hundred mol/μmol. However, the solvent level and its impacts are seldom reported in most works about ASSLBs. More attention from academia is urgently needed to address the mechanistic understanding of solvent impacts and to develop efficient solvent removal technologies for ASSLBs.

3.1.4 Polymer Modification to Enhance the Ionic Conductivity of SSEs

Electrospinning is versatile and universal for processing most polymers into nanofibers. Because of this inherent merit, chemical modification of existing Li-ion conductive polymers could be implemented in electrospinning technology. In this section, we review current chemical modifications of polymer structures for enhanced ionic conductivity and transference number. The regulated polymer structures can be integrated with the structural design of electrospinning, as discussed above, to enable superior SSEs. Although the possible impacts of such chemical modifications on the geometry and ion-conducting properties of the resultant nanofibers have not yet been reported, the existing strategies for enhancing polymer ionic conductivity by regulating polymer properties could concurrently improve the electrospinnability and elaborate structural design of electrospun nanofibers. In this section, we systematically reviewed how chemical regulation of polymers can enable high-performance SSEs, which can provide guidance for SSE improvement that could be of great interest to readers.

PEO was the first polymer reported by Fenton et al. [143] to conduct Li ions and has attracted extensive attention for making SPEs because PEO has a high donor number for Li^+ ions, chain flexibility, high dielectric constant, and strong Li^+ solvating ability [144]. The mechanism, as revealed, involves the dissociation of a Li salt by the polymer backbone and the transport of the resulting ionic species via ion hopping or chain segmental motion (Fig. 8A) [31]. Although PEO is among the best Li-ion conductive polymers known to date, its ion conductivity and transference number along with those of many other polymer electrolytes have been sought and still need to be improved. Numerous chemical modifications and polymer structural designs have been developed in recent years, focusing on (1) lowering the T_g and reducing the crystallinity of polymers to enhance Li ion transport, and (2) controlling the dielectric constant and the solvation site of polymers to enhance Li salt dissociation and the transference number. These chemical modifications have enabled the high ionic conductivity of polymers and could improve the miscibility of the modified polymer with guest molecules for enhanced electrospinnability, especially polymers with decreased T_g and increased dielectric constants.

3.1.4.1 Strategies for Polymer Design to Enhance Ionic Conductivity

The design of polymer structures to enhance ionic conductivity mainly addresses the reduction of polymer crystallinity to decrease the number of Li transport blocks and the decrease in T_g to improve polymer segmental motion. Several strategies have been developed to regulate and synthesize novel structured polymers. The first strategy is to engineer polymer side chains (Fig. 8B). As developed by Sun et al. [145] three types of comb-like peptoid ($n = 20$) homopolymers with ethylene oxide $(EO)_n$ side chains of different lengths were synthesized. When the side chain increased from one EO unit to three EO units, the T_g of the polymer decreased from 38.6 to − 26.4 °C. As a result, the ionic conductivity increased ten-fold, although it was measured at a very high temperature of 100 °C.

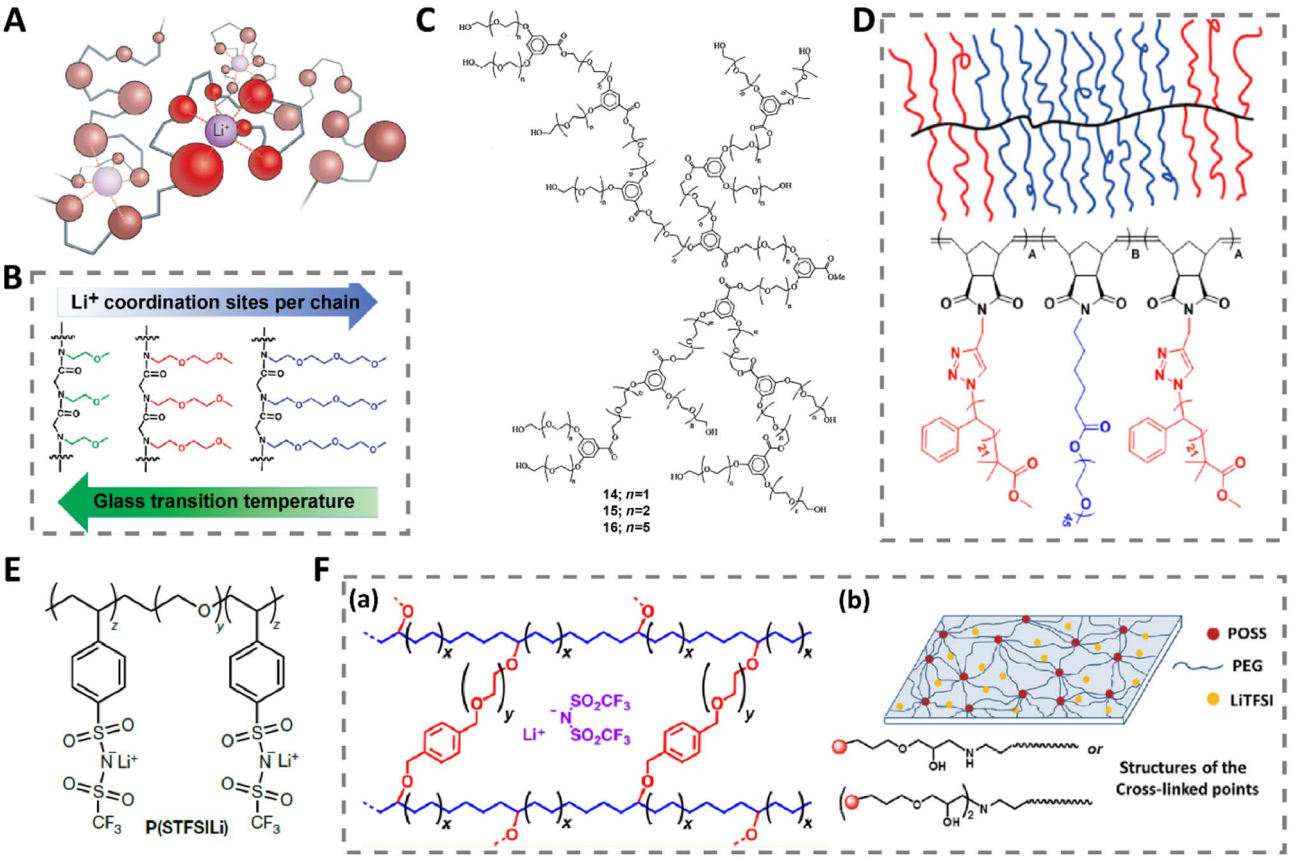

Fig. 8 Strategies to enhance the ionic conductivity of solid polymer electrolytes by modifying polymer molecular structures: **A** mechanism of ionic conduction. Reprinted with permission from Ref. [31]. Copyright © 2019, Springer Nature; **B** side-chain engineering of polymer. Reprinted with permission from Ref. [145]. Copyright © 1999, American Chemical Society; **C** polymer branching. Reprinted with permission from Ref. [147]. Copyright © 2012, IOP Publishing; **D** polymer brush. Reprinted with permission from Ref. [151]. Copyright © 2013, Springer Nature; **E** block copolymer for the single polymer conductor (ionomer). Reprinted with permission from Ref. [152]. Copyright © 2021, Elsevier Ltd.; and **F** polymer crosslinking. Reprinted with permission from Ref. [154]. Reprinted with permission from Ref. [155]. Copyrights © 2015 and 1995, John Wiley & Sons, Inc. and IOP Publishing, respectively

The second extensively used strategy is to synthesize hyperbranched EO-based polymers [146], which can reduce polymer crystallinity to enhance ionic conductivity. Hawker et al. [147] used methyl 3,5-dihydroxybenzoate as the branching point to prepare a PEG-based hyperbranched polymer (Fig. 8C) that had an ionic conductivity of 7×10^{-5} S cm^{-1} at 60 °C. Moreover, Nishimoto et al. [146] copolymerized 2-(2-methoxyethoxy)ethyl glycidyl ether (MEEGE) with EO to form a P(EO/MEEGE) with ether branching units that was followed by photopolymerization in the presence of acrylic acid to form a hyperbranched polymer. The ion conductivity was as high as 1×10^{-4} S cm^{-1} at room temperature.

Third, many block copolymers have been synthesized to form well-ordered molecular structures and to suppress polymer crystallinity, such as PS-*b*-PEO [148], PP-*b*-PEO-*b*-PP [149], and PS-*b*-PEO-*b*-PS [150]. In addition to these linear AB and ABA block copolymers, more complex brushed block copolymers have been synthesized (Fig. 8D), which have a polynorbornene backbone with PS and PEO (PS-*b*-PEO-*b*-PS) brushes [151]. In comparison with linear AB and ABA block copolymers, this ABA brush block copolymer had improved ion conductivity and lower elastic modulus [151]. A triblock copolymer was also synthesized by grafting a Li salt (poly(styrene trifluoromethane sulfonylimide of lithium, P(STFSILi)) to the PEO polymer [152]. The resultant BAB block copolymer of P(STFSILi)-*b*-PEO-*b*-P(STFSILi), as shown in Fig. 8E, has revealed synthetic improvement in single-ion conductivity (1.3×10^{-5} S cm^{-1} at 60 °C), transference number, mechanical strength, and stable electrochemical window up to 5 V versus Li^+/Li [152]. Recently, a three-dimensional intercalated block copolymer of PEG-*b*-hexamethylene diisocyanate trimer was reported, which had a high ionic conductivity of 5.7×10^{-4} S cm^{-1}, a high transference number of 0.49, and a wide electrochemical window up to 4.65 V [153].

Fourth, crosslinked polymers were designed with tunable structures to concurrently enhance the ionic conductivity and lower the mechanical properties to resist Li dendrite growth. For example, a polyethylene-PEO polymer was synthesized by ring-opening metathesis polymerization (ROMP) in which PEO served as the cross linker (Fig. 8F-a) [154]. Pan et al. [155] used an inorganic crosslinker, polyhedral oligomeric silsesquioxane (POSS), to synthesize a PEG-based crosslinked polymer electrolyte (Fig. 8F-b). The structure of the crosslinked polymer can be easily tuned by changing the ratio of POSS and PEO.

Finally, low molecular weight polymers that have a high dielectric constant have been used as polymer plasticizers, such as PEG [154], propylene carbonate [156], butylene carbonate [156] and ethylene carbonate [156, 157], to enhance the ion conductivity of polymer electrolytes. Such plasticizers can decrease the crystallinity of the polymer and enhance Li-ion dissolution. Moreover, with the help of plasticizers, it is possible to tune the processability of the polymer electrolyte by changing the rheology of the polymer composites to assemble polymer electrolyte membranes into all-solid-state batteries.

3.1.4.2 Strategies for Polymer Design to Increase Li-Salt Dissociation and Ion Transference Number Despite the crystallinity and segmental motion of the polymers, their

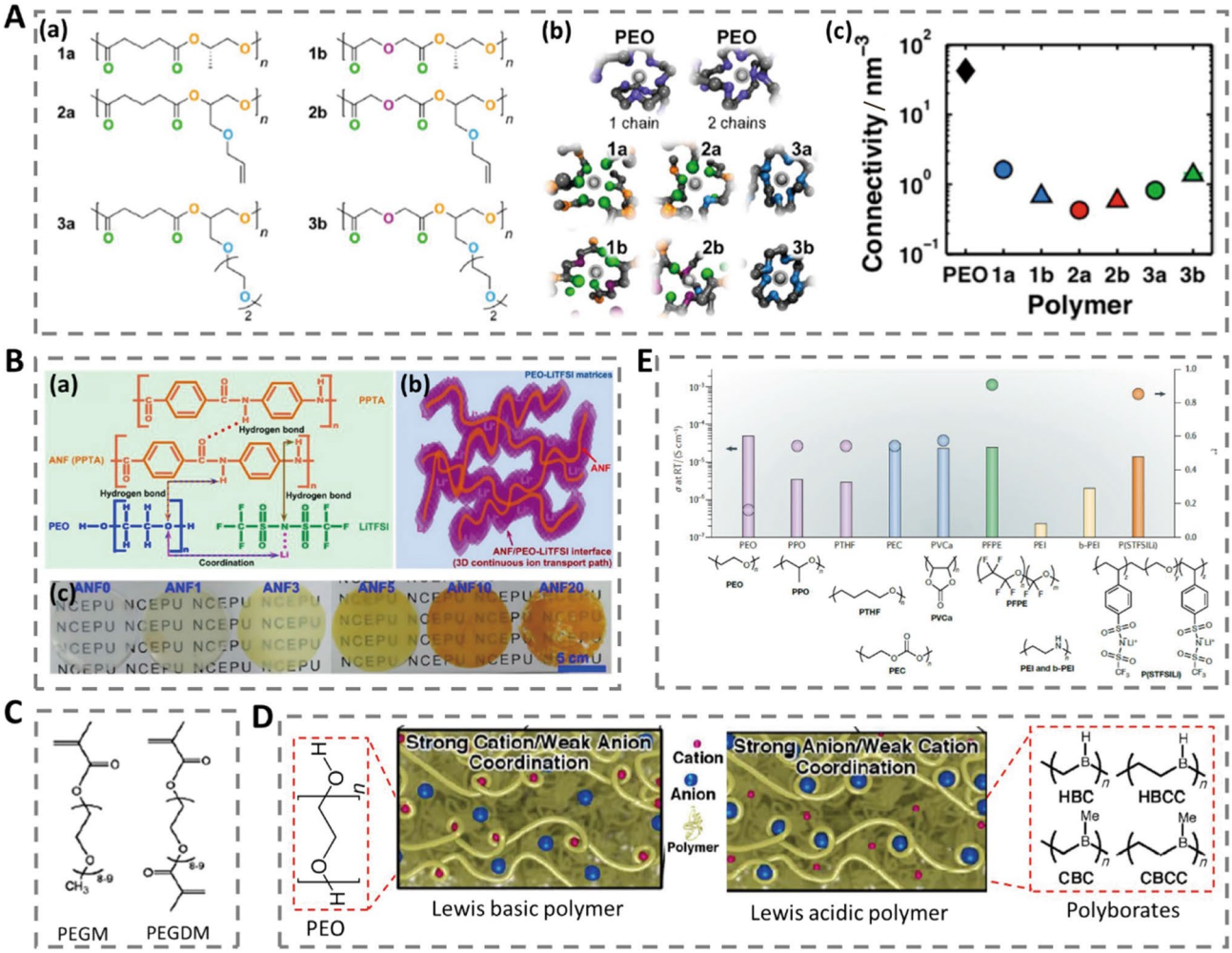

Fig. 9 Strategies to enhance Li-salt dissociation and the ionic transference number of solid polymer electrolytes by modifying polymer molecular structures, functional groups, and interactions: **A** tuning solvation sites to enhance ion conductivity through the synthesis of polymer structures. Reprinted with permission from Ref. [158]. Copyright © 2020, Elsevier Ltd.; **B** enhancement of the hydrogen bonding system. Reprinted with permission from Ref. [159]. Copyright © 2016, American Chemical Society; **C** modification of PEG polymer functional groups. Reprinted with permission from Ref. [160]. Copyright © 2014, American Chemical Society; **D** utilization of Lewis acid polymers. Reprinted with permission from Ref. [144]. Copyright © 2012, American Chemical Society; and **E** comparison of ionic conductivity and the transference number of reported polymers. Reprinted with permission from Ref. [31]. Copyright © 2019, Springer Nature

interactions and connectivity with Li ions are other main considerations for ionic conduction. Another pathway to enhance Li-ion conductivity, therefore, is to alter Li-salt dissociation and ion-polymer interactions. For this purpose, polymer backbone and side-chain structures, functional groups, and ion-polymer coordination have been designed. As shown in Fig. 9A, a series of polymers with polyester-based backbones and PEG-based side chains were synthesized [158]. These polymers differed with respect to oxygen-containing links, including double-bonded carbonyl oxygens (green), ester oxygens (orange) and ether oxygens (purple) in the backbone and ether oxygens (blue) in the side chains (Fig. 9A-a), therefore providing different solvation sites for Li ions. According to the molecular dynamics simulation, these oxygen atoms displayed different distributions in the polymers (Fig. 9A-b), and a more uniform distribution of solvation sites (1a and 3b in Fig. 9A-b and 9A-c) instead of a higher number of binding atoms has been reported to enhance the connectivity of Li ions to the polymers (Fig. 9A-c).

Regarding ion-polymer interactions, Liu et al. [159] reported regulation through the formation of hydrogen bonds, where aramid nanofibers (ANFs) were added into the PEO/LiTFSI polymer electrolyte to form hydrogen bonds with both PEO and LiTFSI (Fig. 9B-a), which facilitated Li-ion dissociation, prevented PEO crystallization, and regulated the ionic transport path along the ANF (Fig. 9B-b). In their study, up to 5% addition of ANF (Fig. 9B-c) displayed the most improved ionic conductivity. The ASSLBs assembled using this ANF-based solid polymer electrolyte, $LiFePO_4$ cathode, and Li-metal anode exhibited a high specific capacity (159 mAh g^{-1} at 0.1 C, 30 °C) and cycling stability (135 mAh g^{-1} after 100 cycles at 0.4 C, 40 °C).

Moreover, a strategy has been reported to change the chain-end functional groups of PEG to increase both the Li ion transference number and ionic conductivity at room temperature [160]. As shown in Fig. 9C, the end-chain hydroxyl groups of PEG were methacrylated and produced two types of PEG-derived polymers with methacrylate at one end (poly(ethylene glycol) methyl ether methacrylate, PEGM) or both ends (poly(ethylene glycol) methyl ether dimethacrylate, PEGDM).

Finally, the Li-ion transference number was enhanced by improving the ion-polymer coordination. Most strategies to increase the ion-polymer coordination focused on the intermolecular interaction between Li^+ and the polymer, for example, decreasing T_g and thus the segmental motion of the polymers. These strategies have been applied for Lewis base polymers such as the traditional PEO polymer, which can form relatively strong cation-polymer interactions. Unlike from these modifications, Savoie et al. [144] used Lewis acid polymers (polyborates) that exhibit strong anion-polymer coordination to indirectly enhance Li-ion dissociation and transference numbers (Fig. 9D).

In summary, the ionic conductivity and transference number of the generally used polymers are shown in Fig. 9E. Polyesters of poly(ethylene carbonate) (PEC) and poly(vinylene carbonate) (PVCa) showed balanced values of the ionic conductivity and the transference number [31]. However, the higher ionic conductivity and its trade-off with the transference number still need to be much improved to reach values on the order of 10^{-3} S cm^{-1} at room temperature, which is critical for achieving the implementation of ASSLBs in the near future.

3.2 Electrospinning of Nanofibers for the Electrodes of ASSLBs

The current focus of applying electrospinning technology to ASSLBs is heavily focused on SSEs, as systematically reviewed in Sect. 3.1. For electrodes, to the best of our knowledge, only a few published works have used electrospinning technology to make anodes or cathodes of ASSLBs, although numerous works have utilized electrospun nanofibers for the electrodes of liquid Li-ion batteries. Since a large number of reviews have already introduced state-of-the-art applications of electrospinning in liquid Li-ion battery systems [25, 28, 42, 161–165], we focus only on ASSLB electrodes in this section. The inherent advantages of nanofibers, including their shortened ionic diffusion pathways, higher specific surface area with improved interfacial contact between electrodes and electrolytes, and the freestanding feature of the formed nanomats, contribute to the foundation of flexible ASSLB electrodes [161]. Basically, electrospun nanofibers in ASSLB electrodes have been advanced as skeletons to support or confine the deposition of active materials. The versatility of electrospinning technology in controlling porosity has been exploited for the anodes of ASSLBs. Such functionalization has also been enabled by electrospinning highly ion-conductive ceramic nanofibers as sulfur hosts for the cathodes of all-solid-state Li-sulfur batteries. These advancements could initiate further development of both anodes and cathodes by exploring the versatility of electrospinning in the structural design of electrodes for addressing current challenges in ASSLBs.

3.2.1 Fabrication of ASSLBs Anodes Through Electrospinning

Anodes in ASSLBs generally include conventionally utilized graphite and its alternatives, such as silicon (Si), tin (Sn), and germanium (Ge) [100]. Carbon nanofibers have been made by using electrospinning to confine the active materials that are used as the anode of the ASSLBs. One of the most challenging issues of the ASSLB anode lies in the large

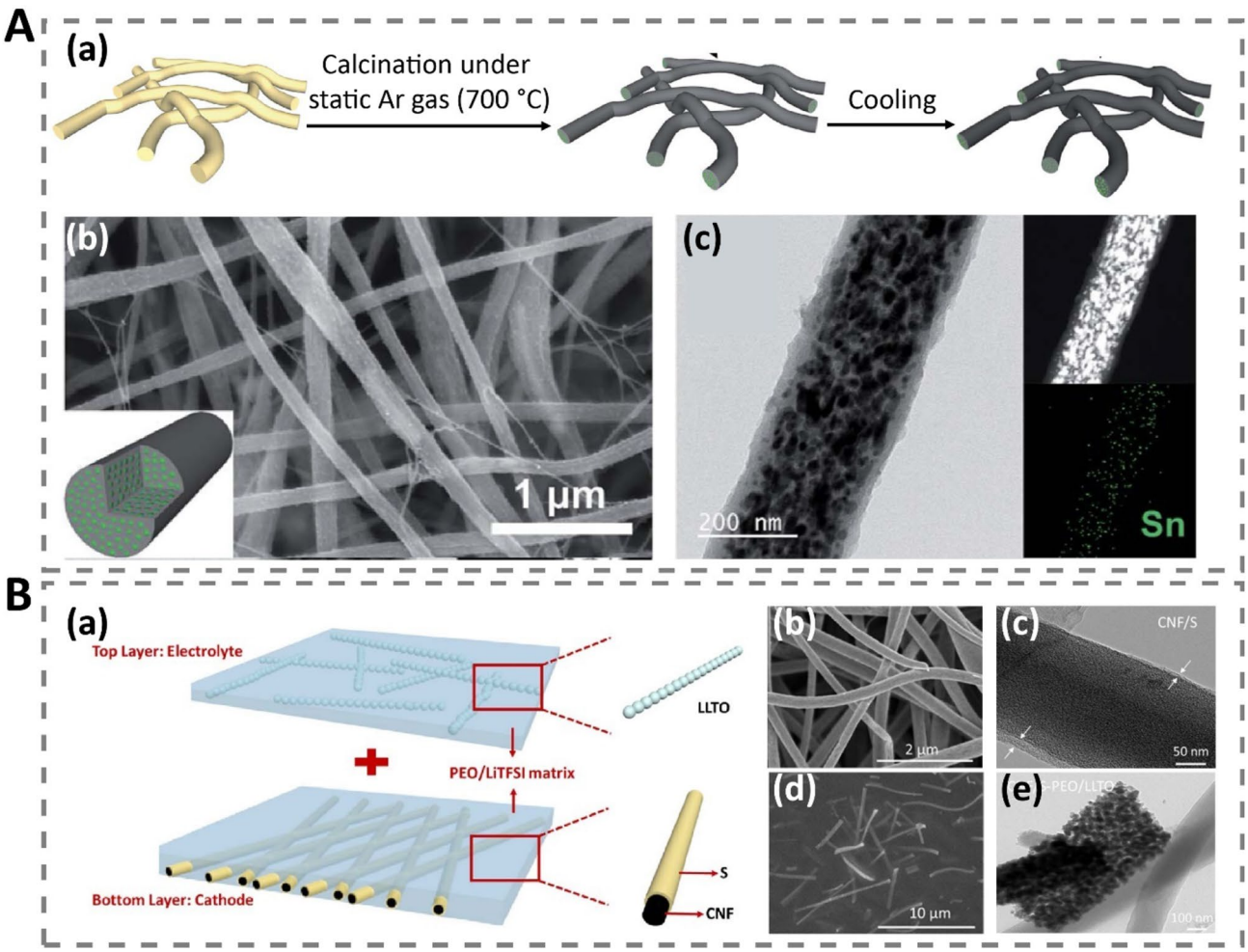

Fig. 10 Applications of electrospinning technology to electrodes of all-solid-state batteries: **A**preparation of an anodeof an all-solid-state Li-ion batterythrough electrospinning (Reprinted with permission from Ref. [100]. Copyright © 2015, Royal Society of Chemistry.) where (a) is the fabrication scheme of Sn/carbon nanofibers, and (b) and (c) are FE-SEM (field emission scanning electron microscopy), HR-TEM (high-resolution transmission electron microscopy) and EDS (energy-dispersive X-ray spectroscopy) elemental mapping of Sn of the Sn/carbon nanofibers, respectively; **B** fabrication of a cathode of an all-solid-state Li-sulfur battery through electrospinning (Reprinted with permission from Ref. [36]. Copyright © 2019, Elsevier Ltd.) where (a) is the schematic of a CNF/S-PEO/LLTO bilayer structure, (b) and (c) are FE-SEM and HR-TEM images of the prepared CNF/S nanofibers, respectively, and (d) and (e) are FE-SEM and HR-TEM images of the PEO/LLTO solid composite electrolyte, respectively.

volumetric expansion, such as 320% for Li–Si alloy during charging [166] and 260% for Li-Sn alloy during Li insertion [100], which can generate anisotropic stresses on pulverized alloy nanoparticles and thus significantly reduce the stability of the resultant ASSLBs. To address the challenge, Nam et al. [100] reported a confining strategy through the electrospinning of alloy-carbon nanofibers in which tin was confined by carbon to prevent pulverization. To fabricate this alloy-carbon fiber, tin acetate and PAN polymers were electrospun into nanofibers and then calcinated to form tin@carbon nanofibers (Fig. 10A-a). Controlling the porosity of the PAN-derived carbon nanofibers was critical to confine the tin in the carbon nanofibers. The carbon matrix also served as the conductive framework to minimize anisotropic stress during charge–discharge processes. As shown in Fig. 10A-b and 10A-c, tin nanoparticles (average diameter 15.18 nm) were evenly distributed inside carbon nanofibers without the exposure of tin, which was achieved by effectively controlling the calcination conditions. The total pore volume of the resultant tin@carbon nanofiber was as low as 0.021 7, enabling excellent cycling performance of the anode after assembly with glass SSEs ($77.5Li_2S$-$22.5P_2S_5$), which had an initial capacity of 762 mAh g^{-1} at 0.05 C and 592 mAh g^{-1} at 0.5 C, and a coulombic efficiency over 99.5% after 50 cycles (60 °C).

Likewise, other nanofiber fabrication technology with plasma-enhanced chemical vapor deposition (PECVD) has been used to make a core–shell, Si-coated, vertically aligned

carbon nanofiber (Si-VACNF) anode [166, 167]. The single Si-coated fiber had an average diameter at approximately 450 nm at the tip and a gradually tapered structure, which reduced the polarization and increased the electrochemical surface area. Although this Si-VACNF anode was employed as the host to infiltrate a flexible gel polymer electrolyte (GPE) composed of poly (vinylidenefluoride-hexafluoropropylene) (PVDF-HFP) and LiTFSI, its functionalization in minimizing the interfacial resistance and accommodating the anisotropic stress could motivate the fabrication of an ASSLB anode for high capacity and cycling performance.

3.2.2 Fabrication of an ASSLB Cathode Through Electrospinning

Regarding the cathode of ASSLBs, electrospinning technology has been applied to all-solid-state Li sulfur batteries and all-solid-state sodium-ion batteries. Therefore, we review current applications of electrospun nanofibers in these two types of all-solid-state batteries in this section. Most all-solid-state Li-sulfur batteries have to be operated at or above 60 °C because of the low electronic and ionic conductivity of the sulfur cathode. A mechanically robust conductive matrix is necessary to buffer the volume change of sulfur during charging and discharging. Carbon nanofibers with micro- and mesopores are ideal matrices for loading sulfur because of their good electrical conductivity and numerous porous structures to confine sulfur expansion during lithiation and avoid pulverization during delithiation. Zhu et al. [36] prepared PAN-based carbon nanofibers (the average diameter 224 nm) through electrospinning and then dropped sulfur/carbon disulfide solution onto them (Fig. 10B-a, -b, and -c), which served as the cathode of an all-solid-state Li-sulfur battery. Electrospinning was also used to prepare LLTO ceramic nanofibers in their study, which were then added to a PEO polymer solution for polymer/ceramic composite electrolytes. The PEO-LLTO mixture was directly dropped onto the sulfur/carbon nanofiber (CNF-S) cathode to assemble a bilayer structure without an additional electrolyte and separator layer for an all-solid-state Li-sulfur battery assembly (Fig. 10B-a, -d and -e). At room temperature, the bilayer framework of CNF-S/PEO-LLTO had a reversible capacity of 384 mAh g^{-1} at 0.05 C and 262 mAh g^{-1} at 0.2 C, and over 99% coulombic efficiency after 50 cycles.

Sodium-ion batteries (SIBs) have also attracted extensive attention for several advantages of sodium, including its natural abundance, low price, and similar chemical properties to Li [168–171]. However, the large radius of Na^+ (1.02 Å) requires cathode materials with a large open framework and robust structure [172, 173]. Nanofibers represent a promising solution to this challenge, although typical solvothermal methods other than electrospinning have been used to prepare cathodes for all-solid-state sodium batteries. With this nanofiber fabrication technology, Gao et al. [174] prepared a $Na_3V_2(PO_4)_3$ (NVP) nanofiber for the cathode of an all-solid-state sodium-ion battery. The cathode was assembled with an electrolyte of PEO/$NaClO_4$/Al_2O_3, and metallic sodium served as the anode. The prepared nanofiber had shortened Na^+ insertion/extraction pathways and improved interfacial contact, and avoided NVP agglomeration, thereby achieving high packing density and high sodium-ion conductivity. The assembled all-solid-state sodium-ion battery using this NVP nanofiber as the cathode had a high reversible capacity of 107 mAh g^{-1} at 0.2 C and 96 mAh g^{-1} at 2 C, and a good cycling stability of 87.5% capacity remained after 1 000 cycles at 2 C.

In summary, even though electrospinning has been used only to prepare the cathode of all-solid-state Li-sulfur batteries, nanofiber-based cathodes represent a promising way to enhance the rate performance of all-solid-state batteries. The good electrochemical performance of the abovementioned all-solid-state Li-sulfur batteries and all-solid-state sodium-ion batteries indicated that electrospinning as a facile technology for nanofiber fabrication could open a new avenue for cathode fabrication. It is also highly expected that the versatility of electrospinning in nanostructure engineering, as discussed in Sect. 2, could guide the structural design of both the cathode and anode of all-solid-state batteries toward high capacity, good cycling stability, and superior mechanical flexibility.

3.3 Relationship Between the Electrospun Nanostructure, Ionic Conductivity, and Electrochemical Performance of ASSLBs

As discussed in Sect. 3.1.3, the current application of electrospun nanofibers for ASSLBs has been focused on the design of aligned structures, especially aligned ceramic nanofibers for composite polymer electrolytes. However, the relationship between the alignment of nanofibers and the electrochemical performance of ASSLBs is still elusive because various factors beyond the alignment of the ionic conductive material could play critical roles in defining ASSLB performance, such as the polymer binder, active materials of the cathode, solid electrolyte thickness, and temperature. Therefore, it is necessary to keep these variants constant to obtain comparable results to determine the relationship between nanofiber alignment and electrochemical performance of ASSLBs. In regard to this consideration, only Liu et al. [35] reported solid evidence that aligned electrospun LLTO nanofibers can significantly enhance the ionic conductivity compared to LLTO nanoparticles and filler-free solid polymer electrolytes (Table 3). In their work [35], aligned LLTO nanofibers were electrospun on interdigital Pt

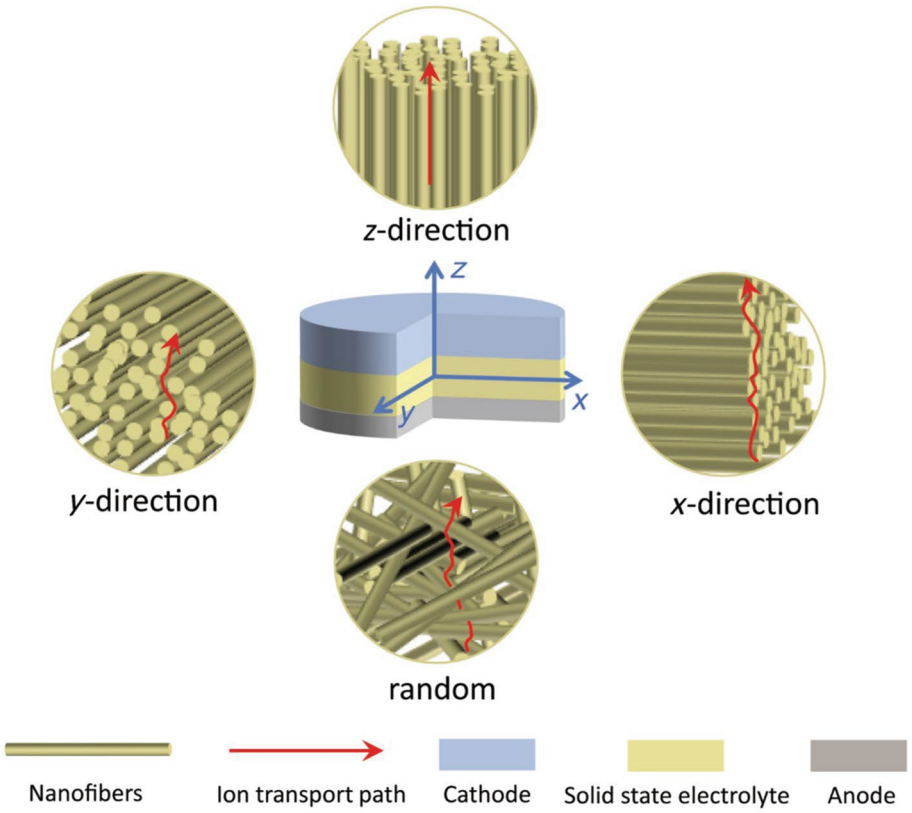

Fig. 11 Schematics of the electrospun nanofiber alignments in the SSEs. The red arrows suggest the possible ion transportation paths in electrospun nanofiber-derived SSEs

electrodes; nevertheless, the electrochemical performances of the assembled ASSLBs were not presented.

More importantly, the angle of the alignment with respect to the ionic transportation path can result in significantly different ionic conductivities. As shown in Table 3, regarding the ionic transport direction from one interdigital Pt electrode to the other, the CPEs (composite polymer electrolytes) derived from the parallelly aligned LLZO nanofibers (0°) had higher ionic conductivity than the CPEs with diagonally aligned LLZO nanofibers (45°) and much higher ionic conductivity than that of the CPEs with vertically aligned LLZO nanofibers (90°). A high ion conductivity (1.16×10^{-4} S cm^{-1}) was also reported for the CPEs with parallelly aligned LLZO nanofibers (Table 4). For the full cell, the direction of the electrospun nanofibers should be extremely important for regulating the ion transport path among electrodes. As displayed in Fig. 11, nanofibers with *Z*-directions could have straighter ion transport paths along the nanofibers, and the ions could be efficiently transferred through the interfaces formed between the ceramic nanofibers and solid electrolyte. As a comparison, the ion transport between the nanofibers with in-plane alignment (*X*- and *Y*-directions) is directed perpendicular to the fiber direction, which could decrease the ionic conductivity. The randomly deposited nanofibers, as discussed above, have cross junctions that could result in lower ionic conductivity than that of the aligned nanofibers.

Nevertheless, ceramic nanofibers with *Z*-direction alignment, as shown in Fig. 11, have not yet been reported by using electrospinning technology. Other technologies, such as anode aluminum oxide (AAO) templating [175], ice templating [176, 177], free drying [178, 179], and porous films [180] have also been used to fabricate *Z*-directed alignments. All these *Z*-aligned solid electrolytes presented a high ionic conductivity at the level of 10^{-4} S cm^{-1}, which is much higher than that of the randomly deposited ceramic nanofibers, as presented in Table 3. For example, AAO has been used as the template to prepare *Z*-aligned PEO polymers [175]. Lithium ions were reported to be transported at the interface of the ceramic (namely, AAO) and PEO, where the *Z*-aligned transport path significantly enhanced the ionic conductivity to 5.82×10^{-4} S cm^{-1} at the electrode level [175]. These data were nearly ten-fold higher than the ionic conductivity of the parallelly aligned LLTO/PAN composite polymer electrolyte (6.05×10^{-5} S cm^{-1}, Table 3). The high ionic conductivity of the CPEs with *Z*-directed alignments can be attributed to the *Z*-direction having the shortest ionic transportation path [181]. These studies could motivate the

electrospinning community to prepare *Z*-aligned ceramic nanofibers for the fabrication of CPEs with much improved ionic conductivity.

With regard to the relationship between the electrochemical performances of the assembled ASSLBs and the alignment of nanofibers, we compared the reported ASSLBs using LLZO nanofibers with and without alignment. As shown in Table 4, the ASSLBs using the CPEs made of parallelly aligned LLZO nanofibers had a higher initial discharge capacity than those using the CPEs made from randomly aligned LLZO nanofibers; however, their cycling performance and coulombic efficiency were even lower. As the CPEs were infiltrated with different polymers and LLZO nanofibers, and the cells were assembled with different cathodes using different active materials, it is difficult to conclude how the alignments of the nanofibers can impact the electrochemical performances of the ASSLBs based on current studies. Nevertheless, it is a matter of fact that higher ionic conductivity generally induces faster ion conduction and lower internal resistance, which can result in enhanced rate performances. That is, *Z*-aligned nanofibers associated with higher ionic conductivity than other parallelly, vertically, or diagonally aligned nanofibers could present better electrochemical performance for the assembled ASSLBs provided the cells were made from the same cathode, anode, and other active materials, and the characterizations were conducted under consistent conditions.

3.4 Mechanical Properties of Electrospun Nanofiber-Based ASSLBs

In comparison with the great efforts that have been devoted to investigating high lithium-ion conductivity, the mechanical performances of SSEs and ASSLBs are less frequently discussed (see Table 5, where many publications lack mechanical strength data), although their importance has been realized by the research community. Mechanical performance is an essential demand for the practical implementation of ASSLBs. On the one hand, mechanical properties must meet the requirements for cell processing, assembly, and operation [182]. On the other hand, the mechanical properties of SSEs play critical roles in suppressing lithium dendrite growth, facilitating the interfacial resistances between the electrode and electrolyte, increasing the interfacial stability, and preventing the propagation of mechanical fractures and cracks during fabrication, manufacturing

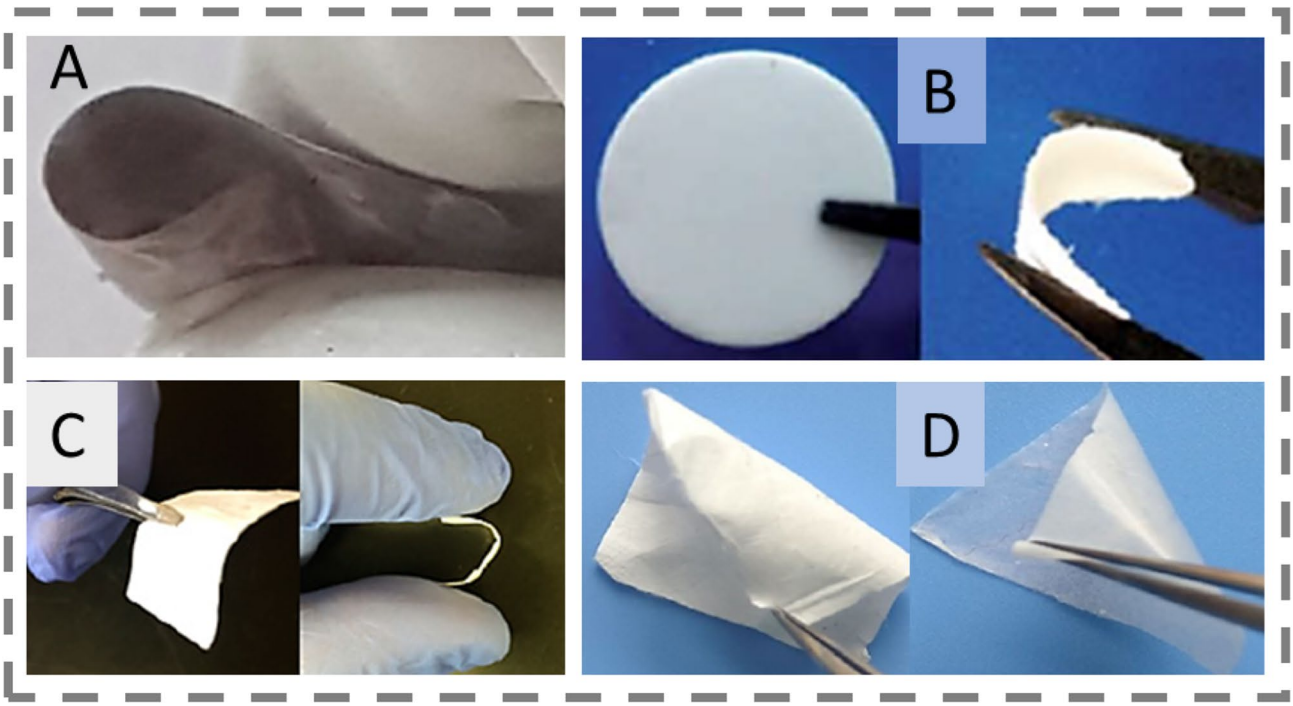

Fig. 12 Representative SSEs derived from electrospinning displayed excellent flexibility and bendability: **A** a representative solid polymer electrolyte made of electrospun PI, $Li_6PS_5Cl_{0.5}Br_{0.5}$ and LiTFSI. Reprinted with permission from Ref. [119]. Copyright © 2020, Elsevier Ltd.; **B** a representative LLTO-based composite ceramic electrolyte made from electrospun LLTO, PAN, SN and LiTFSI. Reprinted with permission from Ref. [184]. Copyright © 2018, American Chemical Society; **C** a representative LLZO-based composite ceramic electrolyte made from electrospun LLZO and infiltrated with PEO. Reprinted with permission from Ref. [128]. Copyright © 2018, Royal Society of Chemistry and **D** a representative LATP-based composite ceramic electrolyte made from electrospun LATP with PAN (left) and PAN/PEO (right) and LiTFSI. Reprinted with permission from Ref. [185]. Copyright © 2020, Springer Nature

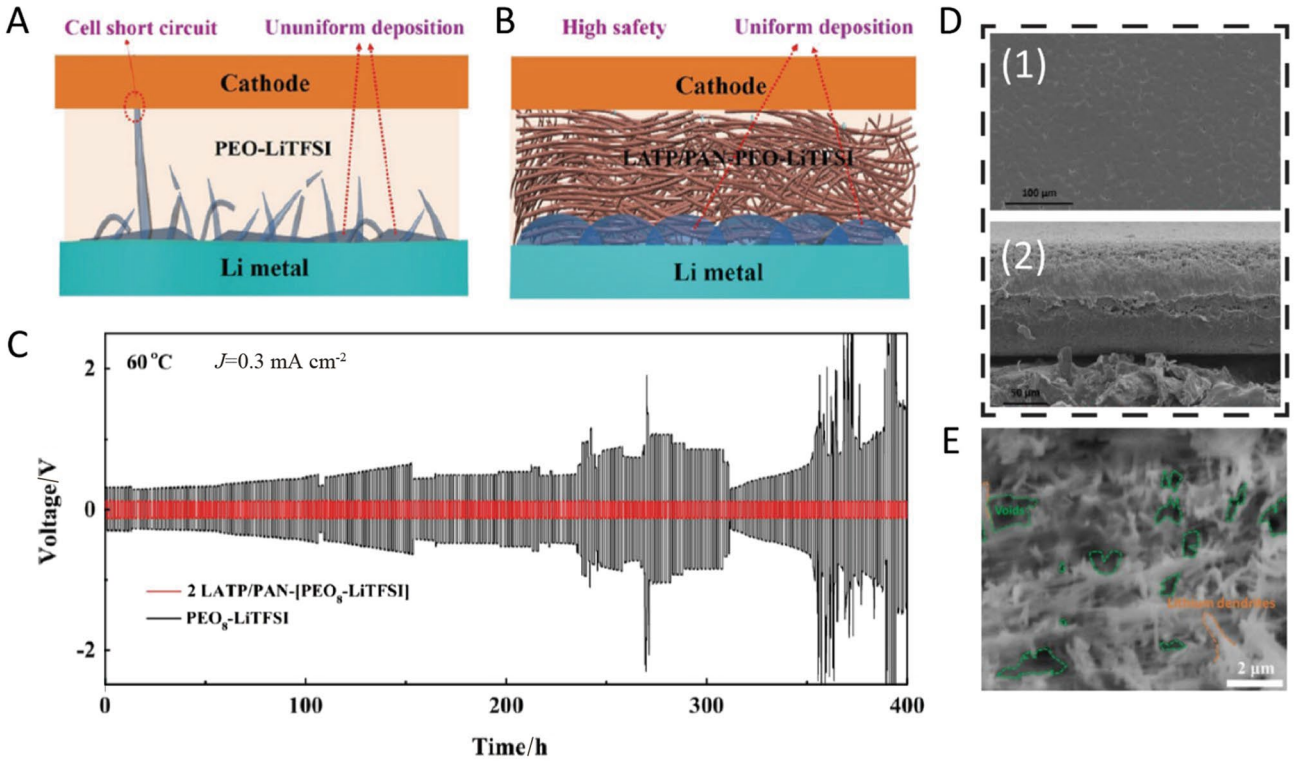

Fig. 13 Lithium dendrites in electrospun ceramic nanofiber-based SSEs and assembled ASSLBs: **A** and **B** lithium plating and/or stripping processes in ASSLBs of Li||PEO-LiTFSI||$LiFePO_4$ and Li||LATP/PAN-PEO-LiTFSI||$LiFePO_4$, respectively. Reprinted with permission from Ref. [185]. Copyright © 2020, Springer Nature. **C** voltage profiles of the LATP/PAN-based ASSLBs at 0.3 mA cm^{-2} current density, 60 °C. Reprinted with permission from Ref. [127]. Copyright © 2016, National Academy of Science. **D** SEM images of the surface (D1) and the cross section (D2) of an SSE of LLZO/PVDF-HFP/LiTFSI; and **E** lithium dendrite growth in an LLATO/PVDF-HFP/LiTFSI SSE when LLATO exceeds a certain content (40 wt%). Reprinted with permission from Ref. [134]. Copyright © 2019, Elsevier

and usage [183]. The demands for ASSLBs with superior mechanical properties have grown significantly with the thriving development of flexible and wearable ASSLBs and electronics. An ideal SSE design for ASSLBs is to concurrently enable high ionic conductivity, low areal resistance, a wide electrochemical stability window, and superior mechanical performance.

The nanomeshes produced by electrospinning generally have good flexibility and bendability. It has been widely revealed that the as-electrospun nanomeshes of both polymers and ceramic-polymer composites are highly flexible, free-standing, bendable, and foldable. The assembled ASSLBs can even remain working after partial cutting (-. 5B). Such flexibility and bendability are normally demonstrated in photographs; for example, representative electrospinning-derived solid polymer electrolytes [119], and LLTO-based [184], LLZO-based [128], and lithium aluminum titanium phosphate (LATP)-based [185] ceramic polymer electrolytes are shown in Fig. 12-A, -B, -C, and -D, respectively. However, quantitative characterizations of flexibility and bendability are still largely lacking.

Tensile performances, including tensile strength, Young's modulus, and elongation, have been presented for some electrospinning-derived solid-state electrolytes and electrodes. As shown in Table 5, SPEs made of electrospun polymer nanomeshes with infiltrated polymers or ceramics normally have tensile strengths less than 15 MPa, but there are large variances in Young's modulus and elongation. These mechanical performances could be largely defined by the applied polymers, in which the tensile strength, Young's modulus, and elongation generally increase with increasing molecular weight, crystallinity, and crosslinking of the polymer [31].

For the ceramic polymer electrolytes, as shown in Table 5, most electrospun ceramics, after infiltration with different kinds of polymers and ion conductive materials, had a tensile strength of approximately 10 MPa but exhibited significant variances in Young's modulus and elongation, similar to those of the CPEs. It is unexpected that Wang et al. [131] reported that a CPE made from electrospun LLTO with the infiltration of PEO and LiTFSI had a remarkably higher Young's modulus (980 MPa) and tensile strength

Table 2 Solvents used for electrospinning ceramic nanofibers, and the derived SSEs and the methods to remove the used solvents

Fiber (Fiber precursor)	Solvent for electrospinning	Solvent removal from the fiber	Fiber-based SSEs	Solvent for SSEs (b.p./°C)	Solvent removal from the SSEs	Reference
LLTO[a] ($LiNO_3$, $La(NO_3)_3{\cdot}6H_2O$, $Ti(OC_4H_9)_4$ with PVP)	DMF/AA[g]	Evaporation during electrospinning + calcination	LLTO/PAN/$LiClO_4$	DMF (153)	80 °C vacuum dry, 48 h + 80 °C heating in glove box, 48 h	[35]
Li_2SO_4-doped SiO_2, (TEOS/Li_2SO_4 with PVA)	dd-H_2O	Evaporation during electrospinning + calcination	Li_2SO_4-SiO_2/PEO/LiTFSI	AN (82)	60 °C air dry	[62]
LLTO[a] ($LiNO_3$, $La(NO_3)_3{\cdot}6H_2O$, $Ti(OC_4H_9)_4$ with PVP)	DMF/AA[g]	Evaporation during electrospinning + calcination	LLTO/PAN/ $LiClO_4$	DMF (153)	High vacuum dry, overnight	[125]
LLTO[b] ($LiNO_3$, $La(CH_3CO_2)_3 \cdot xH_2O$, $Ti(OC_4H_9)_4$ with PVP)	EtOH/AA[h]	Evaporation during electrospinning + calcination	LLTO/PVDF/LiTFSI	NMP (202)	60 °C, 12 h	[126]
LLZO[c] ($LiNO_3$, $La(NO_3)_3{\cdot}6H_2O$, $Zr(OCH_2CH_2CH_3)_4$ with PVP)	DMF/AA[g]	Evaporation during electrospinning + sintering	LLZO/PVDF-HFP/LiTFSI	DMF (153)	70 °C vacuum dry, 12 h	[127]
LLZO[d] ($LiNO_3$, $La(NO_3)_3{\cdot}6H_2O$, $ZrO(NO_3)_2{\cdot}6H_2O$, $Al(NO_3)_3{\cdot}9H_2O$ with PVP)	DMF/AA[i]	Evaporation during electrospinning, vacuum drying for 24 h + calcination	LLZO/PEO-LiTFSI	AN (82)	Air dry, 1 h + vacuum dry, 12 h	[128]
LLTO[a] ($LiNO_3$, $La(NO_3)_3{\cdot}6H_2O$, $Ti(OC_4H_9)_4$ with PVP)	DMF/AA[j]	Evaporation during electrospinning + calcination	LLTO/PEO-LiTFSI	AN (82)	60 °C vacuum dry overnight	[129]
LLTO[a] ($LiNO_3$, $La(NO_3)_3{\cdot}6H_2O$,T $i(OC_4H_9)_4$ with PVP)	DMF/AA/acetylacetone[k]	Evaporation during electrospinning and then sintering & calcination	LLTO/PEO-LiTFSI	AN (82)	RT dry, 4 h + vacuum dry, 12 h	[131]
LLTO[a] ($LiNO_3$, $La(NO_3)_3{\cdot}6H_2O$, $Ti(OC_4H_9)_4$ with PVP)	DMF/AA[g]	Evaporation during electrospinning + calcination	LLTO/PEO-LiTFSI	AN (82)	Air dry, 6 h + 65 °C vacuum dry, 24 h	[132]
s@LLAZO[e] ($LiNO_3$, $La(NO_3)_3{\cdot}6H_2O$, $Zr(OCH_2CH_2CH_2CH_3)_4$, $Al(NO_3)_3{\cdot}9H_2O$ with PVP)	DMF/AA[i] for LLAZO preparation, AA/H_2O/EtOH for s@LLAZO preparation	Evaporation during electrospinning + calcination, ethanol washing of s@LLAZO	s@LLAZO/PEGDA/LiTFSI	NMP (202)	80 °C vacuum dry, overnight	[133]
LLATO[g] ($LiNO_3$, $La(NO_3)_3{\cdot}6H_2O$, $Ti(OC_4H_9)_4$, $Al(NO_3)_3{\cdot}9H_2O$ with PVP)	dd-H_2O & isopropanol/AA to dissolve precursors, DMF/AA[i] to dissolve PVP	Evaporation during electrospinning + calcination	LLATO/OVDF-HFP/LiTFSI	Acetone (56)	Air dry + vacuum dry	[134]
LLZO[d] ($LiNO_3$, $La(NO_3)_3{\cdot}6H_2O$, $ZrO(NO_3)_2{\cdot}6H_2O$, $Al(NO_3)_3{\cdot}9H_2O$, $C_8H_{12}O_8Zr$ with PVP)	dd-H_2O/EtOH[l]	Evaporation during electrospinning + 60 °C vacuum dry for 2 h + calcination	LLZO/PVDF/$LiClO_4$	NMP (202)	Natural dry in glove box + 80 °C vacuum dry, 2 h	[135]

TEOS tetraethyl orthosilicate; AA acetic acid; DMF *N,N*-dimethylformamide; AN acetonitrile; NMP *N*-methyl-2-pyrrolidone; PEGDA, poly(ethylene glycol) diacrylate; RT room temperature

[a]$Li_{0.33}La_{0.557}TiO_3$; [b]$Li_{0.35}La_{0.55}TiO_3$; [c]$Li_7La_3Zr_2O_{12}$; [d]$Li_{6.4}La_3Zr_2Al_{0.2}O_{12}$; [e]silane-modified $Li_{6.28}La_3Al_{0.24}Zr_2O_{12}$; [f]$Li_{0.33}La_{0.557}Ti_{1-x}Al_xO_3$; [g]DMF and 20 vol.% acetic acid cosolvent; [h]DMF/acetic acid cosolvent with unknown mixing ratio; [i]DMF and 15 vol.% acetic acid cosolvent; [j]DMF and acetic acid cosolvent (8:2, in volume ratio); [k]DMF, acetic acid and acetylacetone acid cosolvent (5:2:2, in volume ratio); [l]dd H_2O and ethanol cosolvent (1:1, in weight ratio)

Table 3 Structural design of LLTO nanofibers by electrospinning and its impacts on the ionic conductivity of composite solid electrolytes [35]

LLTO pattern	Composite polymer electrolyte	Ion conductivity/(S cm^{-1}), 30 °C
Filler-free electrolyte	PAN/$LiClO_4$	3.62×10^{-7}
Nanoparticle filling	LLTO/PAN/$LiClO_4$	1.02×10^{-6}
Electrospun nanofiber without alignment		5.40×10^{-6}
Electrospun nanofiber with parallel alignment (0°)		6.05×10^{-5}
Electrospun nanofiber with vertical alignment (90°)		1.78×10^{-7}
Electrospun nanofiber with diagonal alignment (45°)		2.44×10^{-5}

Table 4 Structural design of LLZO nanofibers by electrospinning and its impacts on the electrochemical performance of the assembled ASSLBs

Solid Li-ion electrolyte	Composite polymer electrolyte	Cell	Ion conductivity/(S cm^{-1})	ASSLBs performances					
				Capacity/(mAh g^{-1})	Voltage/V	Cycling performance (capacity retention)	Energy density	Coulombic efficiency	Reference
Electrospun LLZO nanofiber without alignment	LLZO/PEO/LiTFSI	Li‖ CPE‖Li	2.5×10^{-4}, room temperature	N.D	N.D	N.D	N.D	N.D	[128]
	s@LLAZO/PEGDA/LiTFSI	$LiFePO_4$ or NMC‖CPE‖Li	4.9×10^{-4}, room temperature	158 at 0.2 C, 44 at 10 C, 25 °C	N.D	95%, 100 cycles	N.D	99.4%	[133]
	LLZO/PVDF-HFP/LiTFSI (+10% LE)	Li‖ CPE‖Li	9.5×10^{-4}, room temperature	140 at 0.2 C, 81 at 2 C, 25 °C	N.D	93%, 150 cycles	N.D	99.9%	[127]
	LLZO/PAN/$LiClO_4$	Li‖ CPE‖Li	1.31×10^{-4}, 20 °C	N.D	N.D	N.D	N.D	N.D	[129]
Electrospun LLZO nanofiber with alignment	LLZO/PVDF/LiTFSI	NCA ‖CPE ‖Li	1.16×10^{-4}, 30 °C	213 at 0.2 C, 25 °C	4.6	~82%, 20 cycles	N.D	>95%	[135]

NCA, $LiNi_{0.8}Co_{0.15}Al_{0.05}O_2$; NMC, $Li[Ni_{1/3}Mn_{1/3}Co_{1/3}]O_2$; s@LLAZO, silane-modified $Li_{6.28}La_3Al_{0.24}Zr_2O_{12}$

(16.18 MPa) than all other reported SSEs, as summarized in Table 5. In their study, hot pressing at 75 °C under a pressure of 2 N cm^{-2} was applied to the as-prepared SPE, which might be responsible for the extremely strong mechanical performance.

Different from the SSEs, the electrode made from electrospinning had a much lower mechanical performance (Table 5) [36]. The reason has been attributed to weak carbon fibers made from electrospun PAN [36]; however, the performance of the fibers could be modified by optimizing the carbonization conditions, including temperature, ramp rate, vacuum, and inert gas.

For future directions to improve the mechanical performance of SSEs and electrodes, process optimization and ceramic-polymer interlinking could be given more attention. First, as mentioned above, pressure can be applied to SPEs to make denser membranes, which could increase the interactions and thus, the mechanical performance. Likewise, the carbonization process should be carefully controlled to produce high-quality carbon nanofibers. Second, ceramics can enhance the mechanical performance of fabricated SSEs. The most commonly used ceramics have excellent mechanical properties; for example, the Young's moduli of LLTOs, LLZOs, and LATPs are as high as 200, 150, and 115 GPa, respectively [182]. Meanwhile, the fracture toughness of LLTO, LLZO, and LATP is approximately 1 MPa m^{-2} [182]. In fact, ceramics have been reported to increase the mechanical performance of SSEs [36]. However, most composite polymer electrolytes still exhibited weak mechanical performance (Table 5), which might be induced by the limited

Table 5 Mechanical performances of SSEs and electrodes of ASSLBs fabricated by using electrospinning technology

Application of electrospinning in ASSLBs	Nanofiber precursor	Nanofiber structure		SSE		Mechanical properties			Reference
		Pattern	Diameter/nm	Composition	Thickness/μm	T.S./MPa	MOE/MPa	Elongation/%	
Solid polymer electrolyte	PI, PEI	Random	500	PI, PEI/LPSClBr/LiTFSI	40–70	N.D	N.D	N.D	[119]
	PI	Random	N.D	PI/LLZTO-PVDF/LiFSI	20	11.50	N.D	24.40	[120]
	PVDF	Random	500	PVDF/C3mpy-rFSI/LiTFSI	100	3.60	11.2	200*	[121]
	PI-*g*-PEO	Random	150	PI-*g*-PEO/PEO/LiTFSI	20	3.30	93.0	7.30	[123]
	LATP-PAN	Random	400	LATP-PAN/PEO/LiTFSI	N.D	10.72	N.D	43.00*	[185]
Ceramic polymer electrolyte	LLTO	Random	138	LLTO/PAN/$LiClO_4$	N.D	N.D	N.D	N.D	[125]
	LLTO	Aligned	645	LLTO/PAN/$LiClO_4$	N.D	N.D	N.D	N.D	[35]
	LLTO	Random	N.D	LLTO/PEO/$LiClO_4$	50–80	5.30*	8.50	60.00	[187]
	LLTO	Random	281–383	LLTO/PEO/LiTFSI + hot pressing	70–100	16.18	980.0	200.00	[131]
	LLTO	Random	276	LLTO/PAN/$LiClO_4$	N.D	N.D	N.D	N.D	[129]
	LLTO	Random	260	LLTO/PEO/$LiClO_4$	N.D	N.D	N.D	N.D	[188]
	LLTO	Random	740	LLTO/PVDF/LiTFSI	N.D	9.50	N.D	341.00	[126]
	LLTO, PAN	Random	500	LLTO@PAN/SN/LiTFSI	55	3.10	N.D	41.00	[184]
	LLATO	Random	155	LLATO/PVDF-HFP/LiTFSI	80	N.D	N.D	N.D	[134]
	LLZO	Random	100	LLZO/PVDF-HFP/LiTFSI (+ 10% LE)	100	5.30	N.D	47.00	[127]
	LLZO	Random	138	LLZO/PEO/LiTFSI	40–50	N.D	N.D	N.D	[128]
	LLAZO	Random	N.D	s@LLAZO/PEGDA/LiTFSI	50–80	4.20	29.5	19.10	[133]
	Al_2O_3[#]	Random	200	Al_2O_3/PEO-PPO-PEO/SiO_2/LiTFSI	50	N.D	N.D	N.D	[189]
	Al_2O_3[#]	Random	300	Al_2O_3/HPEI-PGC-PCL/LiTFSI	N.D	N.D	N.D	N.D	[190]
	Li_2SO_4/SiO_2	Random & porous	80	Li_2SO_4-SiO_2/PEO/LiTFSI	200*	4.20**	N.D	170.00*	[62]
	YSZ	Random	55	YSZ/PAN/$LiClO_4$	N.D	N.D	N.D	N.D	[191]
Anode	Sn@PAN	Confined	200–300**	77.5Li_2S-22.5P_2S_5 glass SSE	N.D	N.D	N.D	N.D	[100]
Cathode	PAN	Random	237[##]	PEO/LLTO	15	0.12	2.0	8.45	[36]

HPEI-PGC-PCL, hyperbranched polyethylenimine-polyglycolide-poly-ε-caprolactone; PEO-PPO-PEO polyethylene oxide-polypropylene oxide-polyethylene oxide; YSZ Y_2O_3-doped ZrO_2; ND no data

*Estimated from the reported stress–strain curve; **estimated from SEM; [#]melt electrospinning; [##]the diameter refers to sulfur-incorporated carbon nanofibers derived from PAN electrospun nanofibers; T.S., tensile strength; MOE, modulus of elasticity; LATP, lithium aluminum titanium phosphate; LiFSI, lithium bis(fluorosulfonyl)imide; LLATO, $Li_{0.33}La_{0.557}Ti_{1-x}Al_xO_3$; LPSClBr, $Li_6PS_5Cl_{0.5}Br_{0.5}$

Table 6 Comparison of the advantages, challenges, and performances of different types of electrospun nanofiber-based SSEs

Electrospun nanofiber-based SSEs	Advantages	Challenges	Performances
Conventional casted SSEs	Facial preparation, good uniformity of SSEs film	Low IC, high thickness, poor processability of some polymers	IC 10^{-7}–10^{-5} S cm^{-1}
Solid polymer nanofibers-based SSEs	Amenable for most polymers, thin SSEs, robust mechanical flexibility, strength, and bendability	Low IC of polymer, uniformity of SSEs	IC 10^{-5}–10^{-4} S cm^{-1}
Solid ceramic nanofibers-based SSEs	Enhanced interfacial transport and thus IC, enhanced mechanical strength, effective dendrite suppression	Mechanical rigidity, aggregation of ceramic nanofibers in SSEs, high cost of ceramics and their processing	IC≈10^{-4} S cm^{-1}
Solid aligned/porous ceramic/inorganic nanofibers-based SSEs	Designed ion transport pathway and porous structure, high IC	Elaborate control of electrospinning condition and structure formation, high cost of ceramics and their processing	IC≈10^{-4} S cm^{-1} (up to tenfold increase as to SSEs without alignment)

compatibility between ceramics and the polymer. Such weak compatibility could limit the interconnected bonding, hinder dislocation mobility, and lead to brittle and weak behavior. Rational design can regulate polymer structures, enhance ceramic-polymer interfacial bonding, and improve the bulk mechanical properties of solid-state electrolytes [31, 186].

3.5 Lithium Dendrites in Electrospun Ceramic Nanofiber-Based ASSLBs

Lithium dendrites originate from uneven deposition and dissolution of lithium metal; they can cause internal short circuits, which are a serious safety concern [182, 185], and thus represent a major challenging issue for ASSLBs. In our previous review, we systematically revisited the growth mechanism and suppression strategies addressing lithium dendrites in ASSLBs [192]. For ceramic-based SSEs, a mechanistic understanding of lithium dendrites refers to: (1) nonuniform interfacial contact (such as porous structure, void defects, and surface microstructure) that initiate dendrite growth; (2) grain boundary-induced lithium dendrite propagation; (3) lithium plating inside SSEs; and (4) interphase-triggered lithium dendrite growth [192]. Nevertheless, for a long time, SSEs with a high shear modulus have been sought as an effective solution to suppress lithium dendrites [192]. As discussed in Sect. 3.4, most ceramics have excellent mechanical performance, which enables the high mechanical strength of the derived SSEs to meet the needs of ASSLBs (Table 5).

Several publications have reported that dendrite-free ASSLBs were fabricated by using ceramic-based SSEs prepared by electrospinning [127, 184, 185, 187, 193]. In addition to the high mechanical performance discussed above, the underlying mechanism of dendrite suppression was attributed to the structure of the prepared SSEs. As shown in Fig. 13A, an ASSLB of Li||LATP/PAN-PEO-LiTFSI||$LiFePO_4$ was assembled by using LATP/PAN electrospun nanofiber-based SSEs. Compared with the ASSLB of Li||PEO-LiTFSI||$LiFePO_4$ using the polymer SSE without electrospun LATP/PAN nanofibers (Fig. 13B), LATP/PAN nanofibers formed a layer that improved the interfacial property between LATP/PAN-PEO-LiTFSI and the lithium anode, which promoted the uniform deposition of lithium (Fig. 13A). In contrast, Li||PEO-LiTFSI||$LiFePO_4$ had nonuniform lithium deposition (Fig. 13B). Electrochemical testing showed that Li||LATP/PAN-PEO-LiTFSI||$LiFePO_4$ had stable lithium plating/stripping behavior with a relatively steady voltage at 120 mV and no short circuit for 400-h charging-discharging cycles, but Li||PEO-LiTFSI||$LiFePO_4$ had a fluctuating voltage and large voltage polarization during charge–discharge cycling (Fig. 13C). It was concluded that together with the much smaller change in impedance for the 400-h cycling time, the electrospun nanofiber layer in Li||LATP/PAN-PEO-LiTFSI||$LiFePO_4$ significantly improved the interfacial compatibility between SSEs and the lithium anode, which prevented lithium dendrite growth [185]. Furthermore, an LLZO nanofiber-based LLZO/PVDF-HFP/LiTFSI SSE was reported to have a smooth surface without cracks or interparticle spaces for dendrite penetration (Fig. 13D1), and it also had multiple LLZO nanofiber stacking layers (Fig. 13D2) that blocked lithium dendrite growth and thus prevented ASSLB short circuits [127].

To prevent the formation of cracks and spaces for lithium dendrite penetration, the pores and voids formed between electrospun nanofibers should be carefully eliminated by infiltrating polymers. In this process, the ratio of ceramic nanofibers to polymers is important for lithium dendrite suppression. Yang et al. [134] infiltrated a porous film composed of LLATO nanofibers by PVDF-HFP/LiTFSI to prepare an SSE. When the content of the LLATO nanofiber exceeded 40 wt%, it was difficult to infiltrate the void spaces in the LLATO nanofiber film with the PVDF-HFP polymer. The remaining spaces formed cracks after assembling the ASSLBs, which induced penetration of the lithium dendrites (Fig. 13E). The content

of the added ceramic nanofibers (LLAZO) can be further increased to 70 wt% by the modification of the ceramic nanofiber surface, which resulted in the improved percolation of the polymer matrix (PEGDA) in the ceramic nanofiber film [133].

In summary, the high mechanical strength and layered structure of electrospun ceramic nanofibers in SSEs improved the interfacial stability between the solid electrolyte and lithium anode and blocked lithium dendrite growth. Meanwhile, the pores and voids formed between the electrospun ceramic nanofibers should be carefully eliminated by infiltrating with polymers to prevent lithium dendrite penetration. However, other effects, such as those of grain boundaries, interphases, and lithium plating, on lithium dendrite formation and growth in electrospun ceramic nanofiber-based ASSLBs, are still elusive based on the available literature and await further study.

4 Summary and Perspective

ASSLBs have attracted widespread attention due to their numerous advantages, such as high degree of safety, electrochemical stability, and good cycling performance. ASSLBs with a high degree of flexibility have extensive applications as flexible and wearable electronics, where safety, mechanical bendability, foldability, and stretchability are essential characteristics. Electrospinning is a versatile technology that can prepare nanofibers in the form of single fibers, randomly deposited nanomeshes, and well-aligned nanowires or nanomeshes, all of which can be endowed with well-controlled orientation, high surface area, and superior mechanical flexibility. These merits are often augmented by the ease of design and synthesis of nanostructures in electrospun nanofibers, including interfibrous pores, hierarchical meso and microporous structures, and various nanoengineered hollow fiber, fiber-in-tube, nanoparticle-in-tube, tube-in-tube, multichannel microtube, and lamellar nanostructures and fused physical interactions. Nevertheless, the current application of electrospinning in ASSLBs is still in the early stage. Electrospun nanofibers have been used to prepare SSEs, including mainly: (1) electrospinning polymers into nanofibers to serve as electrolyte matrices; (2) electrospinning ion-conductive ceramics into nanofibers (generally enabled in polymer blends) to infiltrate or mix with polymer electrolytes; and (3) electrospinning aligned and/or porous ceramic or inorganic nanofibers to infiltrate or mix with polymer electrolytes. The advantages, challenges, and performance of these types of SSEs are summarized in Table 6. Compared to conventional SSEs made by polymer casting, electrospinning is amenable for most polymers. In addition, electrospun nanofiber-based SSEs have relatively reduced thickness and enhanced ionic conductivity and mechanical strength, although they generally involve more fabrication steps and less uniform SSEs. When the three types of electrospun nanofiber-based SSEs are compared, as shown in Table 6, solid polymer nanofiber-based SSEs are easily prepared and have robust mechanical flexibility, strength and bendability but lower ionic conductivity limited by the polymer. Ceramic nanofiber-based SSEs have much enhanced ionic conductivity and further enhanced mechanical strength, but their fabrication needs more elaborate control, especially the electrospinning of aligned and/or porous nanofibers. However, the high cost of the raw materials of ceramics and the associated high cost in using high-temperature sintering processes are major challenges for current ceramic-based SSEs [194]. Moreover, ceramic nanofibers should be well dispersed to avoid aggregation in composite SSEs. For the highest ionic conductivity, ceramic nanofiber-based SSEs with well-aligned structures and cost-effectiveness represent state-of-the-art for future SSEs.

Nanofiber structural design, as discussed in this review, can certainly enhance structure and charge transfer in energy storage; however, a very limited number of publications report synergies between nanofiber structural design and ASSLB fabrication. Such synergy of nanofiber engineering and ASSLB manufacturing for robust mechanical flexibility and electrochemical performance will transform future Li-battery design according to the following perspectives.

First, pore generation and porous structure control have been widely used to increase the surface area and enhance electrolyte accessibility in conventional electrodes for energy storage in liquid electrolytes, such as aqueous supercapacitors. Meanwhile, the porous structure has great potential to enable better flexibility of devices (Eq. 1). However, pores might impact Li-ion conduction differently in solid electrolytes. The pores formed among nanofibers are generally between hundreds of nanometers and several microns in size, and they can be functionalized for hosting polymer electrolytes or accommodating ceramics, thus enabling considerable Li-ion conduction. Most likely, the macropores (> 50 nm) formed on nanofiber surfaces or in nanofibers generated by numerous technologies (Sect. 2.3) can perform the same functions; however, it might be difficult for polymer electrolytes or ceramics to enter fine pores, such as some mesopores (2–50 nm) and micropores (< 2 nm), and the resulting vacancies could play negative roles in Li-ion conduction. Further elucidation and direct evidence of such effects of different pore types on Li-ion conduction in the solid-state are urgently needed.

Second, the transportation pathways of Li ions could be designed with versatile electrospinning. Currently, aligned ceramic nanofibers made from electrospinning are deposited in planes that are perpendicular to the Li ion transportation direction. *Z*-aligned transportation pathways that are parallel to Li-ion transport directions could largely enhance the ionic conductivity of the ASSLBs. With specially designed

collector structures, *Z*-aligned nanofibers might be produced through electrospinning. Other complex nanostructures, such as electrospinning variant tubular structures, could open new avenues for structural engineering of SSEs and might shed new light on regulating the interfaces of polymer-Li salts and overcoming the mechanical limit of ceramic-derived SSEs.

Third, the molecular structures of ion-conductive polymers are of essential importance for Li-ion conduction. Chemical modifications of polymer structures are indubitably an effective way to augment SSE ion conductivity and transference number as well as the mechanical flexibility of ASSLBs. Because electrospinning technology is highly feasible for most polymers, it is adaptable for polymer structure modification and processing, which thus could provide a universal platform for manufacturing safe and flexible ASSLBs with superior electrochemical stability and good cycling performance.

Finally, controlling the uniformity of the nanomesh thickness and surface roughness during electrospinning represents a challenging issue to be overcome for applications in ASSLBs. In general, an as-spun nanomesh is thicker at the center and thinner at the periphery. This nonuniform distribution of the electrospun nanofibers is induced by the inherent difference in the electrical potential between the jet and the deposition area because the electrical potential tapers off from the center to the periphery of the deposition area. The nonuniformity of a nanomesh can render poor contact at the SSE||electrode interface, increasing the interface impedance and thus deteriorating the electrochemical performance of the ASSLB [195]. Further development in the practical application of electrospinning in ASSLBs may encounter even more pronounced challenges related to uniformity when multiple spinnerets are used in electrospinning. Instrumental design, such as movable spinnerets or collectors, could help improve the uniform deposition of electrospun nanofibers. Other technologies focusing on reducing the impacts of the potential field gradient on the deposition of the electrospinning jets might provide other pathways for addressing the challenge. In the meantime, thin, robust and cost-effective SSEs represent a promising direction for future ASSLBs [186, 194, 196]. ASSLBs can benefit from thin SSEs with the advantages of high energy density, high power density, less utilization of inactive materials, and relatively low cost [186, 196]. Electrospinning is efficient for fabricating very thin films, which might easily reach the ideal SSE thickness, which is < 20 μm [189]. Electrospinning is thus expected to offer a highly desirable solution for thin and high energy density ASSLBs.

Overall, ASSLBs have emerged as the next generation energy storage devices for many flexible and wearable electronics and functional materials. Future technological advances will lead to the development of novel SSEs with superior mechanical properties and high ionic conductivity, electrodes with high capacity, and assembled ASSLBs with good cycling stability. Versatile electrospinning will undoubtedly play a significant role in nanoengineering both SSEs and electrodes with designed nanostructures to realize implementable ASSLBs.

Acknowledgements Financial supports to Hongli Zhu from the National Science Foundation Electrochemical Systems Program at the Division of Chemical, Bioengineering, Environmental, and Transport Systems (CBET-1924534) and Rogers Corporation, United States are acknowledged.

Declaration

Conflict of interest All authors declare no conflicts of interest.

Ethics approval Not applicable.

References

1. Wang, S.J., Xiong, P., Zhang, J.Q., et al.: Recent progress on flexible lithium metal batteries: composite lithium metal anodes and solid-state electrolytes. Energy Storage Mater. **29**, 310–331 (2020). https://doi.org/10.1016/j.ensm.2020.04.032
2. Fan, L., Wei, S.Y., Li, S.Y., et al.: Recent progress of the solid-state electrolytes for high-energy metal-based batteries. Adv. Energy Mater. **8**, 1702657 (2018). https://doi.org/10.1002/aenm.201702657
3. Zhu, J., Chen, L.B., Xu, Z., et al.: Electrospinning preparation of ultra-long aligned nanofibers thin films for high performance fully flexible lithium-ion batteries. Nano Energy **12**, 339–346 (2015). https://doi.org/10.1016/j.nanoen.2014.10.026
4. Sun, B., Long, Y.Z., Chen, Z.J., et al.: Recent advances in flexible and stretchable electronic devices via electrospinning. J. Mater. Chem. C **2**, 1209–1219 (2014). https://doi.org/10.1039/c3tc31680g
5. Qian, G.Y., Liao, X.B., Zhu, Y.X., et al.: Designing flexible lithium-ion batteries by structural engineering. ACS Energy Lett. **4**, 690–701 (2019). https://doi.org/10.1021/acsenergylett.8b02496
6. Yetisen, A.K., Qu, H., Manbachi, A., et al.: Nanotechnology in textiles. ACS Nano **10**, 3042–3068 (2016). https://doi.org/10.1021/acsnano.5b08176
7. Chinnappan, A., Baskar, C., Baskar, S., et al.: An overview of electrospun nanofibers and their application in energy storage, sensors and wearable/flexible electronics. J. Mater. Chem. C **5**, 12657–12673 (2017). https://doi.org/10.1039/c7tc03058d
8. Kenry, Lim, C.T.: Nanofiber technology: current status and emerging developments. Prog. Polym. Sci. **70**, 1–17 (2017). https://doi.org/10.1016/j.progpolymsci.2017.03.002
9. Yang, G., Li, X.L., He, Y., et al.: From nano to micro to macro: electrospun hierarchically structured polymeric fibers for biomedical applications. Prog. Polym. Sci. **81**, 80–113 (2018). https://doi.org/10.1016/j.progpolymsci.2017.12.003
10. Wang, X.F., Ding, B., Sun, G., et al.: Electro-spinning/netting: a strategy for the fabrication of three-dimensional polymer nano-fiber/nets. Prog. Mater. Sci. **58**, 1173–1243 (2013). https://doi.org/10.1016/j.pmatsci.2013.05.001
11. Zhang, Z.M., Duan, Y.S., Xu, Q., et al.: A review on nanofiber fabrication with the effect of high-speed centrifugal force field. J. Eng. Fibers Fabr. **14**, 155892501986751 (2019). https://doi.org/10.1177/1558925019867517
12. Thenmozhi, S., Dharmaraj, N., Kadirvelu, K., et al.: Electrospun nanofibers: new generation materials for advanced applications.

Mater. Sci. Eng. B **217**, 36–48 (2017). https://doi.org/10.1016/j.mseb.2017.01.001
13. Xing, X.B., Yu, H.Q., Zhu, D.B., et al.: Subwavelength and nanometer diameter optical polymer fibers as building blocks for miniaturized photonics integration. In: Xing, X.B.(ed.): Optical Communication, pp.289–320. InTechOpen (2012) https://doi.org/10.5772/47822
14. Huang, Z.M., Zhang, Y.Z., Kotaki, M., et al.: A review on polymer nanofibers by electrospinning and their applications in nanocomposites. Compos. Sci. Technol. **63**, 2223–2253 (2003). https://doi.org/10.1016/S0266-3538(03)00178-7
15. Teo, W.E., Ramakrishna, S.: A review on electrospinning design and nanofibre assemblies. Nanotechnology **17**, R89–R106 (2006). https://doi.org/10.1088/0957-4484/17/14/R01
16. Lallave, M., Bedia, J., Ruiz-Rosas, R., et al.: Filled and hollow carbon nanofibers by coaxial electrospinning of Alcell lignin without binder polymers. Adv. Mater. **19**, 4292–4296 (2007). https://doi.org/10.1002/adma.200700963
17. Bhardwaj, N., Kundu, S.C.: Electrospinning: a fascinating fiber fabrication technique. Biotechnol. Adv. **28**, 325–347 (2010). https://doi.org/10.1016/j.biotechadv.2010.01.004
18. Persano, L., Camposeo, A., Tekmen, C., et al.: Industrial upscaling of electrospinning and applications of polymer nanofibers: a review. Macromol. Mater. Eng. **298**, 504–520 (2013). https://doi.org/10.1002/mame.201200290
19. Peng, S.J., Li, L.L., Kong Yoong Lee, J., et al.: Electrospun carbon nanofibers and their hybrid composites as advanced materials for energy conversion and storage. Nano Energy **22**, 361–395 (2016). https://doi.org/10.1016/j.nanoen.2016.02.001
20. Li, X.Y., Chen, Y.M., Huang, H.T., et al.: Electrospun carbon-based nanostructured electrodes for advanced energy storage: a review. Energy Storage Mater. **5**, 58–92 (2016). https://doi.org/10.1016/j.ensm.2016.06.002
21. Inagaki, M., Yang, Y., Kang, F.Y.: Carbon nanofibers prepared via electrospinning. Adv. Mater. **24**, 2547–2566 (2012). https://doi.org/10.1002/adma.201104940
22. Zhang, B., Kang, F.Y., Tarascon, J.M., et al.: Recent advances in electrospun carbon nanofibers and their application in electrochemical energy storage. Prog. Mater. Sci. **76**, 319–380 (2016). https://doi.org/10.1016/j.pmatsci.2015.08.002
23. Kim, C., Yang, K., Kojima, M., et al.: Fabrication of electrospinning-derived carbon nanofiber webs for the anode material of lithium-ion secondary batteries. Adv. Funct. Mater. **16**, 2393–2397 (2006). https://doi.org/10.1002/adfm.200500911
24. Li, W.H., Li, M.S., Adair, K.R., et al.: Carbon nanofiber-based nanostructures for lithium-ion and sodium-ion batteries. J. Mater. Chem. A **5**, 13882–13906 (2017). https://doi.org/10.1039/c7ta02153d
25. Dong, Z.X., Kennedy, S.J., Wu, Y.Q.: Electrospinning materials for energy-related applications and devices. J. Power Sources **196**, 4886–4904 (2011). https://doi.org/10.1016/j.jpowsour.2011.01.090
26. Cavaliere, S., Subianto, S., Savych, I., et al.: Electrospinning: designed architectures for energy conversion and storage devices. Energy Environ. Sci. **4**, 4761 (2011). https://doi.org/10.1039/c1ee02201f
27. Lu, X.F., Wang, C., Favier, F., et al.: Electrospun nanomaterials for supercapacitor electrodes: designed architectures and electrochemical performance. Adv. Energy Mater. **7**, 1601301 (2017). https://doi.org/10.1002/aenm.201601301
28. Jung, J.W., Lee, C.L., Yu, S., et al.: Electrospun nanofibers as a platform for advanced secondary batteries: a comprehensive review. J. Mater. Chem. A **4**, 703–750 (2016). https://doi.org/10.1039/c5ta06844d
29. Lv, F., Wang, Z.Y., Shi, L.Y., et al.: Challenges and development of composite solid-state electrolytes for high-performance lithium ion batteries. J. Power Sources **441**, 227175 (2019). https://doi.org/10.1016/j.jpowsour.2019.227175
30. Xia, S.X., Wu, X.S., Zhang, Z.C., et al.: Practical challenges and future perspectives of all-solid-state lithium-metal batteries. Chem **5**, 753–785 (2019). https://doi.org/10.1016/j.chempr.2018.11.013
31. Lopez, J., Mackanic, D.G., Cui, Y., et al.: Designing polymers for advanced battery chemistries. Nat. Rev. Mater. **4**, 312–330 (2019). https://doi.org/10.1038/s41578-019-0103-6
32. Zhou, Q., Ma, J., Dong, S.M., et al.: Intermolecular chemistry in solid polymer electrolytes for high-energy-density lithium batteries. Adv. Mater. **31**, 1902029 (2019). https://doi.org/10.1002/adma.201902029
33. Li, S., Zhang, S.Q., Shen, L., et al.: Progress and perspective of ceramic/polymer composite solid electrolytes for lithium batteries. Adv. Sci. **7**, 1903088 (2020). https://doi.org/10.1002/advs.201903088
34. Balazs, A.C., Emrick, T., Russell, T.P.: Nanoparticle polymer composites: where two small worlds meet. Science **314**, 1107–1110 (2006). https://doi.org/10.1126/science.1130557
35. Liu, W., Lee, S.W., Lin, D.C., et al.: Enhancing ionic conductivity in composite polymer electrolytes with well-aligned ceramic nanowires. Nat. Energy **2**, 17035 (2017). https://doi.org/10.1038/nenergy.2017.35
36. Zhu, P., Yan, C.Y., Zhu, J.D., et al.: Flexible electrolyte-cathode bilayer framework with stabilized interface for room-temperature all-solid-state lithium-sulfur batteries. Energy Storage Mater. **17**, 220–225 (2019). https://doi.org/10.1016/j.ensm.2018.11.009
37. Xue, J., Wu, T., Dai, Y., et al.: Electrospinning and electrospun nanofibers: methods, materials, and applications. Chem. Rev. **119**, 5298–5415 (2019). https://doi.org/10.1021/acs.chemrev.8b00593
38. Sill, T.J., von Recum, H.A.: Electrospinning: applications in drug delivery and tissue engineering. Biomaterials **29**, 1989–2006 (2008). https://doi.org/10.1016/j.biomaterials.2008.01.011
39. Doshi, J., Reneker, D.H.: Electrospinning process and applications of electrospun fibers. J. Electrost. **35**, 151–160 (1995). https://doi.org/10.1016/0304-3886(95)00041-8
40. Agarwal, S., Wendorff, J.H., Greiner, A.: Progress in the field of electrospinning for tissue engineering applications. Adv. Mater. **21**, 3343–3351 (2009). https://doi.org/10.1002/adma.200803092
41. Li, Q., Hu, C., Clarke, H., et al.: Microstructure defines the electroconductive and mechanical performance of plant-derived renewable carbon fiber. Chem. Commun. **55**, 12655–12658 (2019). https://doi.org/10.1039/c9cc05016g
42. Zhang, X.W., Ji, L.W., Toprakci, O., et al.: Electrospun nanofiber-based anodes, cathodes, and separators for advanced lithium-ion batteries. Polym. Rev. **51**, 239–264 (2011). https://doi.org/10.1080/15583724.2011.593390
43. Hwang, T.H., Lee, Y.M., Kong, B.S., et al.: Electrospun core-shell fibers for robust silicon nanoparticle-based lithium ion battery anodes. Nano Lett. **12**, 802–807 (2012). https://doi.org/10.1021/nl203817r
44. Li, Q., Serem, W.K., Dai, W., et al.: Molecular weight and uniformity define the mechanical performance of lignin-based carbon fiber. J. Mater. Chem. A **5**, 12740–12746 (2017). https://doi.org/10.1039/c7ta01187c
45. Raghavan, P., Lim, D.H., Ahn, J.H., et al.: Electrospun polymer nanofibers: the booming cutting edge technology. React. Funct. Polym. **72**, 915–930 (2012). https://doi.org/10.1016/j.reactfunctpolym.2012.08.018
46. Li, Q., Xie, S.X., Wilson, K.: Quality carbon fibers from fractionated lignin. Green Chem. **19**, 1628–1634 (2017). https://doi.org/10.1039/c6gc03555h

47. Theron, S.A., Zussman, E., Yarin, A.L.: Experimental investigation of the governing parameters in the electrospinning of polymer solutions. Polymer **45**, 2017–2030 (2004). https://doi.org/10.1016/j.polymer.2004.01.024
48. Li, Q., Naik, M.T., Lin, H.S., et al.: Tuning hydroxyl groups for quality carbon fiber of lignin. Carbon **139**, 500–511 (2018). https://doi.org/10.1016/j.carbon.2018.07.015
49. Xu, C.Y., Inai, R., Kotaki, M., et al.: Aligned biodegradable nanofibrous structure: a potential scaffold for blood vessel engineering. Biomaterials **25**, 877–886 (2004). https://doi.org/10.1016/S0142-9612(03)00593-3
50. Murugan, R., Ramakrishna, S.: Design strategies of tissue engineering scaffolds with controlled fiber orientation. Tissue Eng. **13**, 1845–1866 (2007). https://doi.org/10.1089/ten.2006.0078
51. Hohman, M.M., Shin, M., Rutledge, G., et al.: Electrospinning and electrically forced jets. I. Stability theory. Phys. Fluids **13**, 2201–2220 (2001). https://doi.org/10.1063/1.1383791
52. Theron, A., Zussman, E., Yarin, A.L.: Electrostatic field-assisted alignment of electrospun nanofibres. Nanotechnology **12**, 384–390 (2001). https://doi.org/10.1088/0957-4484/12/3/329
53. Chawla, S., Cai, J.Z., Naraghi, M.: Mechanical tests on individual carbon nanofibers reveals the strong effect of graphitic alignment achieved via precursor hot-drawing. Carbon **117**, 208–219 (2017). https://doi.org/10.1016/j.carbon.2017.02.095
54. Naraghi, M., Arshad, S.N., Chasiotis, I.: Molecular orientation and mechanical property size effects in electrospun polyacrylonitrile nanofibers. Polymer **52**, 1612–1618 (2011). https://doi.org/10.1016/j.polymer.2011.02.013
55. Xie, J., Macewan, M.R., Ray, W.Z., et al.: Radially aligned, electrospun nanofibers as dural substitutes for wound closure and tissue regeneration applications. ACS Nano **4**, 5027–5036 (2010). https://doi.org/10.1021/nn101554u
56. Kessick, R., Fenn, J., Tepper, G.: The use of AC potentials in electrospraying and electrospinning processes. Polymer **45**, 2981–2984 (2004). https://doi.org/10.1016/j.polymer.2004.02.056
57. Li, L.L., Peng, S.J., Lee, J.K.Y., et al.: Electrospun hollow nanofibers for advanced secondary batteries. Nano Energy **39**, 111–139 (2017). https://doi.org/10.1016/j.nanoen.2017.06.050
58. Mao, X.W., Hatton, T., Rutledge, G.: A review of electrospun carbon fibers as electrode materials for energy storage. Curr. Org. Chem. **17**, 1390–1401 (2013). https://doi.org/10.2174/13852728113171300 06
59. Hedayati, R., Sadighi, M., Mohammadi-Aghdam, M., et al.: Mechanical properties of regular porous biomaterials made from truncated cube repeating unit cells: analytical solutions and computational models. Mater. Sci. Eng. C **60**, 163–183 (2016). https://doi.org/10.1016/j.msec.2015.11.001
60. Kim, B.H., Yang, K.S., Kim, Y.A., et al.: Solvent-induced porosity control of carbon nanofiber webs for supercapacitor. J. Power Sources **196**, 10496–10501 (2011). https://doi.org/10.1016/j.jpowsour.2011.08.088
61. Yu, Y., Gu, L., Zhu, C.B., et al.: Tin nanoparticles encapsulated in porous multichannel carbon microtubes: preparation by single-nozzle electrospinning and application as anode material for high-performance Li-based batteries. J. Am. Chem. Soc. **131**, 15984–15985 (2009). https://doi.org/10.1021/ja906261c
62. Yu, J.M., Wang, C., Li, S.H., et al.: Li^+-containing, continuous silica nanofibers for high Li^+ conductivity in composite polymer electrolyte. Small **15**, 1902729 (2019). https://doi.org/10.1002/smll.201902729
63. Chen, H.Y., Di, J.C., Wang, N., et al.: Fabrication of hierarchically porous inorganic nanofibers by a general microemulsion electrospinning approach. Small **7**, 1779–1783 (2011). https://doi.org/10.1002/smll.201002376
64. Moon, S., Choi, J., Farris, R.J.: Highly porous polyacrylonitrile/polystyrene nanofibers by electrospinning. Fibers Polym. **9**, 276–280 (2008). https://doi.org/10.1007/s12221-008-0044-y
65. Li, Z., Zhang, J.T., Chen, Y.M., et al.: Pie-like electrode design for high-energy density lithium–sulfur batteries. Nat. Commun. **6**, 8850 (2015). https://doi.org/10.1038/ncomms9850
66. Kim, C., Ngoc, B. . ., Yang, K. ., et al.: Self-sustained thin webs consisting of porous carbon nanofibers for supercapacitors via the electrospinning of polyacrylonitrile solutions containing zinc chloride. Adv. Mater. **19**, 2341–2346 (2007). https://doi.org/10.1002/adma.200602184
67. Li, J., Liu, E.H., Li, W., et al.: Nickel/carbon nanofibers composite electrodes as supercapacitors prepared by electrospinning. J. Alloy. Compd. **478**, 371–374 (2009). https://doi.org/10.1016/j.jallcom.2008.11.024
68. Im, J.S., Woo, S.W., Jung, M.J., et al.: Improved capacitance characteristics of electrospun ACFs by pore size control and vanadium catalyst. J. Colloid Interface Sci. **327**, 115–119 (2008). https://doi.org/10.1016/j.jcis.2008.08.030
69. Kim, B.H., Yang, K.S., Woo, H.G.: Thin, bendable electrodes consisting of porous carbon nanofibers via the electrospinning of polyacrylonitrile containing tetraethoxy orthosilicate for supercapacitor. Electrochem. Commun. **13**, 1042–1046 (2011). https://doi.org/10.1016/j.elecom.2011.06.024
70. Zhang, L.F., Aboagye, A., Kelkar, A., et al.: A review: carbon nanofibers from electrospun polyacrylonitrile and their applications. J. Mater. Sci. **49**, 463–480 (2014). https://doi.org/10.1007/s10853-013-7705-y
71. Ghasemi, M., Shahgaldi, S., Ismail, M., et al.: Activated carbon nanofibers as an alternative cathode catalyst to platinum in a two-chamber microbial fuel cell. Int. J. Hydrog. Energy **36**, 13746–13752 (2011). https://doi.org/10.1016/j.ijhydene.2011.07.118
72. Wang, G., Dong, Q., Ling, Z., et al.: Hierarchical activated carbon nanofiber webs with tuned structure fabricated by electrospinning for capacitive deionization. J. Mater. Chem. **22**, 21819 (2012). https://doi.org/10.1039/c2jm34890j
73. Lee, K.J., Shiratori, N., Lee, G.H., et al.: Activated carbon nanofiber produced from electrospun polyacrylonitrile nanofiber as a highly efficient formaldehyde adsorbent. Carbon **48**, 4248–4255 (2010). https://doi.org/10.1016/j.carbon.2010.07.034
74. Kim, C., Yang, K.S.: Electrochemical properties of carbon nanofiber web as an electrode for supercapacitor prepared by electrospinning. Appl. Phys. Lett. **83**, 1216–1218 (2003). https://doi.org/10.1063/1.1599963
75. You, X.Y., Misra, M., Gregori, S., et al.: Preparation of an electric double layer capacitor (EDLC) using miscanthus-derived biocarbon. ACS Sustainable Chem. Eng. **6**, 318–324 (2018). https://doi.org/10.1021/acssuschemeng.7b02563
76. You, X.Y., Koda, K., Yamada, T., et al.: Preparation of high-performance internal tandem electric double-layer capacitors (IT-EDLCs) from melt-spun lignin fibers. J. Wood Chem. Technol. **36**, 418–431 (2016). https://doi.org/10.1080/02773813.2016.1212893
77. Chen, Y.J., Amiri, A., Boyd, J.G., et al.: Promising trade-offs between energy storage and load bearing in carbon nanofibers as structural energy storage devices. Adv. Funct. Mater. **29**, 1901425 (2019). https://doi.org/10.1002/adfm.201901425
78. Zhou, Z.P., Liu, G.L.: Controlling the pore size of mesoporous carbon thin films through thermal and solvent annealing. Small **13**, 1603107 (2017). https://doi.org/10.1002/smll.201603107
79. Zhou, Z.P., Liu, T., Khan, A.U., et al.: Block copolymer–based porous carbon fibers. Sci. Adv. **5**, eaau6852–eaau6860 (2019). https://doi.org/10.1126/sciadv.aau6852

80. Liu, T., Zhou, Z., Guo, Y., et al.: Block copolymer derived uniform mesopores enable ultrafast electron and ion transport at high mass loadings. Nat. Commun. **10**, 675–684 (2019). https://doi.org/10.1038/s41467-019-08644-w
81. Liu, T., Liu, G.L.: Block copolymers for supercapacitors, dielectric capacitors and batteries. J. Phys.: Condens. Matter **31**, 233001 (2019). https://doi.org/10.1088/1361-648x/ab0d77
82. Yu, D.G., Wang, M.L., Li, X.Y., et al.: Multifluid electrospinning for the generation of complex nanostructures. Wiley Interdiscip. Rev.-Nanomed. Nanobiotechnol.**12**, e1601 (2020). https://doi.org/10.1002/wnan.1601
83. Sun, Z., Zussman, E., Yarin, A.L., et al.: Compound core–shell polymer nanofibers by Co-electrospinning. Adv. Mater. **15**, 1929–1932 (2003). https://doi.org/10.1002/adma.200305136
84. Dror, Y., Salalha, W., Avrahami, R., et al.: One-step production of polymeric microtubes by Co-electrospinning. Small **3**, 1064–1073 (2007). https://doi.org/10.1002/smll.200600536
85. Tuncel, D., Matthews, J., Anderson, H.: Synthesis of nanowalled polymer microtubes using glass fiber templates. Adv. Funct. Mater. **14**, 851–855 (2004). https://doi.org/10.1002/adfm.200305201
86. Kim, S.W., Kim, M., Lee, W.Y., et al.: Fabrication of hollow palladium spheres and their successful application to the recyclable heterogeneous catalyst for Suzuki coupling reactions. J. Am. Chem. Soc. **124**, 7642–7643 (2002). https://doi.org/10.1021/ja026032z
87. Wen, X.J., Tresco, P.A.: Fabrication and characterization of permeable degradable poly(dl-lactide-co-glycolide) (PLGA) hollow fiber phase inversion membranes for use as nerve tract guidance channels. Biomaterials **27**, 3800–3809 (2006). https://doi.org/10.1016/j.biomaterials.2006.02.036
88. Li, D., Xia, Y.N.: Direct fabrication of composite and ceramic hollow nanofibers by electrospinning. Nano Lett. **4**, 933–938 (2004). https://doi.org/10.1021/nl049590f
89. McCann, J.T., Li, D., Xia, Y.N.: Electrospinning of nanofibers with core-sheath, hollow, or porous structures. J. Mater. Chem. **15**, 735 (2005). https://doi.org/10.1039/b415094e
90. Loscertales, I.G., Barrero, A., Márquez, M., et al.: Electrically forced coaxial nanojets for one-step hollow nanofiber design. J. Am. Chem. Soc. **126**, 5376–5377 (2004). https://doi.org/10.1021/ja049443j
91. Liu, X.K., Yang, Y.Y., Yu, D.G., et al.: Tunable zero-order drug delivery systems created by modified triaxial electrospinning. Chem. Eng. J. **356**, 886–894 (2019). https://doi.org/10.1016/j.cej.2018.09.096
92. Yang, C., Yu, D.G., Pan, D., et al.: Electrospun pH-sensitive core–shell polymer nanocomposites fabricated using a tri-axial process. Acta Biomater. **35**, 77–86 (2016). https://doi.org/10.1016/j.actbio.2016.02.029
93. Chen, H., Wang, N., Di, J., et al.: Nanowire-in-microtube structured core/shell fibers via multifluidic coaxial electrospinning. Langmuir **26**, 11291–11296 (2010). https://doi.org/10.1021/la100611f
94. Yang, H.F., Lightner, C.R., Dong, L.: Light-emitting coaxial nanofibers. ACS Nano **6**, 622–628 (2012). https://doi.org/10.1021/nn204055t
95. Moghe, A.K., Gupta, B.S.: Co-axial electrospinning for nanofiber structures: preparation and applications. Polym. Rev. **48**, 353–377 (2008). https://doi.org/10.1080/15583720802022257
96. Qu, H.L., Wei, S.Y., Guo, Z.H.: Coaxial electrospun nanostructures and their applications. J. Mater. Chem. A **1**, 11513 (2013). https://doi.org/10.1039/c3ta12390a
97. Yu, Y., Gu, L., Wang, C.L., et al.: Encapsulation of sn@carbon nanoparticles in bamboo-like hollow carbon nanofibers as an anode material in lithium-based batteries. Angew. Chem. Int. Edit. **121**, 6607–6611 (2009). https://doi.org/10.1002/ange.200901723
98. Park, G.D., Kang, Y.C.: Enhanced Li-ion storage performance of novel tube-in-tube structured nanofibers with hollow metal oxide nanospheres covered with a graphitic carbon layer. Nanoscale **12**, 8404–8414 (2020). https://doi.org/10.1039/d0nr00592d
99. Gao, S.W., Wang, N., Li, S., et al.: A multi-wall Sn/SnO_2@carbon hollow nanofiber anode material for high-rate and long-life lithium-ion batteries. Angew. Chem. Int. Edit. **59**, 2465–2472 (2020). https://doi.org/10.1002/anie.201913170
100. Nam, D.H., Kim, J.W., Lee, J.H., et al.: Tunable Sn structures in porosity-controlled carbon nanofibers for all-solid-state lithium-ion battery anodes. J. Mater. Chem. A **3**, 11021–11030 (2015). https://doi.org/10.1039/c5ta00884k
101. Zhao, Y., Cao, X.Y., Jiang, L.: Bio-mimic multichannel microtubes by a facile method. J. Am. Chem. Soc. **129**, 764–765 (2007). https://doi.org/10.1021/ja068165g
102. Zhao, Y., Jiang, L.: Hollow micro/nanomaterials with multilevel interior structures. Adv. Mater. **21**, 3621–3638 (2009). https://doi.org/10.1002/adma.200803645
103. Mai, Y.Y., Eisenberg, A.: Self-assembly of block copolymers. Chem. Soc. Rev. **41**, 5969–5985 (2012). https://doi.org/10.1039/c2cs35115c
104. Ma, M.L., Krikorian, V., Yu, J.H., et al.: Electrospun polymer nanofibers with internal periodic structure obtained by microphase separation of cylindrically confined block copolymers. Nano Lett. **6**, 2969–2972 (2006). https://doi.org/10.1021/nl062311z
105. Ma, M.L., Titievsky, K., Thomas, E.L., et al.: Continuous concentric lamellar block copolymer nanofibers with long range order. Nano Lett. **9**, 1678–1683 (2009). https://doi.org/10.1021/nl900265y
106. Schacher, F.H., Rupar, P.A., Manners, I.: Functional block copolymers: nanostructured materials with emerging applications. Angew. Chem. Int. Edit. **51**, 7898–7921 (2012). https://doi.org/10.1002/anie.201200310
107. Blanazs, A., Armes, S.P., Ryan, A.J.: Self-assembled block copolymer aggregates: from micelles to vesicles and their biological applications. Macromol. Rapid Commun. **30**, 267–277 (2009). https://doi.org/10.1002/marc.200800713
108. Niu, H.T., Zhang, J., Xie, Z.L., et al.: Preparation, structure and supercapacitance of bonded carbon nanofiber electrode materials. Carbon **49**, 2380–2388 (2011). https://doi.org/10.1016/j.carbon.2011.02.005
109. Wu, H., Hu, L., Rowell, M.W., et al.: Electrospun metal nanofiber webs as high-performance transparent electrode. Nano Lett. **10**, 4242–4248 (2010). https://doi.org/10.1021/nl102725k
110. Dallmeyer, J.L.: Preparation and characterization of lignin nanofibre-based materials obtained by electrostatic spinning. Doctoral dissertation, University of British Columbia (2013)
111. Schlee, P., Hosseinaei, O., Baker, D., et al.: From waste to wealth: from kraft lignin to free-standing supercapacitors. Carbon **145**, 470–480 (2019). https://doi.org/10.1016/j.carbon.2019.01.035
112. Roman, J., Neri, W., Derré, A., et al.: Electrospun lignin-based twisted carbon nanofibers for potential microelectrodes applications. Carbon **145**, 556–564 (2019). https://doi.org/10.1016/j.carbon.2019.01.036
113. Tenhaeff, W.E., Rios, O., More, K., et al.: Highly robust lithium ion battery anodes from lignin: an abundant, renewable, and low-cost material. Adv. Funct. Mater. **24**, 86–94 (2014). https://doi.org/10.1002/adfm.201301420
114. Milczarek, G., Inganäs, O.: Renewable cathode materials from biopolymer/conjugated polymer interpenetrating networks.

Science **335**, 1468–1471 (2012). https://doi.org/10.1126/science.1215159
115. Peng, Z.Y., Zou, Y.B., Xu, S.Q., et al.: High-performance biomass-based flexible solid-state supercapacitor constructed of pressure-sensitive lignin-based and cellulose hydrogels. ACS Appl. Mater. Interfaces **10**, 22190–22200 (2018). https://doi.org/10.1021/acsami.8b05171
116. Wang, S.X., Yang, L.P., Stubbs, L.P., et al.: Lignin-derived fused electrospun carbon fibrous mats as high performance anode materials for lithium ion batteries. ACS Appl. Mater. Interfaces **5**, 12275–12282 (2013). https://doi.org/10.1021/am4043867
117. Wang, X.E., Kerr, R., Chen, F.F., et al.: Toward high-energy-density lithium metal batteries: opportunities and challenges for solid organic electrolytes. Adv. Mater. **32**, 1905219 (2020). https://doi.org/10.1002/adma.201905219
118. Kim, D.H.: Thin and flexible solid electrolyte membranes with ultrahigh thermal stability derived from solution-processable Li argyrodites for all-solid-state Li-ion batteries. ACS Energy Lett. **5**, 718–727 (2020)
119. Hu, J.K., He, P.G., Zhang, B.C., et al.: Porous film host-derived 3D composite polymer electrolyte for high-voltage solid state lithium batteries. Energy Storage Mater. **26**, 283–289 (2020). https://doi.org/10.1016/j.ensm.2020.01.006
120. Wang, X.E., Girard, G.M.A., Zhu, H.J., et al.: Poly(ionic liquid) s/electrospun nanofiber composite polymer electrolytes for high energy density and safe Li metal batteries. ACS Appl. Energy Mater. **2**, 6237–6245 (2019). https://doi.org/10.1021/acsaem.9b00765
121. Zhou, Y.D., Wang, X.E., Zhu, H.J., et al.: Solid-state lithium conductors for lithium metal batteries based on electrospun nanofiber/plastic crystal composites. Chemsuschem **10**, 3135–3145 (2017). https://doi.org/10.1002/cssc.201700691
122. Watanabe, T., Inafune, Y., Tanaka, M., et al.: Development of all-solid-state battery based on lithium ion conductive polymer nanofiber framework. J. Power Sources **423**, 255–262 (2019). https://doi.org/10.1016/j.jpowsour.2019.03.066
123. Wang, C.S., Zhang, X.W., Appleby, A.J.: Solvent-free composite PEO-ceramic fiber/mat electrolytes for lithium secondary cells. J. Electrochem. Soc. **152**, A205 (2005). https://doi.org/10.1149/1.1828952
124. Liu, W., Liu, N., Sun, J., et al.: Ionic conductivity enhancement of polymer electrolytes with ceramic nanowire fillers. Nano Lett. **15**, 2740–2745 (2015). https://doi.org/10.1021/acs.nanolett.5b00600
125. Li, B.Y., Su, Q.M., Yu, L.T., et al.: $Li_{0.35}La_{0.55}TiO_3$ nanofibers enhanced poly(vinylidene fluoride)-based composite polymer electrolytes for all-solid-state batteries. ACS Appl. Mater. Interfaces **11**, 42206–42213 (2019). https://doi.org/10.1021/acsami.9b14824
126. Li, Y., Zhang, W., Dou, Q.Q., et al.: $Li_7La_3Zr_2O_{12}$ ceramic nanofiber-incorporated composite polymer electrolytes for lithium metal batteries. J. Mater. Chem. A **7**, 3391–3398 (2019). https://doi.org/10.1039/c8ta11449h
127. Fu, K.K., Gong, Y., Dai, J., et al.: Flexible, solid-state, ion-conducting membrane with 3D garnet nanofiber networks for lithium batteries. Proc. Natl. Acad. Sci. U. S. A. **113**, 7094–7099 (2016). https://doi.org/10.1073/pnas.1600422113
128. Zhu, P., Yan, C.Y., Dirican, M., et al.: $Li_{0.33}La_{0.557}TiO_3$ ceramic nanofiber-enhanced polyethylene oxide-based composite polymer electrolytes for all-solid-state lithium batteries. J. Mater. Chem. A **6**, 4279–4285 (2018). https://doi.org/10.1039/c7ta10517g
129. Yu, L., Canfield, N.L., Chen, S.R., et al.: Enhanced stability of lithium metal anode by using a 3D porous nickel substrate. ChemElectroChem **5**, 761–769 (2018). https://doi.org/10.1002/celc.201701250
130. Wang, X.Z., Zhang, Y.B., Zhang, X., et al.: Lithium-salt-rich PEO/$Li_{0.3}La_{0.557}TiO_3$ interpenetrating composite electrolyte with three-dimensional ceramic nano-backbone for all-solid-state lithium-ion batteries. ACS Appl. Mater. Interfaces **10**, 24791–24798 (2018). https://doi.org/10.1021/acsami.8b06658
131. Liu, K., Zhang, R.H., Sun, J., et al.: Polyoxyethylene (PEO)|PEO-Perovskite|PEO composite electrolyte for all-solid-state lithium metal batteries. ACS Appl. Mater. Interfaces **11**, 46930–46937 (2019). https://doi.org/10.1021/acsami.9b16936
132. Yan, C.Y., Zhu, P., Jia, H., et al.: Garnet-rich composite solid electrolytes for dendrite-free, high-rate, solid-state lithium-metal batteries. Energy Storage Mater. **26**, 448–456 (2020). https://doi.org/10.1016/j.ensm.2019.11.018
133. Yang, H., Bright, J., Chen, B.H., et al.: Chemical interaction and enhanced interfacial ion transport in a ceramic nanofiber-polymer composite electrolyte for all-solid-state lithium metal batteries. J. Mater. Chem. A **8**, 7261–7272 (2020). https://doi.org/10.1039/c9ta12495k
134. Zhao, Y., Yan, J.H., Cai, W.P., et al.: Elastic and well-aligned ceramic LLZO nanofiber-based electrolytes for solid-state lithium batteries. Energy Storage Mater. **23**, 306–313 (2019). https://doi.org/10.1016/j.ensm.2019.04.043
135. Wu, Q.Y., Chen, X.N., Wan, L.S., et al.: Interactions between polyacrylonitrile and solvents: density functional theory study and two-dimensional infrared correlation analysis. J. Phys. Chem. B **116**, 8321–8330 (2012). https://doi.org/10.1021/jp304167f
136. Foran, G., Mankovsky, D., Verdier, N., et al.: The impact of absorbed solvent on the performance of solid polymer electrolytes for use in solid-state lithium batteries. iScience **23**, 101597 (2020). https://doi.org/10.1016/j.isci.2020.101597
137. Huttner, F., Haselrieder, W., Kwade, A.: The influence of different post-drying procedures on remaining water content and physical and electrochemical properties of lithium-ion batteries. Energy Technol. **8**, 1900245 (2020). https://doi.org/10.1002/ente.201900245
138. Fu, L.J., Zhang, H.P., Wu, Y.P., et al.: Surface active sites: an important factor affecting the sensitivity of carbon anode material toward humidity. Electrochem. Solid-State Lett. **8**, A456 (2005). https://doi.org/10.1149/1.1990047
139. Rupich, M.W., Pitts, L., Abraham, K.M.: Characterization of reactions and products of the discharge and forced overdischarge of Li/SO_2 cells. J. Electrochem. Soc. **129**, 1857–1861 (1982). https://doi.org/10.1149/1.2124314
140. Li, J.L., Daniel, C., An, S.J., et al.: Evaluation residual moisture in lithium-ion battery electrodes and its effect on electrode performance. MRS Adv. **1**, 1029–1035 (2016). https://doi.org/10.1557/adv.2016.6
141. Stich, M., Pandey, N., Bund, A.: Drying and moisture resorption behaviour of various electrode materials and separators for lithium-ion batteries. J. Power Sources **364**, 84–91 (2017). https://doi.org/10.1016/j.jpowsour.2017.08.009
142. Fenton, D.E., Parker, J.M., Wright, P.V.: Complexes of alkali metal ions with poly(ethylene oxide). Polymer **14**, 589 (1973). https://doi.org/10.1016/0032-3861(73)90146-8
143. Savoie, B.M., Webb, M.A., Miller, T.F., III.: Enhancing cation diffusion and suppressing anion diffusion via lewis-acidic polymer electrolytes. J. Phys. Chem. Lett. **8**, 641–646 (2017). https://doi.org/10.1021/acs.jpclett.6b02662
144. Sun, J., Stone, G.M., Balsara, N.P., et al.: Structure–conductivity relationship for peptoid-based PEO–mimetic polymer electrolytes. Macromolecules **45**, 5151–5156 (2012). https://doi.org/10.1021/ma300775b
145. Nishimoto, A., Agehara, K., Furuya, N., et al.: High ionic conductivity of polyether-based network polymer electrolytes with hyperbranched side chains. Macromolecules **32**, 1541–1548 (1999). https://doi.org/10.1021/ma981436q
146. Hawker, C.J., Chu, F.K., Pomery, P.J., et al.: Hyperbranched Poly(ethylene glycol)s: a new class of ion-conducting materials.

Macromolecules **29**, 3831–3838 (1996). https://doi.org/10.1021/ma951909i
147. Stone, G.M., Mullin, S.A., Teran, A.A., et al.: Resolution of the modulus versus adhesion dilemma in solid polymer electrolytes for rechargeable lithium metal batteries. J. Electrochem. Soc. **159**, A222–A227 (2012). https://doi.org/10.1149/2.030203jes
148. Young, N.P., Devaux, D., Khurana, R., et al.: Investigating polypropylene-poly(ethylene oxide)-polypropylene triblock copolymers as solid polymer electrolytes for lithium batteries. Solid State Ionics **263**, 87–94 (2014). https://doi.org/10.1016/j.ssi.2014.05.012
149. Bouchet, R., Phan, T.N.T., Beaudoin, E., et al.: Charge transport in nanostructured PS-PEO-PS triblock copolymer electrolytes. Macromolecules **47**, 2659–2665 (2014). https://doi.org/10.1021/ma500420w
150. Bates, C.M., Chang, A.B., Momčilović, N., et al.: ABA triblock brush polymers: synthesis, self-assembly, conductivity, and rheological properties. Macromolecules **48**, 4967–4973 (2015). https://doi.org/10.1021/acs.macromol.5b00880
151. Bouchet, R., Maria, S., Meziane, R., et al.: Single-ion BAB triblock copolymers as highly efficient electrolytes for lithium-metal batteries. Nat. Mater. **12**, 452–457 (2013). https://doi.org/10.1038/nmat3602
152. Lin, Z.Y., Guo, X.W., Yang, Y.B., et al.: Block copolymer electrolyte with adjustable functional units for solid polymer lithium metal battery. J. Energy Chem. **52**, 67–74 (2021). https://doi.org/10.1016/j.jechem.2020.04.052
153. Khurana, R., Schaefer, J.L., Archer, L.A., et al.: Suppression of lithium dendrite growth using cross-linked polyethylene/poly(ethylene oxide) electrolytes: a new approach for practical lithium-metal polymer batteries. J. Am. Chem. Soc. **136**, 7395–7402 (2014). https://doi.org/10.1021/ja502133j
154. Pan, Q.W., Smith, D.M., Qi, H., et al.: Hybrid electrolytes with controlled network structures for lithium metal batteries. Adv. Mater. **27**, 5995–6001 (2015). https://doi.org/10.1002/adma.201502059
155. Peramunage, D., Pasquariello, D.M., Abraham, K.M.: Polyacrylonitrile-based electrolytes with ternary solvent mixtures as plasticizers. J. Electrochem. Soc. **142**, 1789–1798 (1995). https://doi.org/10.1149/1.2044195
156. Watanabe, M., Kanba, M., Nagaoka, K., et al.: Ionic conductivity of hybrid films composed of polyacrylonitrile, ethylene carbonate, and $LiClO_4$. J. Polym. Sci.: Polym. Phys. Ed. **21**, 939–948 (1983). https://doi.org/10.1002/pol.1983.180210610
157. Webb, M.A., Jung, Y., Pesko, D.M., et al.: Systematic computational and experimental investigation of lithium-ion transport mechanisms in polyester-based polymer electrolytes. ACS Central Sci. **1**, 198–205 (2015). https://doi.org/10.1021/acscentsci.5b00195
158. Liu, L.H., Lyu, J., Mo, J.S., et al.: Comprehensively-upgraded polymer electrolytes by multifunctional aramid nanofibers for stable all-solid-state Li-ion batteries. Nano Energy **69**, 104398 (2020). https://doi.org/10.1016/j.nanoen.2019.104398
159. Porcarelli, L., Shaplov, A.S., Bella, F., et al.: Single-ion conducting polymer electrolytes for lithium metal polymer batteries that operate at ambient temperature. ACS Energy Lett. **1**, 678–682 (2016). https://doi.org/10.1021/acsenergylett.6b00216
160. Mai, L., Tian, X., Xu, X., et al.: Nanowire electrodes for electrochemical energy storage devices. Chem. Rev. **114**, 11828–11862 (2014). https://doi.org/10.1021/cr500177a
161. Li, X.Y., Chen, W.C., Qian, Q.R., et al.: Electrospinning-based strategies for battery materials. Adv. Energy Mater. **11**, 2000845 (2021). https://doi.org/10.1002/aenm.202000845
162. Wang, H.G., Yuan, S., Ma, D.L., et al.: Electrospun materials for lithium and sodium rechargeable batteries: from structure evolution to electrochemical performance. Energy Environ. Sci. **8**, 1660–1681 (2015). https://doi.org/10.1039/c4ee03912b
163. Liu, M., Deng, N.P., Ju, J.G., et al.: A review: electrospun nanofiber materials for lithium-sulfur batteries. Adv. Funct. Mater. **29**, 1905467 (2019). https://doi.org/10.1002/adfm.201905467
164. Liu, Q., Zhu, J.H., Zhang, L.W., et al.: Recent advances in energy materials by electrospinning. Renew. Sustain. Energy Rev. **81**, 1825–1858 (2018). https://doi.org/10.1016/j.rser.2017.05.281
165. Pandey, G.P., Klankowski, S.A., Li, Y.H., et al.: Effective infiltration of gel polymer electrolyte into silicon-coated vertically aligned carbon nanofibers as anodes for solid-state lithium-ion batteries. ACS Appl. Mater. Interfaces **7**, 20909–20918 (2015). https://doi.org/10.1021/acsami.5b06444
166. Klankowski, S.A., Rojeski, R.A., Cruden, B.A., et al.: A high-performance lithium-ion battery anode based on the core–shell heterostructure of silicon-coated vertically aligned carbon nanofibers. J. Mater. Chem. A **1**, 1055–1064 (2013). https://doi.org/10.1039/c2ta00057a
167. Slater, M.D., Kim, D., Lee, E., et al.: Sodium-ion batteries. Adv. Funct. Mater. **23**, 947–958 (2013). https://doi.org/10.1002/adfm.201200691
168. Nayak, P.K., Yang, L.T., Brehm, W., et al.: From lithium-ion to sodium-ion batteries: advantages, challenges, and surprises. Angew. Chem.-Int. Edit. **57**, 102–120 (2018). https://doi.org/10.1002/anie.201703772
169. Kim, S.W., Seo, D.H., Ma, X.H., et al.: Electrode materials for rechargeable sodium-ion batteries: potential alternatives to current lithium-ion batteries. Adv. Energy Mater. **2**, 710–721 (2012). https://doi.org/10.1002/aenm.201200026
170. Vaalma, C., Buchholz, D., Weil, M., et al.: A cost and resource analysis of sodium-ion batteries. Nat. Rev. Mater. **3**, 18013 (2018). https://doi.org/10.1038/natrevmats.2018.13
171. Hwang, J.Y., Myung, S.T., Sun, Y.K.: Sodium-ion batteries: present and future. Chem. Soc. Rev. **46**, 3529–3614 (2017). https://doi.org/10.1039/c6cs00776g
172. Yabuuchi, N., Kubota, K., Dahbi, M., et al.: Research development on sodium-ion batteries. Chem. Rev. **114**, 11636–11682 (2014). https://doi.org/10.1021/cr500192f
173. Gao, R.T., Tan, R., Han, L., et al.: Nanofiber networks of $Na_3V_2(PO_4)_3$ as a cathode material for high performance all-solid-state sodium-ion batteries. J. Mater. Chem. A **5**, 5273–5277 (2017). https://doi.org/10.1039/c7ta00314e
174. Zhang, X., Xie, J., Shi, F., et al.: Vertically aligned and continuous nanoscale ceramic-polymer interfaces in composite solid polymer electrolytes for enhanced ionic conductivity. Nano Lett. **18**, 3829–3838 (2018). https://doi.org/10.1021/acs.nanolett.8b01111
175. Liu, K., Wu, M.C., Wei, L., et al.: A composite solid electrolyte with a framework of vertically aligned perovskite for all-solid-state Li-metal batteries. J. Membr. Sci. **610**, 118265 (2020). https://doi.org/10.1016/j.memsci.2020.118265
176. Zhai, H.W., Xu, P.Y., Ning, M.Q., et al.: A flexible solid composite electrolyte with vertically aligned and connected ion-conducting nanoparticles for lithium batteries. Nano Lett. **17**, 3182–3187 (2017). https://doi.org/10.1021/acs.nanolett.7b00715
177. Tang, W.J., Tang, S., Guan, X.Z., et al.: High-performance solid polymer electrolytes filled with vertically aligned 2D materials. Adv. Funct. Mater. **29**, 1900648 (2019). https://doi.org/10.1002/adfm.201900648
178. Wang, X., Zhai, H.W., Qie, B.Y., et al.: Rechargeable solid-state lithium metal batteries with vertically aligned ceramic nanoparticle/polymer composite electrolyte. Nano Energy **60**, 205–212 (2019). https://doi.org/10.1016/j.nanoen.2019.03.051
179. Wan, J.Y., Xie, J., Kong, X., et al.: Ultrathin, flexible, solid polymer composite electrolyte enabled with aligned nanoporous host for lithium batteries. Nat. Nanotechnol. **14**, 705–711 (2019). https://doi.org/10.1038/s41565-019-0465-3

180. Wang, X., Wang, T.Y., Borovilas, J., et al.: Vertically-aligned nanostructures for electrochemical energy storage. Nano Res. **12**, 2002–2017 (2019). https://doi.org/10.1007/s12274-019-2392-x
181. Wolfenstine, J., Allen, J.L., Sakamoto, J., et al.: Mechanical behavior of Li-ion-conducting crystalline oxide-based solid electrolytes: a brief review. Ionics **24**, 1271–1276 (2018). https://doi.org/10.1007/s11581-017-2314-4
182. Ke, X.Y., Wang, Y., Ren, G.F., et al.: Towards rational mechanical design of inorganic solid electrolytes for all-solid-state lithium ion batteries. Energy Storage Mater. **26**, 313–324 (2020). https://doi.org/10.1016/j.ensm.2019.08.029
183. Bi, J.Y., Mu, D.B., Wu, B.R., et al.: A hybrid solid electrolyte $Li_{0.33}La_{0.557}TiO_3$/poly(acylonitrile) membrane infiltrated with a succinonitrile-based electrolyte for solid state lithium-ion batteries. J. Mater. Chem. A **8**, 706–713 (2020). https://doi.org/10.1039/c9ta08601c
184. Li, D., Chen, L., Wang, T.S., et al.: 3D fiber-network-reinforced bicontinuous composite solid electrolyte for dendrite-free lithium metal batteries. ACS Appl. Mater. Interfaces **10**, 7069–7078 (2018). https://doi.org/10.1021/acsami.7b18123
185. Jia, M.Y., Zhao, N., Huo, H.Y., et al.: Comprehensive investigation into garnet electrolytes toward application-oriented solid lithium batteries. Electrochem. Energy Rev. **3**, 656–689 (2020). https://doi.org/10.1007/s41918-020-00076-1
186. Yan, C.Y., Zhu, P., Jia, H., et al.: High-performance 3-D fiber network composite electrolyte enabled with Li-ion conducting nanofibers and amorphous PEO-based cross-linked polymer for ambient all-solid-state lithium-metal batteries. Adv. Fiber Mater. **1**, 46–60 (2019). https://doi.org/10.1007/s42765-019-00006-x
187. He, K.Q., Zha, J.W., Du, P., et al.: Tailored high cycling performance in a solid polymer electrolyte with perovskite-type $Li_{0.33}La_{0.557}TiO_3$ nanofibers for all-solid-state lithium ion batteries. Dalton Trans. **48**, 3263–3269 (2019). https://doi.org/10.1039/c9dt00074g
188. Wang, S., Zhang, L., Li, J.Y., et al.: A nanowire-nanoparticle double composite polymer electrolyte for high performance ambient temperature solid-state lithium batteies. Electrochim. Acta **320**, 134560 (2019). https://doi.org/10.1016/j.electacta.2019.134560
189. Zhang, L., Wang, S., Li, J.Y., et al.: A nitrogen-containing all-solid-state hyperbranched polymer electrolyte for superior performance lithium batteries. J. Mater. Chem. A **7**, 6801–6808 (2019). https://doi.org/10.1039/c9ta00180h
190. Liu, W., Lin, D., Sun, J., et al.: Improved lithium ionic conductivity in composite polymer electrolytes with oxide-ion conducting nanowires. ACS Nano **10**, 11407–11413 (2016). https://doi.org/10.1021/acsnano.6b06797
191. Cao, D.X., Sun, X., Li, Q., et al.: Lithium dendrite in all-solid-state batteries: growth mechanisms, suppression strategies, and characterizations. Matter **3**, 57–94 (2020). https://doi.org/10.1016/j.matt.2020.03.015
192. Yang, T., Zheng, J., Cheng, Q., et al.: Composite polymer electrolytes with $Li_7La_3Zr_2O_{12}$ garnet-type nanowires as ceramic fillers: mechanism of conductivity enhancement and role of doping and morphology. ACS Appl. Mater. Interfaces **9**, 21773–21780 (2017). https://doi.org/10.1021/acsami.7b03806
193. Balaish, M., Gonzalez-Rosillo, J.C., Kim, K.J., et al.: Processing thin but robust electrolytes for solid-state batteries. Nat. Energy **6**, 227–239 (2021). https://doi.org/10.1038/s41560-020-00759-5
194. Zhao, Y., Zheng, K., Sun, X.L.: Addressing interfacial issues in liquid-based and solid-state batteries by atomic and molecular layer deposition. Joule **2**, 2583–2604 (2018). https://doi.org/10.1016/j.joule.2018.11.012
195. Yang, X.F., Adair, K.R., Gao, X.J., et al.: Recent advances and perspectives on thin electrolytes for high-energy-density solid-state lithium batteries. Energy Environ. Sci. **14**, 643–671 (2021). https://doi.org/10.1039/d0ee02714f
196. Wang, C.H., Liang, J.W., Zhao, Y., et al.: All-solid-state lithium batteries enabled by sulfide electrolytes: from fundamental research to practical engineering design. Energy Environ. Sci. **14**, 2577–2619 (2021). https://doi.org/10.1039/d1ee00551k

Qiang Li is currently a professor at Huazhong Agricultural University, China. He has solid backgrounds on wood chemistry, carbon materials, and advanced manufacturing. His research focuses on biomass-based carbon fibers, sustainable and renewable materials, and multi-stream integrated biorefinery. From Jan. 2020 to Apr. 2021, he worked at Northeastern University as a postdoc in Prof. Hongli Zhu group. His work covers lignin-based solid-state electrolytes, carbon materials, plastic replacement, and nanocellulose. From 2016 to 2020 and Apr. 2021 to Jan. 2022, he worked as a postdoc and Scientist I, respectively, at Texas A&M University with the research topics on biomass-based carbon fibers and lignocellulosic biorefinery. Before that, he got his Ph.D. degree in 2015 on wood chemistry from Hokkaido University, Japan. He has dedicated to implement a sustainable future by using wood and agriculture residue as resources to produce renewable, economic, and high-value materials and products, which includes renewable energy like biofuels and biodiesels, high quality carbon fibers, and bioplastics.

Xiao Sun is currently a Ph.D. candidate at the department of Mechanical and Industrial Engineering in Northeastern University. She received her M.S. degree in mechanical engineering department from Northeastern University in 2019. Her research is focused on investigating advanced materials for energy storage and developing all solid-state batteries.

Daxian Cao is currently a postdoc in Mechanical and Industrial Engineering at Northeastern University. His research interests include advanced all-solid-state batteries and Li metal anodes. He received his B.S. degree (2014) in Material Science and Engineering and Ph.D. degree (2019) in Electrical Engineering from Xi'an Jiaotong University.

Ying Wang is a Ph.D. student in Professor Hongli Zhu's group at Northeastern University. She received her M.S. degree (2020) in the Department of Mechanical and Industrial Engineering from Northeastern University. She is interested in advanced manufacturing and multifunctional materials for energy storage.

Pengcheng Luan is currently an exchange Ph.D. student between Northeastern University and the State Key Laboratory of Pulp and Paper Engineering in the South China University of Technology. His research interests focus on the extraction and functional modification of lignocellulosic biomass, including eco-friendly delignification processes, lignocellulosic sorbent, and cellulose-based reverse electrodialysis devices. Furthermore, he is also interested in the industrial applications of cellulose in the field of pulp and paper manufacturing and environmental protection.

Hongli Zhu is currently an assistant professor at Northeastern University. Her group focuses on the research of electrochemical energy storage, sustainable materials, and advanced manufacturing. Her current google scholar citations are > 15 000, and the *H* factor is 59. From 2012 to 2015, she works in the University of Maryland as postdoc, focusing on the research of nanocellulose, energy storage, and flexible electronics. From 2009 to 2011, She conducted research on materials science and processing of biodegradable and renewable biomaterials from natural wood in the KTH Royal Institute of Technology in Sweden. Her expertise is on the research of environmentally friendly natural materials and energy storage, design and application of novel, high-value biomaterials from renewable sources towards neutral carbon, and R2R manufacturing. In energy storage, her group in Northeastern University works intensively on flow batteries, solid state batteries, and other alkali metal ion batteries, such as Li^+, Na^+ and K^+ batteries.